BUILDING THERMAL LOAD CONTROL: POTENTIAL, STRATEGY, AND IMPLEMENTATION

A Dissertation
Presented to
The Academic Faculty

by

Di Lu

In Partial Fulfillment
of the Requirements for the Degree
Doctor of Philosophy in the
School of Architecture

Georgia Institute of Technology
December 2020

BUILDING THERMAL LOAD CONTROL:
POTENTIAL, STRATEGY, AND IMPLEMENTATION

Approved by:

Prof. Godfried Augenbroe, Advisor
School of Architecture
Georgia Institute of Technology

Dr. Gregor P. Henze
College of Engineering and Applied Science
University of Colorado Boulder

Dr. Peter Loutzenhiser
School of Mechanical Engineering
Georgia Institute of Technology

Dr. Ali Malkawi
Graduate School of Design
Harvard University

Dr. Jason Brown
School of Architecture
Georgia Institute of Technology

Dr. Zheng O'Neill
College of Engineering
Texas A&M University

Date Approved: November 25, 2020

To my beloved world

ACKNOWLEDGEMENTS

I would like to express my greatest thanks to my advisor Prof. Godfried Augenbroe. His wisdom lightens the path for me in proceeding with academic studies, and his life philosophy guides me as being a man. I will never forget the days we work together and laugh together. It is really a great honor for me to be his student. I would like to extend my thanks to Dr. Jason Brown, who admitted me to Georgia Tech and gave me the chance to enjoy these beautiful years of my Ph.D. study. The rigorous attitude I learned in his classes deeply influences my works.

I want to thank Qi Li, Jianli Chen, Yifu Shi, and Yuna Zhang, who gave me valuable advice on my thesis work. I feel supported by having your help. And I also want to thank my colleagues Gustavo, Alya, Mohanned, Yun Joon, and Zhaoyun, who expand my vision on aspects of professional works. Many thanks to my friends Ruicheng, Junteng, Ning, Shiyang, Chufei, Xi, and Ting. You got me a lot of fun, and I really enjoy the days with you.

I want to give my most profound appreciation to my Mom Junxiu Zhang and my Dad Jinlong Lu. Thank you for your love and encouragement. I feel lucky to be your son. Lastly, I would like to extend my thankfulness to my beloved fiancée Jie Lei. You make my life full of happiness and gratification.

I lost my Grandmother 高桂兰 and my Grandfather 张贵藻 during my Ph.D. study. May they rest in peace.

TABLE OF CONTENTS

ACKNOWLEDGEMENT **iv**

LIST OF TABLES **vii**

LIST OF FIGURES **ix**

SUMMARY **xiii**

CHAPTER 1. Introduction **1**
1.1 Background **1**
1.2 Literature review **5**
1.2.1 Existing MPC studies for building thermal load control 5
1.2.2 Thermal comfort requirement and productivity loss 28
1.3 Research goals **37**

CHAPTER 2. Zonal Control Flexibility to Manage Building Thermal Loads **40**
2.1 Zonal acceptable temperature band **40**
2.1.1 Methodology and approach 41
2.1.2 Results and analysis 46
2.2 Productivity (loss) function **52**
2.2.1 Methodology and Approach 53
2.2.2 Result and analysis 55
2.3 Conclusion **58**

CHAPTER 3. Potential Benefits of Building Thermal Load Control **60**
3.1 Methodology **62**
3.1.1 Prediction Model 62
3.1.2 Linear system and optimization 66
3.1.3 Experiment setups 69
3.2 Results **73**
3.2.1 Inspection 73
3.2.2 Potential cost-saving 75
3.2.3 Potential of organizational benefit increase 79
3.2.4 Extensions 80
3.3 Conclusion **82**

CHAPTER 4. Cost-saving Potential across Building Types and Climates **84**
4.1 Climate conditions **85**
4.1.1 Climate zones and selected cities 85
4.1.2 Time of use rate in cities 86
4.2 Construction types **87**
4.3 Experiment results **89**
4.4 Analysis of influential factors on cost saving potential **95**
4.5 Conclusion **102**

CHAPTER 5. Cost-saving Performance under Scenario Uncertainty 104
5.1 Methodology 107
5.1.1 Definitions and Attributes 107
5.1.2 Definition of the influence of scenario uncertainties on MPC 110
5.2 Uncertainty range 112
5.2.1 Literature review on prediction methods 112
5.2.2 Experiment setups 116
5.2.3 Kalman filter 121
5.2.4 Uncertainty Range defined in this study 123
5.3 Result and analysis 135
5.3.1 Result inspection 135
5.3.2 The influence of scenario uncertainties on MPC 137
5.4 Conclusion and Inference 139

CHAPTER 6. A Possible Road to Real Application 141
6.1 Two-Point Activation control 141
6.1.1 The form of TPA control 143
6.1.2 The significance of TPA control 146
6.2 An example of TPA control 149
6.2.1 Assumptions about the building 149
6.2.2 RC modeling 150
6.2.3 RC model calibration 154
6.2.4 Optimization and simulation result 158
6.3 Conclusion 162

CHAPTER 7. Conclusion and Future Works 164

APPENDIX A. Parameters in the emulator for cost-saving potential estimation 167

APPENDIX B. Comparison of temperature profiles in different MPC cases 168

REFERENCES 171

LIST OF TABLES

Table 1.1 Example design criteria for spaces in various types of buildings [50] 32

Table 2.1 Summary of temperature band in scenarios 49

Table 2.2 The violation instances and percentage 51

Table 2.3 Summary of productivity in scenarios 57

Table 3.1 Electricity time of use rate form Georgia Power 61

Table 3.2 List of scenarios in the analysis of potentials 70

Table 3.3 Building HVAC operation cost in scenarios (T1, T3-T5) 75

Table 3.4 OB in scenarios (T2 & T6) 80

Table 3.5 Zonal OB comparison between A2 and A1 scenarios over 4 months 82

Table 4.1 The list of cities in climate zone 1A to 6B 85

Table 4.2 TOU rate plans in selected cities 86

Table 4.3 The seasonal HVAC energy cost, cost savings, and cost-saving percentage of all simulated scenarios 90

Table 4.4 Correlation matrix of cost-saving percentage and weather parameters 96

Table 4.5 Training error of the regression models 100

Table 4.6 Summary of the emulator's training error 101

Table 4.7 Testing result of the emulator 102

Table 4.8 Summary of the emulator's testing error 102

Table 5.1 The combinations of levels of uncertainty and representing case code 121

Table 5.2 Statistical summary of the ANN model 125

Table 5.3 Statistical summary of online weather forecast 127

Table 5.4 Statistical summary of local weather prediction 130

Table 5.5 Statistical summary of internal gain prediction 133

Table 5.6 Seasonal performance of MPC in cases with levels of scenario uncertainty 137

Table 6.1 Comparison of the performance using original / TPA MPC control 144

Table 6.2 RC parameters in the building level RC model 153

Table 6.3 RC parameters in the south zone RC model 158

Table 6.4 Detailed case setups 160

Table 6.5 Comparison of cost-saving performance in different MPC cases 161

LIST OF FIGURES

Figure 1.1	A typical workflow of MPC	5
Figure 1.2	Structure of the RC model proposed in [25]	10
Figure 1.3	Structure of the RC model proposed in [35]	11
Figure 1.4	Prediction process in white-box or grey-box models using temperature setpoint as the control variable	16
Figure 1.5	Prediction process in black-box models using temperature setpoint as the control variable	16
Figure 1.6	Prediction and actuation process in white-box or grey-box models using energy flow rate as the control variable	18
Figure 1.7	Exponential relation between the number of state variable and number of predefined states (given 10 intervals in each dimension)	27
Figure 1.8	Acceptable temperature band [3]	30
Figure 1.9	Graphic comfort zone method from ASHRAE 55 [4]	31
Figure 1.10	Normalized performance vs. temperature with the maximum performance set to 1. [67]	35
Figure 1.11	Thermal discomfort profiles of six occupants [68]	36
Figure 2.1	The percentage of dissatisfaction over temperature due to cold (left) and hot (right)	42
Figure 2.2	The regressed CDF of the percentage of dissatisfaction over temperature	43
Figure 2.3	The probability distribution of upper and lower bound for individuals	44
Figure 2.4	Overall percentage of dissatisfaction vs. room air temperature	45
Figure 2.5	Percentage of dissatisfaction-Temperature for all zones in 6 scenarios, the reference curve is shown in blue line for comparison.	47
Figure 2.6	Frequency distribution of zonal desired temperature in scenarios	47

Figure 2.7	Frequency distribution of zonal lower temperature bound in scenarios	48
Figure 2.8	Frequency distribution of zonal upper temperature bound in scenarios	48
Figure 2.9	Frequency distribution of zonal temperature bandwidth in scenarios	49
Figure 2.10	Original and fitted productivity curve	53
Figure 2.11	Derived and fitted curves for an example zone	55
Figure 2.12	Fitted productivity curve for all zones in multi-occupant scenarios compared with the reference curve (blue) in Equation 15	56
Figure 2.13	Frequency distributions of specific acceleration of relative productivity loss	56
Figure 2.14	Frequency distributions of temperature with maximum productivity	57
Figure 3.1	Schematic diagram of part of the nodal network	64
Figure 3.2	The connections between nodes in the nodal network	65
Figure 3.3	Temperature, power, and cost in 3 consecutive days	74
Figure 3.4	Daily zonal OB increase in USD	75
Figure 3.5	Building HVAC cost in scenarios with traditional control flexibilities	76
Figure 3.6	Cost-saving percentage at the building level	78
Figure 3.7	Cost-saving percentage of individual zone	79
Figure 3.8	Zonal total OB increase by L&P control	80
Figure 3.9	Cost-saving potentials in the zones of medium and large office buildings	81
Figure 3.10	Zonal total OB loss in zonal desired temperature control	82
Figure 4.1	Construction of the light-weight exterior wall	
Figure 4.2	Construction of the heavy-weight exterior wall with insulation inside	88

Figure 4.3	Construction of the heavy-weight exterior wall with insulation outside	89
Figure 4.4	Seasonal HVAC operation cost of all simulated scenarios	92
Figure 4.5	Seasonal cost-saving percentages of all simulated scenarios	93
Figure 4.6	Scatter plots of weather parameters v.s. the cost-saving percentage in scenarios	97
Figure 4.7	The distributions of the training error of the regression models	100
Figure 4.8	Q-Q plot based on the training dataset of the emulators	101
Figure 5.1	Control workflow of the “all-true” scenario setup	119
Figure 5.2	Control workflow of the “best possible” scenario setup	119
Figure 5.3	Control workflow of the “current reality” scenario setup	120
Figure 5.4	Q-Q plot of the training error of the ANN model	125
Figure 5.5	Q-Q plot of the testing error of the ANN model based on 2017 AMY	126
Figure 5.6	Q-Q plot of the testing error of the ANN model based on 2018 weather station recorded data	126
Figure 5.7	Errors of hourly online weather forecast	128
Figure 5.8	Error distribution of the hourly online weather forecast	128
Figure 5.9	Frequency domain of the error of hourly online weather forecast	128
Figure 5.10	Errors of hourly local weather prediction	130
Figure 5.11	Error distribution of the hourly local weather prediction	131
Figure 5.12	Frequency domain of the error of hourly local weather prediction	131
Figure 5.13	Internal gain profiles of south zone on Monday	133
Figure 5.14	Internal gain profiles of all zones in a week	134
Figure 5.15	Room air temperature and scenario parameter profiles	136
Figure 5.16	Cost-saving percentage under levels of scenario uncertainty	138

Figure 6.1	Temperature profiles based on MPC in levels of scenario uncertainty	142
Figure 6.2	Temperature profiles in AA, LL, and PP scenarios	145
Figure 6.3	Modeling process of the RC model	150
Figure 6.4	Structure of the building level RC model	152
Figure 6.5	Room air temperature profiles of the calibrated RC models	156
Figure 6.6	Error distributions of the calibrated RC models	156
Figure 6.7	Structure of the south zone RC model	157
Figure 6.8	Objective value and optimum in the solution space of each RC model	159
Figure 6.9	Comparison of temperature profiles in different MPC cases	160

SUMMARY

The HVAC system consumes 30-50% of the energy delivered to a building, providing heating and cooling to maintain suitable thermal conditions for occupants. In recent years, advanced control methods, such as model predictive control (MPC), are being studied to lower building energy cost (e.g., by deferring consumption to low rate hours of the day) while still satisfying comfort requirements to an acceptable degree. Two main research gaps are identified from the literature on MPC and human thermal comfort. First, zonal control flexibility employed by MPC in terms of thermal requirements is not well defined. Second, confusion persists about the contribution of MPC vis a vis other energy conservation methods. These two research gaps weaken the acceptance of existing models and thereby frustrate the real-life application of MPC.

The objective of the undertaken research is to analyze the potential, strategy, and implementation of thermal load control with the aim to quantify its ability to minimize the operation cost of HVAC systems. This is achieved in five consecutive steps, 1) understanding zonal control flexibility, 2) evaluating the potential of building thermal load control with zonal control flexibility, 3) analyzing the potential for varying climate zones and construction types, 4) investigating the performance of MPC under scenario uncertainties, and 5) developing a thermal load control strategy that is ready for implementation. In each step, a mathematical formulation of the optimal control problem is formulated and consequently solved by appropriate algorithms. A novel comfort tolerance model for occupant cohorts is developed and implemented as constraints on the

control envelope. The research outcomes expand the understanding of the multiple aspects of building thermal load control.

CHAPTER 1. INTRODUCTION

This chapter provides the background and motivation of this study. A literature review is performed to analyze the existing typical formulations of the topic and identify the gaps in realization, followed by research questions and definitions of scope.

1.1 Background

According to a report from EIA [1], the delivered energy consumed by commercial and residential buildings accounts for 27% of total U.S. delivered energy in 2017 and is expected to grow gradually up to 2050. The increasing demand for building energy use has generated high interest in methods to reduce building energy consumption, such as applying renewable energy sources and regulating energy consumption from non-renewable sources.

Increasing Energy Flexibility of Buildings (EFB) [2] alleviates these challenges by exploiting a flexible response to occurring demands, also known as “demand-response”. From current research and analysis, it is well established that EFB may help avoid excess building energy consumption, increase the stability of energy networks, and enhance the efficiency and cost-effectiveness of energy delivery. Endorsing this trend, IEA-Annex 67 started in 2015 with participants from 16 countries [2].

The building HVAC system consumes 30-50% of delivered energy providing heating and cooling to maintain suitable thermal conditions for occupants. In the domain of thermal energy needs of buildings, there are three main strategies at the demand side, which exploit some form of building energy flexibility, namely 1) overall thermal load reduction, 2) peak

shaving, and 3) load shifting. On the one hand, the method of overall thermal load reduction is usually realized through retrofit that improves static building features, like applying insulation in an exterior wall to reduce heat transfer, adding shading on the façade to reduce solar heat gain, or utilizing energy-efficient lighting to lower internal heat gain. Peak shaving and load shifting rely on the dynamic control of heating and cooling provided by HVAC systems. In this thesis, peak shaving and load shifting are considered as the primary strategies for building thermal load control.

In general, peak shaving is the process of reducing the amount of energy purchased from the utility company during peak demand hours. Peak shaving usually requires the reduction of energy flows for space conditioning, which results in a room temperature offset from the original setpoint. Load shifting essentially moves a certain amount of energy consumption from one period to another. For example, the HVAC system could precool the building in off-peak hours (or when system COP is high) and utilize the building thermal mass to store energy for space cooling in predefined daily "peak hours" (or when system COP is low).

The difference between peak shaving and load shifting is that peak shaving provides less thermal energy for space conditioning and allows the room temperature to go beyond the original setpoint; while load shifting provides more thermal energy and over-conditions the space, which results in temperatures that are lower than the original setpoint. In other words, peak shaving is certain to reduce building thermal load, but load shifting always results in a higher thermal load due to the higher energy losses through the exterior construction. It should be noticed that, even though the thermal load is always higher by applying load shifting, there is still a potential of reducing HVAC energy consumption by

precooling the building when the HVAC system has higher COP than later. The cost saving potentials of these two methods will be examined in Chapter 3. From the perspective of load control to minimize electricity costs, it should be noted that any distinction between the two strategies is purely artificial. In fact, most control strategies that aim to minimize cost will deploy a blend of both where the blend is determined by the relative differences in time of use rates.

Applying either strategy mentioned above will lead to temperature changes in the conditioned space. The resulting temperature deviation from the "ideal" temperatures may impact the thermal comfort of occupants and reduce their productivity. A detailed thermal comfort assessment is elaborated by P.O. Fanger in his book [3]. For a given person at a given activity level, the thermal comfort is met when the skin temperature and sweat secretion are inside narrow limits. Both factors are strongly influenced by the indoor environment. Predicted mean vote (PMV) is commonly used for predicting the thermal comfort level for a large group of people. In ASHRAE standard 55 [4], a comfort zone is defined as "conditions falling within and including PMV levels from -0.5 to +0.5". Based on a study in 2006, the average performance of office occupants is reduced by 10% in both 30^{o}C and 15^{o}C conditions compared with 23^{o}C and 21^{o}C as the baseline [5]; another research indicates a 4% reduction in performance at cooler temperatures and a 6% reduction in warmer conditions [6]. Both studies are endorsed by the World Green Building Council (WGBC), and the results are shown in a report published in 2014 [7]. Although we know that lacking comfort impacts health, productivity, worker retention, and other human factors, it is fair to say that these effects are poorly understood and even harder to quantify, although sparse studies provide indications.

Another complexity is that individual thermal comfort requirements differ. This fact results in different thermal conditioning for each zone that allows user-specified control. This presents another layer of complexity in zones with more than one occupant as the diversity across occupants does not allow an easy determination of optimal conditions. Due to the non-linear relation between temperature change and thermal sensation, the penalty of discomfort and productivity loss, as the temperature deviates from the zonal "optimal" temperature, needs careful attention when applying building thermal load control [8]. For effective zonal temperature control, it is necessary to adapt to the thermal comfort requirements for each zone based on knowledge of the population of occupants.

Model predictive control (MPC) has been suggested by many researchers as an ideal control strategy for finding optimal solutions that balance the thermal comfort requirements and the energy cost [9]. Especially in recent years, due to the advances in computing power and the availability of real-time information in the building automation system, the research efforts on MPC for buildings have increased markedly [10].

Compared with traditional control methods, MPC has the advantage of considering the future system loads and states and utilizing them in the optimization algorithm. The predicted future loads usually include ambient temperature, solar radiation, occupancy profiles, etc. Some inputs, like the occupancy, not only act as thermal loads on the system but also appear in objective functions for optimization through the individual comfort requirements across the occupant pool. A typical workflow of MPC for HVAC system operation is shown in Figure 1.1.

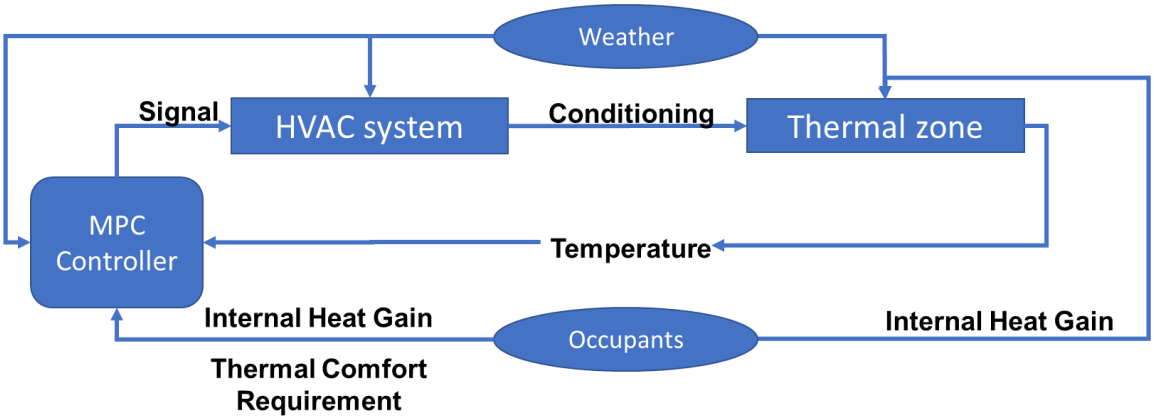

Figure 1.1 A typical workflow of MPC

The MPC paradigm is that an underlying behavioral model informs the control algorithm to reason about the best next control state. The adequate representation of thermal storage property in the model is important as the dynamic storage and release of energy from the building thermal mass primarily enables load shifting and peak shaving. The building thermal mass can be categorized into two types, active and passive. The active thermal mass includes the thermal mass in the HVAC system, such as the thermal storage tank or the fluid in the water loop; the passive thermal mass indicates the thermal capacitance of building envelop, structure, and furniture [11,43]. Most building thermal load control methods discussed in the literature review is mainly about utilizing the latter one, which is elaborated in the next section.

1.2 Literature review

1.2.1 Existing MPC studies for building thermal load control

Several literature reviews on MPC have been done in recent years [19, 44, 45, 48], providing valuable information for succeeding studies. [45] presents a comprehensive review of the control methods for HVAC systems, with an emphasis on the theory and

applications of MPC. The author identifies the factors in the composition of an MPC system and analyzes the reviewed articles from that perspective. In [19], a detailed review of using artificial neural network (ANN) for MPC is presented, followed by a case study on an experimental building. Predictive control strategies for energy storage systems are reviewed in [48]. In this article, the model-free control strategies and MPC are compared, and challenges for MPC in applications are identified. In addition, [44] presents a nearly exhaustive review of building energy models for control and operation. Aside from the detailed review studies, both [9] and [10] give the outlooks on the situations and trends of using MPC for buildings from macro perspectives.

Based on the information provided in the studies above, an in-depth analysis rather than an inclusive review is presented in this section from the following aspects:

1) Usage of the dynamic building model, input, and output
2) Control process and actuation
3) Formulation and algorithms used for the optimization

1.2.1.1 Usage of the dynamic building model, input, and output

In the field of building energy performance simulation, the models can be categorized into three types: white-box, grey-box, and black-box models. This categorization is more or less based on the model's implied translation of physical reality into a mathematical formulation with resulting fidelity. The white-box model uses detailed physics-based equations to model building components and is capable of capturing most of the dynamics of building behavior correctly. Grey-box models are also physics-based models with abstraction in manners by different levels; the simplification of physical description

enables the auto-calibration of this type of model while reducing the level of dynamics. The black-box model is also called statistical model or data-driven model, which bypasses physical-based formulations and only focuses on prediction accuracy. Details of model type and modeling techniques refer to [44]. The applications of these three types of models in MPC are analyzed later in this section.

From the reviewed literature for this study, all three model types are being studied for MPC, in which the white-box model is least used in practice due to the model complexity, but there is no leading trend or model preference that emerges over the 15 years that the reviewed literature covers. The summary of model usage in the literature is as follows:

1) White-box: [11, 12, 14-17, 31, 38]
2) Grey-box: [18, 20, 22, 25-27, 29, 32, 33, 35, 37, 42]
3) Black-box: [13, 16, 19, 21, 23, 24, 28, 30, 34, 36, 39-41]

1) White-box model

White-box modeling commonly relies on commercial building energy simulation tools like EnergyPlus [83] or TRNSYS [84]. In order to reflect dynamic building behaviors, this modeling method requires multiple sources of information, including building geometries, construction, materials, zone functions, detailed HVAC configurations, etc. Some of the information may not be available in applications, which always requires extra effort for model calibration to ensure prediction accuracy [12]. In [17], an MPC optimization environment is established and patented based on EnergyPlus. This method is then applied to a MATLAB-EnergyPlus co-simulation environment to execute real-time

MPC for commercial buildings [15]. The authors, in the latter paper, also point out two challenges of using EnergyPlus as the prediction model, which are the slow simulation speed and the lack of thermal history management [15]. The latter one prevents the prediction model from being initialized at any timestep, which results in the redundancy of repeatedly warming up the model in each iteration of optimization. These disadvantages of EnergyPlus also exist in most other white-box commercial simulation tools.

Thus, due to the high-fidelity of physics-based formulations, the white-box model is commonly used in studies for analyzing the potentials of MPC or for control rule extraction. In [31], the authors examined the saving potential of cooling energy cost by optimizing a time-varying temperature setpoint schedule. A reference EnergyPlus building model is used directly for predicting energy cost and predicted mean vote (PMV). The setpoint scenarios are optimized based on the climate and utility price in three cities separately. In [16], the EnergyPlus model is used in optimizing the control sequences of window operation in a mixed-mode building. On-off control is applied in window operation with a decision interval of 2 hours. The control rule is extracted by using MPC results of binary control sequences to further train a logistic regression model with input variables in 8 categories, including outdoor dry bulb temperature, outdoor dew point temperature, wind speed, wind direction, direct normal solar radiation, core zone temperature, mean temperature of given zones, and states of the window opening. From the author, the logistic regression emulator is able to mimic the decision made by the EnergyPlus optimizer, achieving 70-90% of energy saving, but with a very little computational expense.

The white-box model is only seen as being used practically as a prediction model in [11], which illustrates an MPC scenario for active and passive thermal storage control by

using a TRNSYS building energy model. This scenario is applied in a test facility in real-time, described in [14].

1) Grey-box model

Grey-box models in MPC are mostly in a form analogous to electric resistor-capacitor (RC) networks [45]. Building and room components are simplified as thermal capacitors connected by thermal resistors, which represent the possibly important thermal process. For a given building (zone), there could be different RC network representations of varying complexity, where various components are defined as capacitors. The complexity of the RC network determines its ability to reflect the dynamics of the thermal process. In the RC model development, its composition is predetermined based on the need of the predictor, while the parameters in the RC model are calibrated based on historical data. The RC model indeed blurs a certain amount of dynamics due to its linearity and the simplified models of components. As a trade-off, this modeling method reduces the effort in the model establishment and increases the simulation speed dramatically compared with white-box models.

The model formation of the RC network is flexible in its utilization. In [32], the MPC controller is applied to the heating system of a campus building. In this RC model, a reference room and the water in the heating system are represented by two thermal capacitors. According to the author, this simple RC network is able to capture the dynamics of the heating system, which is a relatively slow-moving process. In [33], an MPC is designed for load shifting of a 5-room test facility with an air-based cooling system, generating the temperature set-points trajectory for on/off controllers. In this study, a five

node RC model is used to reflect the temperature behavior and controller's action in each zone. Compared to the highly abstracted RC model mentioned above, [25] demonstrates a more detailed RC network with explicit components modeled, shown in Figure 1.2. For a single zone, the model contains two capacitors representing zone air and exterior wall, respectively. The two nodes and energy supplies interact through multiple heat transfer processes, including convection, conduction, solar radiation, ventilation, and ground heat transfer. In addition, in [35], the authors model all components, walls and windows, separately formatting a 5-state RC network for a single office room, shown in Figure 1.3. With limited measurements, unscented Kalman filtering (UKF) is exploited to estimate states and parameters simultaneously, outperforming the traditional training method.

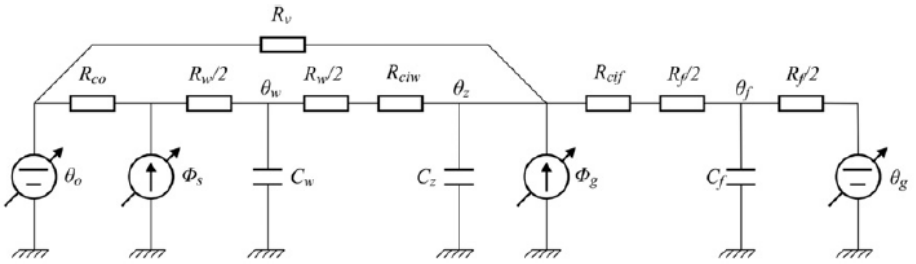

LEGEND

Variables :	**Parameters :**	
Inputs :	***Resistances :***	***Capacities :***
θ_o - outdoor air temperature	R_{co} - outdoor-convection thermal resistance	C_w - equivalent envelope thermal capacity
Φ_s - solar radiation on walls	R_{ciw} - indoor-convection thermal resistance (of the wall)	C_z - equivalent thermal capacity of the zone
Φ_g - direct (internal) gains	R_w - wall conduction resistance	C_f - equivalent floor thermal capacity
θ_g - ground temperature	R_{cif} - indoor-convection thermal resistance (of the floor)	
States :	R_f - floor conduction resistance	
θ_w - wall temperature	R_v - resistance equivalent to ventilation and infiltration	
θ_z - zone temperature		
θ_f - floor temperature		

Figure 1.2 Structure of the RC model proposed in [25]

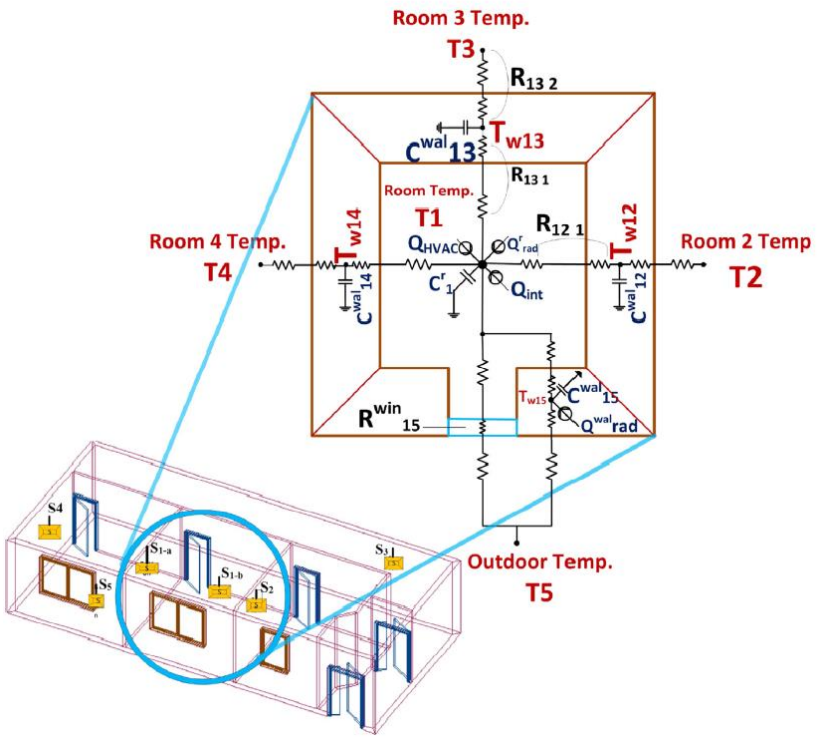

Figure 1.3 Structure of the RC model proposed in [35]

To be noticed, the formulation of the RC model is also influenced by the optimization method. In [18], a single-zone three-node RC model is used for zone temperature prediction, in which the three nodes are representing the zone, the inner layer, and the outer layer of the construction, respectively. The control sequence of the temperature setpoint is optimized by the Markov decision process (MDP), which has a 3-dimensional predefined state space (called "anchor points"). For every time step, the current states of the nodes are matched back to the anchor points to acquire known states to get the optimum action for the present time step. Since MDP selects the action only based on the current states, a multi-state model is required to represent system dynamics, like the three-node RC model in this study. But as the number of states increases, it is necessary to have more and accurate data for calibrating a high-quality model. Furthermore, the inner and outer surface temperatures,

assumed as known states in this study, are not easy to know or measure in real-life applications.

2) Black-box model

Black-box models have multiple formulations fitting linear and nonlinear functions to measured data [45], including the generalized linear model (GLM) [16, 28, 41], state-space model [21, 36], artificial neural network (ANN) [19, 21, 23, 24, 30, 34], transfer function model (TF) [21, 39, 40], process model, auto-regressive exogenous (ARX) [21], and auto-regressive moving average model with exogenous inputs (ARMAX) [13]. Without sticking to the physical law, the black-box model can be explicitly constructed to fit a particular setting, usually showing higher prediction accuracy; on the other hand, it renders black-box models low in extendibility and hard to generalize [21,45]. In addition, since the model parameters are calibrated in building operation conditions during the training period, it may cause large prediction errors when the condition is not within the coverage of training data [44].

As the predictor in MPC, black-box models are usually designed to provide a specific output without calculating the entire system. In other words, there is often only one state variable (or at best a few) in the black-box model; as a result, the system dynamics are captured in the inputs which contain the building and environmental information over several time steps. The literature presents some examples in which black-box models are used for prediction. A 3-layer ANN framework is proposed in [30] for zone air temperature prediction. The categories of the input include zone temperature, outdoor air temperature, neighboring zone temperature, chilled water temperature, etc. Multiple model structures

are tested by varying the input parameter numbers of different historical time steps. From the experiment results in the literature, the ANN model has the highest prediction accuracy when proper variable categories with moderate past time steps are selected in the input. This ANN structure is further improved and applied to a multi-zone MPC study in [23]. Given 10 mins as the timestep length, the model takes 3 timesteps of the historical room air temperature and 2 timesteps of the outdoor air temperature as the input for every prediction. In [28], a multiple linear regression model is proposed for predicting the electricity consumption of the cooling system in a residential building. It uses a backward prediction process similar to the previous example. During the model construction, multiple time steps of room air temperature, setpoint temperature, past energy consumption, the hour of a day, and their second-order coeffects are considered as input variables at the very beginning. After variable selection, 6 variable categories are kept in the linear reduced-order model, which could be effectively used in MPC.

Besides the usage for prediction, black-box models are also designed for decision making directly. As mentioned above, the optimization result based on a white-box model is extracted to train a regression model that is ideal for fast reaction and actuation [16]. Even though this control type is more likely to be categorized, by definition, as a rule-based control rather than an MPC, it has the same functionality as the white-box MPC by taking the same inputs and providing the same outputs (control sequences).

In summary of the model developed in MPC, grey-box and black-box models are generally used for prediction due to their flexible formulation and fast calculation speed; white-box models are more serving as a reference model to evaluate the performance of controllers [45]. The model selection and formulation are highly based on the building

system, control purpose, data availability, and the optimization process. [46] presents a systematic method for model development, in which a two-stage process is suggested for selecting the external disturbances and the system states sequentially. To be noticed, this method is NOT for model selection, but it helps to obtain the ideal formulation of the model after a specific model type is selected.

1.2.1.2 Control process and actuation

MPC configurations can be categorized into hierarchical, cascaded, centralized, decentralized, and distributed structures according to [45]. These categories are not exclusive to each other. For example, MPC controllers could be cascaded with local on/off control to form a decentralized controller for every room [33], or an MPC controller could also collaborate with local rule-based control in a hierarchical structure composing a centralized to distributed control [42].

The control variables in the MPC formulation can be categorized as abstract variables and concrete variables, in which a concrete variable is measurable in HVAC operation while an abstract variable is not. For example, the concrete variables include setpoint temperature, damper position, etc., while the abstract variables include cooling energy flow rate, etc. Notice that abstract and concrete are relative definitions depending on the complexity and process of measurements; a control variable that is abstract in one control system could be concrete in another. The supply air flow rate, as an example, could be used to calculate the cooling energy flow rate, which is a more abstract control variable; or it could be estimated by damper position and(or) supply fan speed, which are more concrete ones.

From the literature review, the commonly used control variables in MPC formulation include zone temperature setpoint [11, 15, 18, 19, 24, 28, 31-34], energy flow rate (some in on/off form) [12, 14, 16, 19, 20, 23, 25, 27, 36, 37], mass flow rate [20, 30], and damper (valve) position [16, 20, 30]. This section discusses the usage and actuation of these control variables.

1) Temperature setpoint

As a control variable, temperature setpoint is usually used directly in white-box models due to its convenience in simulation setups. The HVAC module in white-box models automatically controls the room temperature to the setpoint by adjusting the heating/cooling amount. As mentioned in the previous section, this type of control process is only seen in the analyses of MPC potential due to the limitation of the white-box model in actual implementations. Being ruled by energy balance, three prediction processes need to be known and done in the white-box or grey-box prediction model with temperature setpoint as the control variable, including 1) given temperature setpoint to predict cooling/heating load, 2) given cooling/heating load to predict HVAC energy consumption, and 3) given cooling/heating load to predict room air temperature. The relation is shown in Figure 1.4. These three processes require numerous information in the development of energy balance models and make temperature setpoint hardly being used in real-world applications.

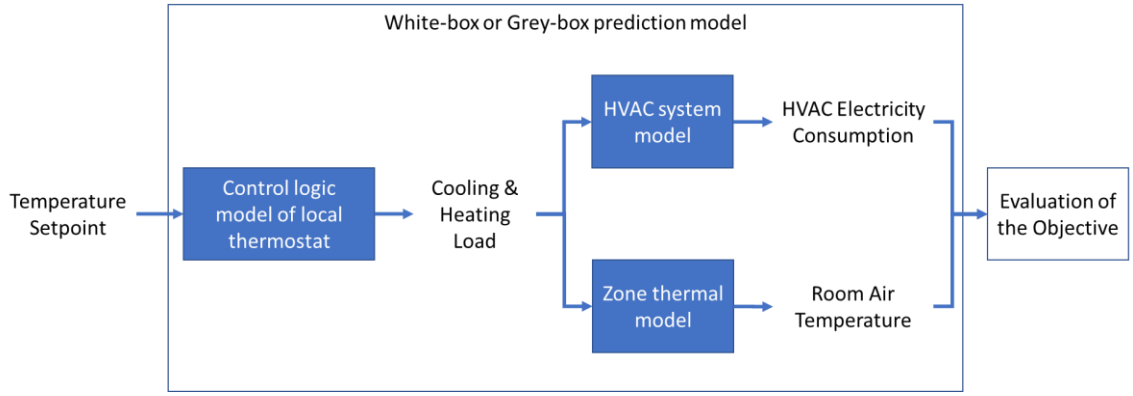

Figure 1.4 Prediction process in white-box or grey-box models using temperature setpoint as the control variable

Temperature setpoint, as a control variable (vector), is also used in black-box model based approaches. The prediction process is shown in Figure 1.5. In [28], a generalized multiple linear regression model (GLM) is developed for HVAC energy consumption prediction, in which the GLM model creates a direct link from room air temperature and temperature setpoint to HVAC energy consumption. In this study, the temperature setpoints are constrained in an acceptable range of thermal comfort, and the room temperature is assumed to be controlled in this range consequently.

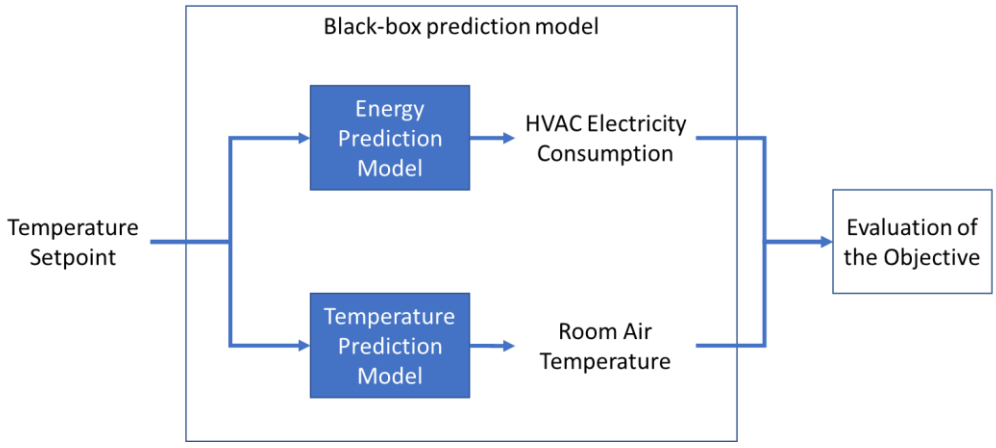

Figure 1.5 Prediction process in black-box models using temperature setpoint as the control variable

The actuation of optimized temperature setpoint generally relies on a "smart thermostat", which interprets the information from higher-level controllers to signals sent to terminal units based on local control logic. At the time of this study, there are several companies that provide products mainly for residential building users [48]. From the advertisements and catalogs of these products, MPC are not seen in existing commercial products.

2) Energy flow rate

The energy flow rate is also widely used as a control variable in MPC regardless of the model type. Since the energy flow is the "link" between the room and the HVAC system, it is automatically a built-in variable in the heat balance of white-box and grey-box models. By using the energy flow rate as the control variable, the computational complexity of the MPC model can be minimized while performing the optimization concisely. However, the energy flow rate is a very abstract variable, which is not only requiring multiple sensors for a reasonable measurement for model development but also relies on predetermined algorithms to translate the optimized value for actuation. Figure 1.6 shows the prediction and actuation process using the energy flow rate as the control variable in white-box or grey-box models.

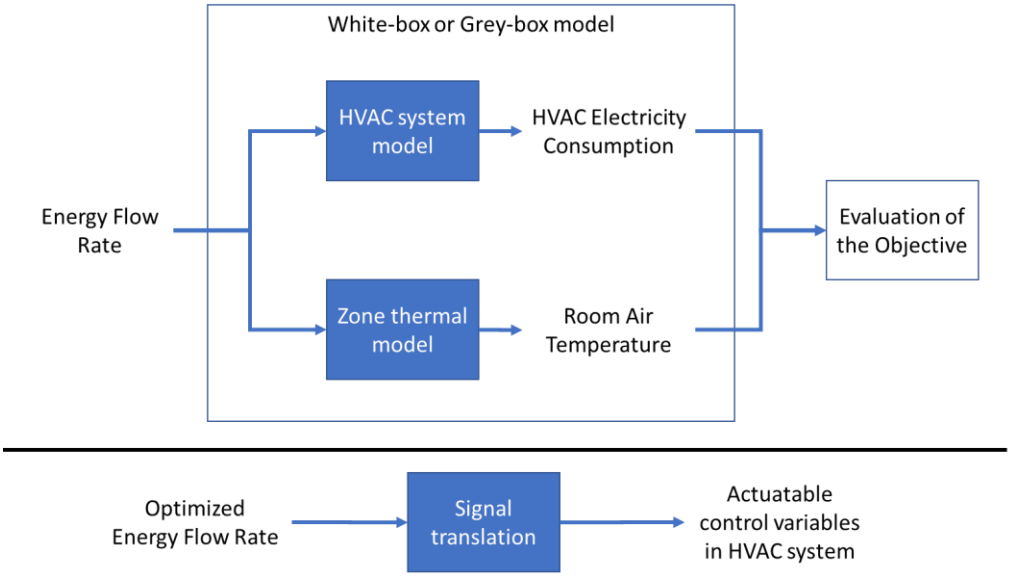

Figure 1.6 Prediction and actuation process in white-box or grey-box models using energy flow rate as the control variable

From the literature review, the predicted energy flow rates are actuated in the discrete form, including on/off control, start-stop time control, and switching operation scenarios. And these MPC decisions are all at the highest level in the control systems. In [27], a framework of a centralized energy management system is proposed for building off-grid operation with PV systems, in which MPC is used for comprehensive decision making. On/off control is applied in HVAC operation, and the control signal for every unit in every step is generated from the central optimizer. In [23], an ANN model is developed to predict the room air temperature in an airport terminal, and the HVAC energy consumption is calculated by a set of empirical equations. In this specific case, the flight departure schedule is also considered in determining the start-stop time. In [14], a white-box MPC model is exploited to optimize the energy flows between chillers and a thermal energy storage (TES) system. After the optimization in every step, a post-processing program is employed to translate the optimal results into the commands of chiller operation modes. Even though

this is an example of utilizing active thermal mass in building load control, it provides crucial information demonstrating the adversity of using energy flow rate as the control variable in MPC.

Some of the studies take concrete variables as the control input, i.e., damper positions or supply fan speed. In model development and optimization, these variables have the same properties of setpoint temperature. But actuating these variables requires the modification of existing local controllers, which dramatically increases the workload and complexity in application.

In summary of the control process and actuation, the questions are always:

1) How are the variables measured?
2) How is the prediction model acquired?
3) How is the optimal control being actuated?

From the limited experience from real building experiments, it is found that two setups of the control process may have good potential for applications, notably 1) black-box model with temperature setpoint as the control variable and 2) energy balance model with energy flow rate as control variable and post-processing.

1.2.1.3 Formulation and algorithms in the optimization

Since the goal of MPC for building thermal load control is essential to find the sweet spot of HVAC operation for balancing energy cost and the thermal comfort requirements, there are thus two “stakeholders” in the optimization. In a building thermal system with numerous states, the control decision made at the current time step will

influence the states and control decisions in the following steps. In most cases, a control sequence optimization is performed recurrently by the MPC optimizer. The two objectives, of lowering the energy cost and satisfying thermal comfort requirements within given limits, can form the optimization as multi-objective optimization or single-objective optimization with constraints, shown in Equation 1-3.

$$\min_{u_i} \sum_{i=1}^{n} (C_{i(u_i)} + \mathrm{P}_{i(u_i)}) \tag{1}$$

$$\min_{u_i} \sum_{i=1}^{n} C_{i(u_i)} \tag{2}$$

$$\text{Subj.to} \qquad T_{lb,i,j} \leq T_{i,j} \leq T_{ub,i,j}\,, \qquad \forall i = 1 \dots n, \forall j = 1 \dots m \tag{3}$$

Where u_i is the control input in every time step i, $C_{i(u_i)}$ is the energy cost, $\mathrm{P}_{i(u_i)}$ is the penalty of the thermal comfort violation, $T_{i,j}$ is the room air temperature for every room j in every step i, $T_{lb,i,j}$ and $T_{ub,i,j}$ are the lower and upper bound of the acceptable temperature range, n represents the prediction horizon, and m represents the total number of simultaneously controlled rooms. The single-objective optimization (Equation 2 and 3) seeks the lowest energy cost over the prediction horizon while taking the thermal comfort requirement as constraints; the multi-objective optimization (Equation 1) seeks the minimum of an overall cost, which is the sum of the scalarized value of both energy cost and the effects of the thermal comfort violation. A standard way to deal with multi-objective optimization is to generate a Pareto front [127], but the resulting front gives theoretical insights but rarely has any relevance for real decision making. It is also good to realize the front represents the same outcome as one finds with an additive weighted approach towards a single objective target by varying the weights over all plausible values.

Thinking this true means that the Pareto front represents the best possible optimization if one has no idea about the weights of the different objectives. Which would cast a shadow on the attempt to optimize in the first place. In general, it is more sensible to put extra emphasis on the determination of relative weights and use the result in a single weighted objective optimization.

In many cases, the role of uncertainties, both in the predicted outcomes as well as in the weights, cannot be ignored. This role leads to a risk-based assessment of the outcomes taking into account that the risk of an unfavorable outcome is weighed against the opportunity of a more favorable one, which calls for the introduction of a utility concept used to express this value over the range of possible outcomes. It is based on an axiomatic theory that assumes the total rationality of the decision-maker. Hazelrigg [128] shows that the concept only holds up in situations where there is a single decision-maker.

In multi-objective optimizations shown in Equation 1, the utility function C_i and P_i are usually acquired from multi-attribute utility analysis [126]. These two utility functions are assumed to be linearly additive. If the multi-attribute utility analysis is performed based on the preferences provided by different stakeholders, an assumption is required, as indicated above, that they are totally rational and able to consistently express the utility toward given outcomes. However, the occupants, the building manager, or the building owner are all stakeholders, and the utility derived from these them will differ significantly. The question of defining the objective functions in the scope of this thesis is extensively discussed in Chapters 2 and 3.

To be noticed, the energy cost function $C_{i(u_i)}$ in Equation 1 and 2 may have different meanings, they share the same representation if and only if the penalty term $P_{i(u_i)}$ is scalarized to a monetary unit. From the reviewed literatures, single-objective optimization is used in [11, 13-15, 18-20, 23, 24, 26, 29, 33, 38, 41], and multi-objective optimization is used in [12, 16, 27, 31, 32, 34-36, 37, 39, 40, 42].

These two optimization formulations are suitable for buildings where the energy cost is charged by the time of use rate (TOU). In reality, buildings may be charged a penalty based on (previous or current) monthly peak demand. This penalty is not covered by either formulation. Theoretically, the optimization for minimizing the energy cost, which contains peak demand terms, requires an extremely long prediction horizon for finding the global optimum. In [103], the minimization of demand charge is addressed by setting a predefined constraint on the peak demand, where the constraint is defined by the peak demand in the reference scenario. As an alternative, [69] analyzes the potential of static building control strategies in realizing demand reduction. This question will not be discussed in this study.

In the formulations, the cost term (C_i) has a tangible representation in general, while the constraint terms (P_i, or T_{lb} and T_{ub}) are highly specific and case dependent throughout the reviewed literature. Any assumed constraint is acceptable in the type of study for model development, but the constraint should be prudentially considered in analyzing potential and application-oriented studies.

Some examples are showing the constraints used for single-objective optimization. In [11], a temperature band of 22 to 24 ^{o}C is assumed based on the free-floating interval

between the original cooling and heating setpoint. In [18], a much wider temperature band of 20 to 26 ^{o}C is assumed, being around the reference setpoint of 24 ^{o}C. Both examples above are for office buildings. Examples for residential buildings are found in [28], where the room temperature constraint is set at 20 to 27.8 ^{o}C for non-occupied hours and at 21.5 to 25.5 for occupied hours. In [19] and [33], a constant temperature band of 22 to 25 is assumed throughout the cooling season.

In [31], a multi-objective optimization is used for minimizing HVAC energy cost and PMV simultaneously by using a set of weighting factors to relatively rank the two objectives. The value of the weighting factors is examined, and Pareto curves, showing relations between HVAC cost and PMV, are concluded to provide guidelines for building operators. In reality, the effects of the weighting factor highly depend on the building type, zone function, TOU pricing, and operator and occupant preferences. An improperly defined weighting factor may result in an overall room temperature offset or no cost saving at all. In other words, determining a weighting factor for building operators is the same as asking the question, "how much money do you want for trading off a certain amount of thermal comfort?", which is very hard to answer without proper training. Some previous work in expert judgment studies [126, 129] uses the type of training that is suitable for this purpose.

To solve the optimizations, various types of techniques are seen practiced in the reviewed literature, including rule-based method [23], linear programming [20, 25, 26, 28], quadratic programming [32], mixed-integer linear programming [27, 41], quasi-newton methods [11, 14], particle swarm optimization [15, 16, 31], genetic algorithm [34], branch and bound algorithm [24], and dynamic programming [11, 14, 18, 38], etc. Besides the

dedicated methods described in the literature, commercial optimization packages are also widely used, like Gurobi [27, 41], YALMIT [35], etc. The usage of the optimization methods is determined by the prediction model and the objective function. The feasibility of optimization methods is discussed as follows.

Linear programming (LP) is an efficient method for solving control sequence optimization, and it requires both the prediction model and the objective function in linear form. This method is usually seen in the form of single-objective optimization. In [25 26], the author details the steps of utilizing LP in RC-MPC, including building thermal modeling, linear transformation, constraint setup, etc. In [28], LP is used for setpoint temperature optimization based on a linearized black-box prediction model. If the control inputs are designated in a binary form like on/off control, mixed-integer (pure-integer) linear programming (MILP / PILP) method could be used; such example is found in [27, 41].

Quadratic programming (QP) is usually encountered for solving multi-objective optimization, in which the prediction model is linear and the penalty of the thermal comfort violation is in a quadratic form. In [32], the penalty term is captured by the squared error of the MPC controlled temperature and reference temperature (original setpoint). With the room temperature and the energy consumption predicted by a linear model, the optimization can be readily solved by a QP solver.

Either LP or QP requires a particular form of the prediction model and the objective function, where the global optimum is ensured by computing the Jacobian or Hessian for the analytical solution. But in some studies, the prediction model and the objective function

is hard to be mathematically evaluated. For example, 1) the prediction model is not accessible (i.e., when using commercial white-box simulation tool as the prediction model), 2) the objective function is complicated and not convex due to its formulation (i.e., when using ANN as the prediction model), or 3) the control input is discrete (i.e., when using "operation mode" as the control variable). In these situations, the analytical solution is not applicable, and general optimization methods have to be used, like quasi-newton methods, particle swarm optimization (PSO), and genetic algorithm (GA).

As described in the previous section, the white-box commercial tools do not explicitly provide the governing equation for building simulations, resulting in an "invisible" formulation of the prediction model. Even though some optimization environment has been proposed specifically for tools like EnergyPlus, the optimization is still limited to running in general optimization methods. An example is shown in [31], a setpoint temperature schedule optimization runs in GenOpt using PSO, with a stated run-time for a one-day optimization of around 80 hours originally. Even after simplification (dimension reduction), the run-time is still around 3 hours. In the cases that ANN is used as the prediction model, the objective function is nested by multiple activation functions, like sigmoid functions. As a result, the objective function is usually non-convex for analytical solutions. As shown in [34], GA can be used to solve an ANN-based objective function for finding the optimized temperature setpoint schedules over the prediction horizon of 24 hours.

In [49], the optimization time costs of different solution methods are compared by running the same optimization problem for an increasing number of decision variables.

According to the results, the computational effort of using general optimization methods may be way many times that of the analytical methods.

The main idea of dynamic programming (DP) is to solve a complicated problem in a recursive manner. It usually requires the knowledge of the full states in the controlled system. This method is widely used for finding the optimal control strategies for active thermal mass and PV with batteries [11, 14, 38], since both the thermal storage tank and the battery can be regarded as a single-state-variable system, in which the states can be explicitly expressed. [18] demonstrates an optimization structure using MDP for optimum room setpoint temperature control, which was explained in the previous section. Figure 1.7 shows the exponential relation between the number of state variables and the number of predefined states in MDP. From the optimization point of view, this method may not be feasible for multizone models when the number of state variable increases, e.g. 2 rooms with 3 walls will require at least 8 state variables (one state variable for each room, and two for each wall). 10 predefined intervals in each dimension will compose 10^8 anchor points in full combination, and the transactions between two predefined states, $T(s, a, s')$, will have 10^{16} possibilities. Thus, for a two-zone centralized control model, the computation has become too expensive in predefining the states and transactions.

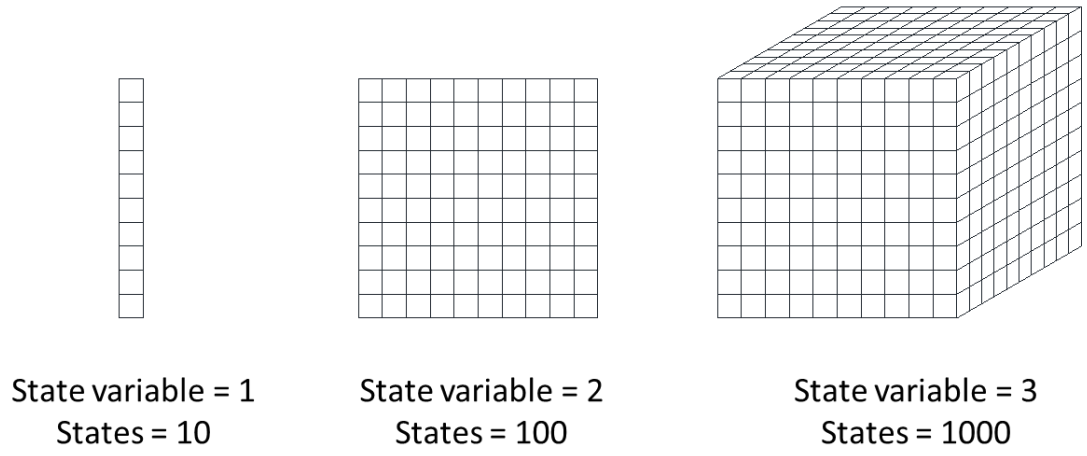

Figure 1.7 Exponential relation between the number of state variable and number of predefined states (given 10 intervals in each dimension)

To summarize the above reflections on optimization formulation and algorithm, the following observations are relevant. Firstly, both single-objective and multi-objective optimizations are widely used in current studies. These two formulations address the constraint term based on different understandings of the thermal comfort requirement. The key question is whether thermal comfort is treated as an acceptability test or a penalty function. There may not be a single correct answer. Either formulation could be correct if the "band" or "function" can be reasonably defined. Secondly, the run-time of optimization is a main concern in MPC development. The analytical solution, like LP and QP, outperforms the general optimization methods in terms of the run speed and the capability in finding the global optimum, but a convex form of the objective function is a prerequisite. Last but not least, the building thermal load control by using passive thermal mass can only be translated into a Markov decision process in very special cases, and dynamic programming is not feasible to this control problem in general.

Throughout the literature review about MPC in building thermal load control, several research questions emerge:

1) How much is the flexibility in controlling room air temperatures to effectively reduce building thermal loads within the constraints of occupant acceptability?
2) How much is the seasonal saving potentials given a certain level of flexibility?
3) How long should the prediction horizon be? And for how long is a prediction valid before it has to be readjusted?
4) What type of model is most suitable for prediction and control decisions?

These research questions have not been comprehensively answered in the literature. The remaining gaps weaken the validity of the existing MPC approaches and diminish the uptake of MPC in industry.

1.2.2 Thermal comfort requirement and productivity loss

Regarding the four questions raised in the previous section, the answer to the first one appears to be the prerequisite for answering the rest. Thermal comfort has been well studied for decades. Some detailed criteria and calculation methods have been established, with multi-variables considered, for thermal comfort evaluations like in ASHRAE 55 [4] and ISO 7730 [50]. In reality, the building HVAC systems, only measuring the temperature in the control feedback loop, usually do not have the full-controllability of all thermal comfort related parameters, i.e., relative humidity and local air velocity, and the thermal comfort is only implicitly realized by controlling a single variable, in most case, the room air temperature. Likewise, in this study, only the room air temperature is considered as the criterion which represents the thermal comfort requirements in MPC. Other indoor

environmental variables are typically maintained within narrow bands, like RH around 50% and average air velocity around 1 m/s. These values will therefore be used in all comfort assessments.

For office buildings, the productivity loss of office work is identified as an effect of the thermal environment on the occupants [5, 6]. The productivity loss function is needed to compare thermal comfort and HVAC operation cost, by scalarization, in a specific form of organizational benefit (OB), which includes two components: the HVAC operation cost and the revenue created by the employees. The mathematical formulation is shown in Equation 4.

$$N_i = -C_i + \nu r_i\left(1 - p_{i(T_i)}\right) \tag{4}$$

Where N_i is the organizational benefit at a certain time interval, C_i is the energy cost for building operation, ν is the number of occupants, r_i is the revenue per employee at time i [53], and $p_{i(T_i)}$ is the productivity loss function. Then the objective function in MPC is to maximize the OB for each zone or, in other words, to minimize the OB loss. Then, Equation 1 can be rewritten as Equation 5.

$$\min_{u_i} \sum_{i=1}^{n} (C_{i(u_i)} + \nu r_i p_{i(T_i)}) \tag{5}$$

Thus, depending on the objective defined in Equation 2 or 5, the flexibility of room air temperature for building thermal load control is defined as the allowable fluctuation of room air temperature under the thermal comfort requirement of occupants, or a cost

function that minimizes the sum of operation cost and productivity loss. Therefore, this definition leads to two specific questions: 1) is there a temperature band that can be objectively defined as the acceptability band, and 2) what is the productivity loss function.

Mathematically, the acceptable temperature band includes three values, which are the desired temperature, upper bound, and lower bound. The early studies on this topic are seen in the 3rd chapter of P.O. Fanger's book [3], and the table of the results is shown in Figure 1.8. From the results, the desired temperature for both males and females of all ages is around 21 ^{o}C, and the mean value of the difference between the upper and lower bound is 3.4 ^{o}C.

Table 8. *Values on the Temperature Scale Estimated as Optimal by the Subjects*

Group	Sex	Estimated Optimal Temperature °C	Estimated Comfort Range °C
College-age	Females + Males.....	20.8 ± 2.0[1]	3.8 ± 1.7
	Females.....	20.6 ± 1.9	3.9 ± 1.8
	Males.....	20.9 ± 2.1	3.6 ± 1.7
Elderly	Females + Males.....	21.2 ± 1.8	3.0 ± 1.9
	Females.....	21.1 ± 1.7	2.8 ± 1.7
	Males.....	21.2 ± 1.8	3.4 ± 2.1

[1] Standard deviation.

Figure 1.8 Acceptable temperature band [3]

P.O. Fanger developed the PMV measure, based on the energy balance of the human body, as an index for assessing thermal environments. The standard ASHRAE 55 [4] highly depends on this index and defines the thermal comfort zone as -0.5<PMV<0.5. A graphic comfort zone method is provided in the standard for thermal comfort evaluation, shown in Figure 1.9. In the situation of the office environment, dress code, and working condition, the comfort range in terms of operative temperature can vary from 21^{o}C to 27^{o}C.

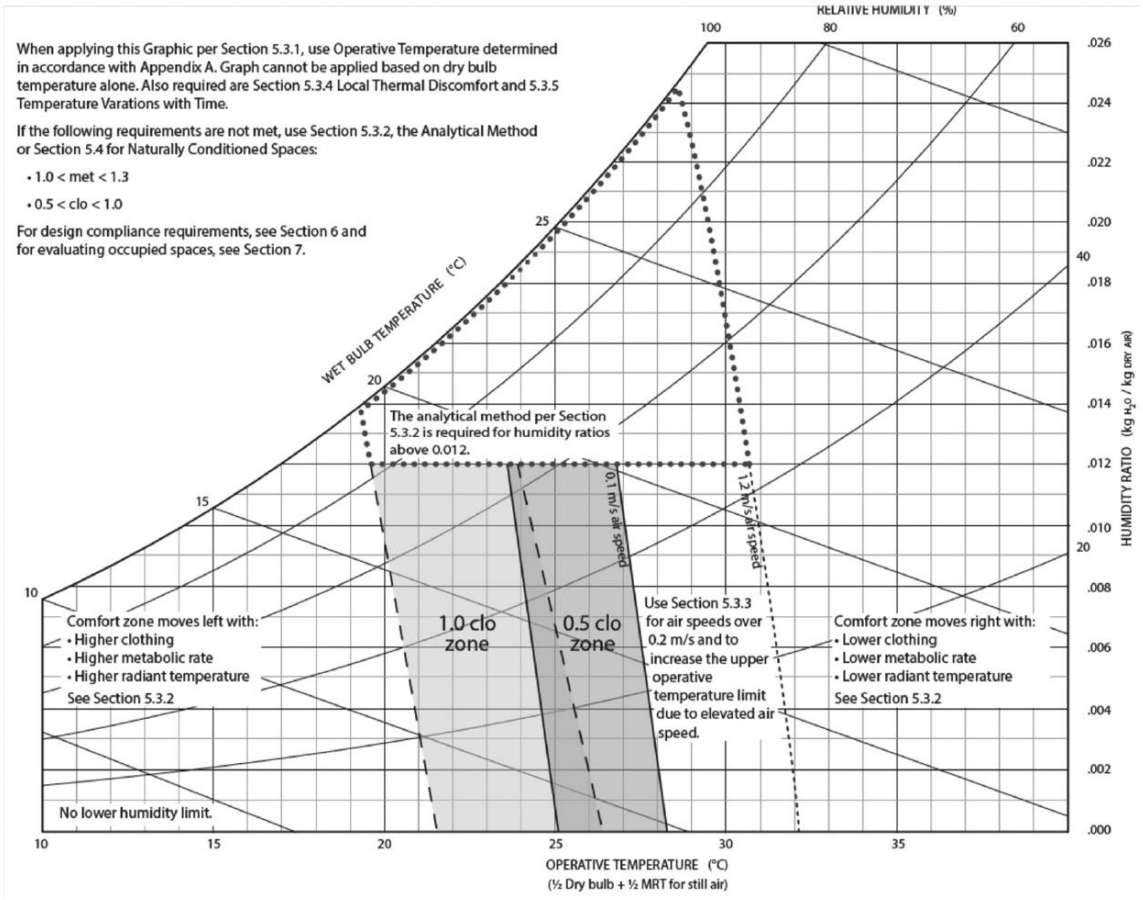

Figure 1.9 Graphic comfort zone method from ASHRAE 55 [4]

Based on the relationship between PMV and PPD, ISO 7730 [50] explicitly shows the example design criteria for spaces in various types of buildings. (Table 1.1) The categories A, B, and C are based on the PPD levels of <6%, <10%, and <15%, respectively, and the clothing-factors are assumed as 0.5 and 1.0 during summer and winter.

Table 1.1 Example design criteria for spaces in various types of buildings [50]

Type of building/space	Activity W/m^2	Category	Operative temperature °C		Maximum mean air velocity [a] m/s	
			Summer (cooling season)	Winter (heating season)	Summer (cooling season)	Winter (heating season)
Single office Landscape office Conference room Auditorium Cafeteria/restaurant Classroom	70	A	24,5 ± 1,0	22,0 ± 1,0	0,12	0,10
		B	24,5 ± 1,5	22,0 ± 2,0	0,19	0,16
		C	24,5 ± 2,5	22,0 ± 3,0	0,24	0,21 [b]
Kindergarten	81	A	23,5 ± 1,0	20,0 ± 1,0	0,11	0,10 [b]
		B	23,5 ± 2,0	22,0 ± 2,5	0,18	0,15 [b]
		C	23,5 ± 2,5	22,0 ± 3,5	0,23	0,19 [b]
Department store	93	A	23,0 ± 1,0	19,0 ± 1,5	0,16	0,13 [b]
		B	23,0 ± 2,0	19,0 ± 3,0	0,20	0,15 [b]
		C	23,0 ± 3,0	19,0 ± 4,0	0,23	0,18 [b]

[a] The maximum mean air velocity is based on a turbulence intensity of 40 % and air temperature equal to the operative temperature according to 6.2 and Figure A.2. A relative humidity of 60 % and 40 % is used for summer and winter, respectively. For both summer and winter a lower temperature in the range is used to determine the maximum mean air velocity.

[b] Below 20 °C limit (see Figure A.2).

During the almost 50 years since the publication of Fanger's book, some researchers have challenged the PMV theory, especially its applicability to daily life. In a study done in 1993 [52], the authors compared the methods for assessing thermal sensation and acceptability in the field studies. Several thermal comfort related questions are asked in the survey, including a seven scale thermal sensation (-3 to 3), six scale comfort level (very uncomfortable to very comfortable), and temperature preference (warmer, no change, and cooler), and the authors seek to equate these indexes with thermal acceptability and to equate the optimum temperature with a neutral thermal sensation. However, the result suggests the opposite: 1) the indirect measures of the acceptability derived from the three indexes deviate from each other by a significant amount, 2) People's preferences for thermal non-neutrality are common, and 3) thermal sensation does not necessarily reflect

thermal satisfaction. At the end of this article, the authors raise the question “what is an acceptable building thermal environment?”, and suggest adding a direct measure/question in surveys for thermal acceptance. A later paper [54] published in 1996 by the same authors state that “Comfort is not a physiological condition but a state of mind”, which fundamentally challenges the PMV theory. Based on the same perspective, [55] draws a critical view of the traditional ‘total indoor environmental control’ method from environmental and human knowledge concerns. This paper potentially leads out the studies on adaptive thermal comfort [81,82]. Practically, [56] criticizes the method for PMV calculation used in ISO 7730 and ASHRAE 55, with the discussion of possible origins of the biases between the PMV and actual mean vote. A statistical model is proposed to improve the PMV calculation based on the data gathered from the ASHRAE thermal comfort database. Unfortunately, the proposed calculation method is not seen in later ISO or ASHRAE standards. More information on research perspectives, models, algorithms, and practices about thermal comfort can be found in [57] and Chapter 5 in [58].

As for the temperature-effected productivity loss, the early study on this topic dates back to 1968 [60], in which 72 students are examined for the speed and accuracy to complete an assignment with various temperatures [61]. In the following years, many studies have addressed this problem from different perspectives. A few comparative examples are shown in follows, and the detailed research approach and outcomes are extensively included in [62] and will not be repeated here.

In [63], the effects of reduced summer indoor temperature, through the renovation of an HVAC system in an office building, are investigated. The self-estimated work efficiency of employees is compared before and after the renovation, and a 4.4%

improvement in the objective productivity is concluded from the result. Controversially, [64] presents a chamber experiment where 26 office workers were asked to do the Cambridge Brain Sciences test in normal and increased-temperature conditions sequentially. The result shows that CBS test scores are not significantly affected by the temperature increase. [65] investigates the effect of air temperature on the labors' productivity in a call center via both controlled and uncontrolled experiments over four months. The result shows a 7% productivity increase when the room air temperature is reduced from 25°C to 23°C. Coincidentally, the research in [66], published in the same year as [65], investigates the influential factors on workers' productivity in call-center as well. Given the productivity benchmark for each individual as the wrap-up time performed at 23 °C, 15%-20% productivity decrease is observed only at temperature higher than 25°C, and the productivity of individuals deviates from each other when the temperature is below 22 °C.

Based on the reviews of 24 studies on this topic, [67] concludes a normalized temperature-productivity curve, shown in Figure 1.10 and Equation 6. This curve summarizes the discrete results from multiple studies and enables the continuous evaluation of the productivity over temperature. Thus, it can be regarded as a general representation of the working performance in office buildings.

$$P = 0.1647524T - 0.0058274T^2 + 0.0000623T^3 - 0.4685328 \qquad (6)$$

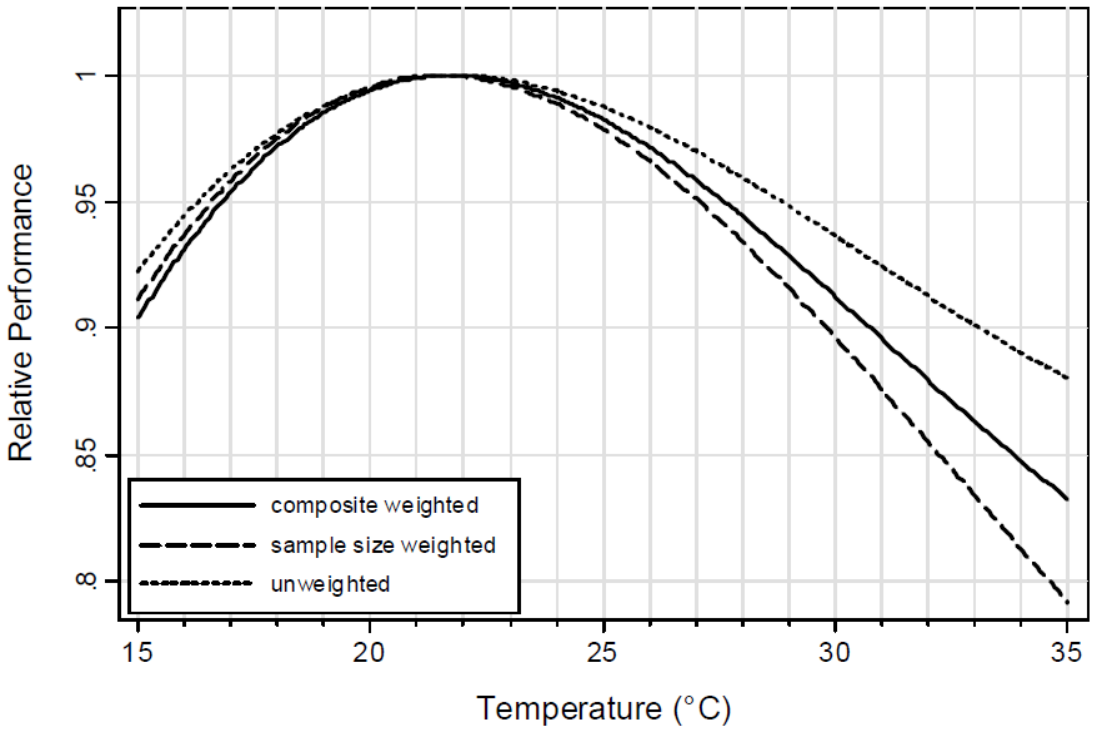

Figure 1.10 Normalized performance vs. temperature with the maximum performance set to 1. [67]

To be noticed, the initial purpose of the standards and some studies cited above, for both acceptable temperature band and productivity loss, is to describe or evaluate the thermal comfort properties for "a large group" of people. The research outcomes with this purpose may not be applicable to every thermal zone with a few occasional occupants. In other words, the criteria of thermal comfort for individual zones may deviate from the general requirement. An example is shown in [68], in which a data-driven approach is proposed for selecting the optimized setpoint for the target zones. The comfort temperature ranges for six occupants are examined, showing a variation from 21.8^{o}C to 25.4^{o}C. Based on the derived thermal discomfort profiles of the occupants (Figure 1.11), the zone temperature setpoint is selected to minimize energy consumption while maintaining the comfort level. The same proof is also found when comparing the conclusions from [65]

and [66], as the productivity loss caused by temperature changes may differ even in highly comparable building functions and work types. Besides, the author in [69] reviews 14 studies and points out the discrepancies in the productivity loss by linearizing the individual results. A detailed review of the individual difference in thermal comfort can be found in [70], which also demonstrates the necessity and possible methods to detect and satisfy the individual difference in thermal comfort.

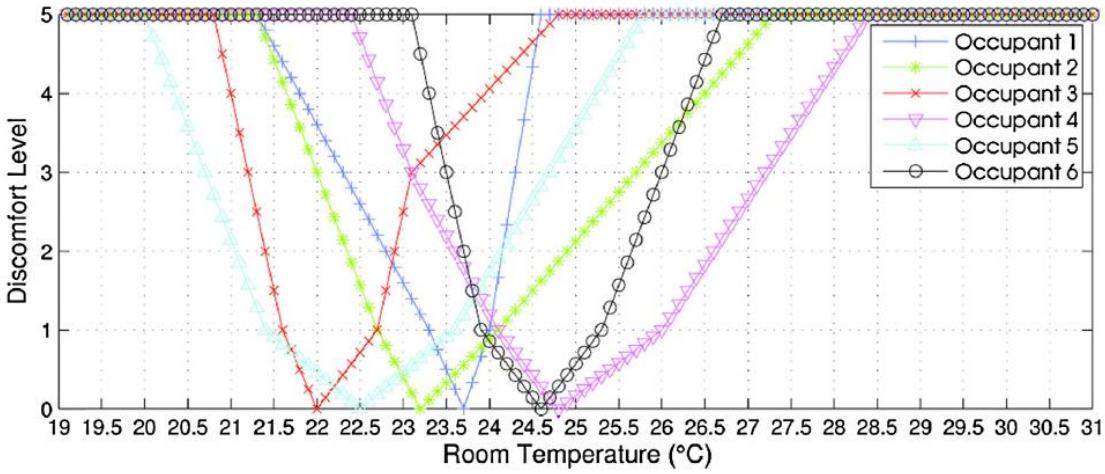

Figure 1.11 Thermal discomfort profiles of six occupants [68]

Summarizing the literature on thermal comfort requirements and productivity loss, it is crucial to understand how to quantify the flexibility that can be exploited by MPC before attempting to quantify the control potentials. From the reviewed literature, the temperature band and productivity loss function are acquirable for a large group of people. However, the diversity across individuals and hence the zonal thermal requirements show the incontrovertible need for adaptive and zonal HVAC control, in which the flexibility for MPC should be defined for each zone separately. An added complexity needs to be confronted in multi-occupancy zones. For a randomly selected set of individuals that

occupy a zone, the “joint” flexibility has to be determined for that ensemble of occupants before a control can be effectively implemented.

1.3 Research goals

Targeting the objective to exploit the energy flexibility of buildings, challenges are identified as the design and implementation issues of MPC and the demands to characterize human needs with regard to a dynamic thermal environment. Given these challenges, it is imperative to apply MPC that is adaptive to the thermal requirements of the occupants in individual zones. Theoretically, this control method addresses the environmental and human knowledge concerns about building thermal environment conditioning raised in [55], by utilizing dynamically and adaptively applied control algorithms. Practically, this control method provides a well-rounded demand response strategy in building operations with the consideration of the organizational benefit and the differentiated thermal requirements of occupants.

Thus, this dissertation aims to analyze the potential, strategy, and implementation of the building thermal load control. In order to perform a comprehensive analysis, this dissertation is proposed to address the following five parts sequentially.

Part 1 takes a fresh look at the role of occupant thermal comfort and investigates the variation of the zonal control flexibility to manage the thermal load. In this step, a cohort of occupants is established first according to a profile of the tenant organization, and occupants of each zone are randomly sampled from this cohort. The zonal control flexibility, including acceptable temperature ranges and productivity (loss) curve, is

derived from the percentage of dissatisfaction curve of the randomly drawn populations in each zone. This knowledge serves as the foundation for the following steps.

Part 2 evaluates the saving potential of building thermal load control using passive building thermal mass in both cost-saving and maximizing organizational benefits. In this step, an abstract HVAC system is assumed with the energy flow rate as the control variable; a high fidelity building thermal model is established to capture the building dynamics; analytical solution methods are employed in optimization to ensure the global optima; and the benefit of implementing MPC is isolated by the case specification. Full-knowledge of inputs (external loads and environmental conditions) is assumed in this part of the study.

Part 3 expands the evaluation method developed in Part 2 on a broader scale, in which cost-saving potentials of building thermal load control are investigated for varying climate zones and construction types. An in-depth analysis is then performed based on the simulation result to identify the influential factors among the varying circumstances. A regression model is established accordingly for the quick evaluation of seasonal cost-saving potentials.

Part 4 addresses the influence of scenario uncertainty on the performance of MPC. In this study, the "influence" is strictly defined in the first place in serving as a research envelope. Different levels of scenario uncertainty are characterized based on the sources and the knowledge of the building's operation conditions. The influence is evaluated based on the simulation results.

Part 5 transforms the research outcomes in the first 4 parts to the application. In which a simple but effective MPC structure is derived dedicated to realizing building

thermal load control. The significance of this MPC structure is illustrated by comparing it with existing MPC methods. A hypothetical case study is performed at the end to further demonstrate its effectiveness.

In the following chapters of this dissertation, the detailed methodology, approach, and results of the aforementioned five studies are elaborated in Chapter 2-6. The overall conclusions of this dissertation are drawn in Chapter 7.

CHAPTER 2. ZONAL CONTROL FLEXIBILITY TO MANAGE BUILDING THERMAL LOADS

As discussed in Chapter 1, the flexibility of room air temperature for building thermal load control is defined as the allowable fluctuation of room air temperature under the thermal comfort requirement of occupants, or a cost function that minimizes the sum of operation cost and productivity loss. The scope of the study performed in this chapter is to provide an elementary understanding of the discrepancies of temperature requirements between zones and to provide the formulations for zonal control flexibility of general offices. The outcomes from this chapter will serve as the assumption for the evaluation of MPC potential. For convenience, "control flexibility" is used to represent the flexibility of room air temperature for building thermal load control, and an "acceptable temperature band" is used to represent the allowable fluctuation of room air temperature under the thermal comfort requirement of occupants. Depending on the objectives, the two forms of control flexibility will be discussed separately in the following sections.

2.1 Zonal acceptable temperature band

The room air temperature is the only parameter controlled in most of the HVAC systems in office buildings. However, the study which connects individual thermal comfort directly and solely to temperature is rare. This fact forces the derivation of zonal acceptable temperature band from existing field survey data directly.

ASHRAE Global Thermal Comfort Database (database) originated from a data collection and assimilation process in an ASHRAE project on adaptive thermal comfort.

The first version of this database is established in 1998 [71] and revised since 2014. The second version is published online in 2018 [72]. 52 field studies with 81,846 sets of objective indoor climatic observations are included in the current version of the database. The online interface of this database provides a convenient filtering system for users to select relevant studies and data. The database can be accessed through the link in [73].

2.1.1 Methodology and approach

Since the zonal acceptable temperature band is determined by the acceptable band of each occupant, it is necessary to extract the distribution of the upper and lower temperature limits for individuals in the first place. Then the zonal band could be acquired by sampling the occupants inside the distribution. In order to collect the data relevant to this study, several keywords are applied in the filter, including building type – Office, Season – Summer, and Cooling strategy – Air conditioned. With all other categories included, the collected data is not limited in age, sex, clothing factor, and culture. By doing so, an assumption is naturally made that the derived zonal temperature band is based on the universal profile of office buildings. Three data categories are used for extracting the distributions of the lower and upper temperature limits, namely Thermal sensation (-3 to 3), Thermal acceptability (0, 1), and Air temperature. The detailed approach is shown as follows.

1) The temperature scale from 16 to 32 ^{o}C is divided into 32 bins with 0.5^{o}C interval. Three 1-by-32 vectors are used to count the number of instances in each temperature interval, representing the total number of people (C_{tot}), people dissatisfied due to cold (C_{cold}) (thermal sensation < 0 and thermal acceptability

= 0) , and people dissatisfied due to hot (C_{hot}) (thermal sensation > 0 and thermal acceptability = 0).

2) The percentage of dissatisfaction due to cold or hot (PD_{cold} or PD_{hot}) is calculated from Equation 7 and 8, and the raw results are shown in Figure 2.1. The temperature intervals with no data collected are left as 0. Just as an observation from the histograms, it shows that office workers are much less dissatisfied by the relatively lower temperatures in the cooling condition.

$$PD_{cold} = \frac{C_{cold}}{C_{tot}} \tag{7}$$

$$PD_{hot} = \frac{C_{hot}}{C_{tot}} \tag{8}$$

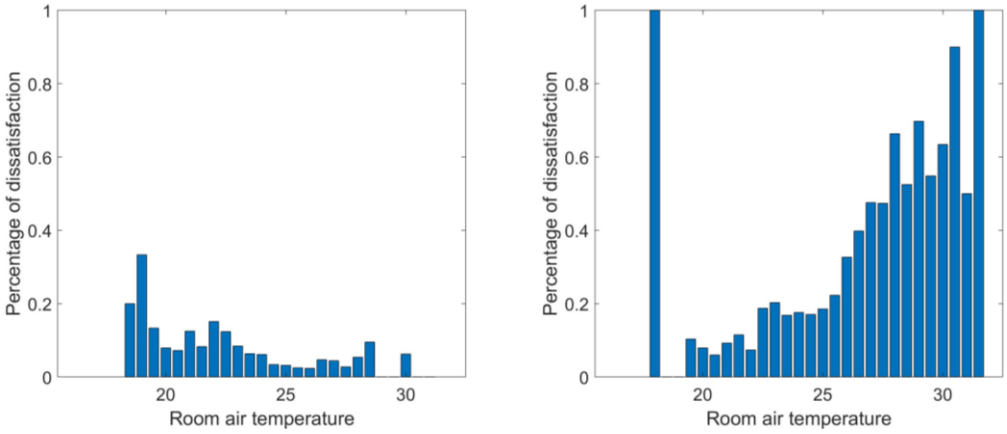

Figure 2.1 The percentage of dissatisfaction over temperature due to cold (left) and hot (right)

3) Given that the samples collected are independent and identically distributed (i.i.d.) across the temperature domain, the histograms of PD_{cold} and PD_{hot} can be statistically regarded as cumulative frequency distributions (CFD). Theoretically, the PD_{cold} approaches 1 in low temperature and approaches 0 when the

temperature is high, vise versa for PD_{hot}. Thus, it is possible to capture the CFDs by cumulative distribution functions (CDF) in the sigmoid form.

4) The erf function is used for quantifying CDFs of PD_{cold} and PD_{hot}, and the percentage of dissatisfaction in each temperature interval is weighted by the sample numbers. The formulation of the regressed CDFs are shown in Equation 9 and 10, and the CDF curves are plotted in Figure 2.2.

$$\widehat{PD}_{cold} = \frac{1}{2}\left[1 - erf\left(\frac{T_i - \mu_c}{\sigma_c\sqrt{2}}\right)\right] \tag{9}$$

$$\widehat{PD}_{hot} = \frac{1}{2}\left[1 + erf\left(\frac{T_i - \mu_h}{\sigma_h\sqrt{2}}\right)\right] \tag{10}$$

Where $\mu_c = 18.58,$ $\sigma_c = 3.05,$ $\mu_h = 26.70,$ $\sigma_h = 2.69$

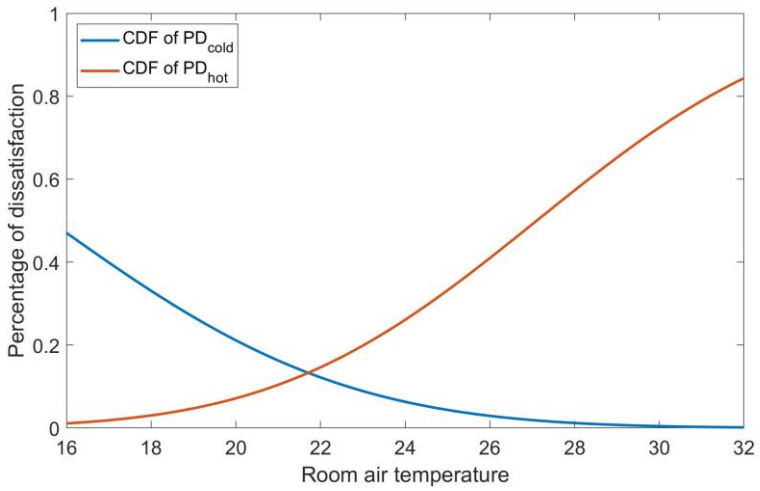

Figure 2.2 The regressed CDF of the percentage of dissatisfaction over temperature

5) By definition, the first-order derivative of the CDF function, in this case, represents the incremental percentage of dissatisfaction (PD) along with temperature increase. The absolute value of the derivatives are the probability density functions (PDF), which describe the "change of PD" that happens at a

specific temperature interval. This “change of PD” could also be used to determine the temperature that exceeds the acceptable range of a certain percentage of people. Thus, the probability distributions of the lower and upper limits for individuals are defined in the PDFs in Equation 11 and 12. As plotted in Figure 2.3, the highest probability (13%/K) of the lowest acceptable temperature for individuals occurs at 18.5 °C, and the highest probability (15%/K) of the highest acceptable temperature is observed at 26.5 °C

$$\Pr_{lb}(T_i) = \frac{1}{\sqrt{2\pi{\sigma_c}^2}} e^{-\frac{(T_i-\mu_c)^2}{2{\sigma_c}^2}} \tag{11}$$

$$\Pr_{ub}(T_i) = \frac{1}{\sqrt{2\pi{\sigma_h}^2}} e^{-\frac{(T_i-\mu_h)^2}{2{\sigma_h}^2}} \tag{12}$$

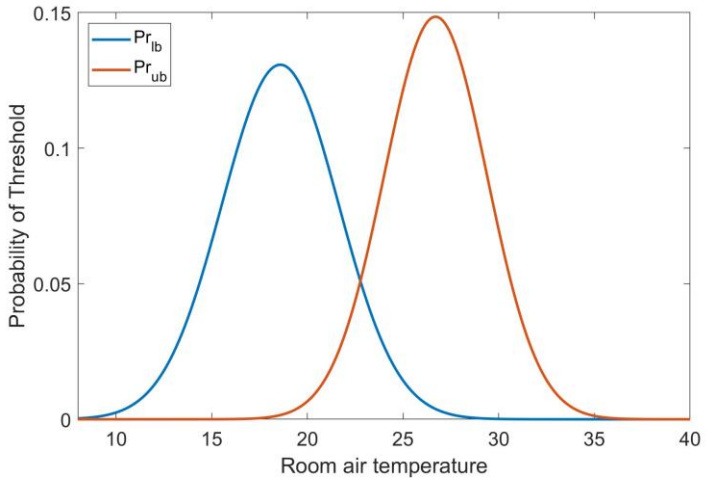

Figure 2.3 The probability distribution of upper and lower bound for individuals

6) Adding up the CDFs of $\widehat{PD}_{cold}$ and $\widehat{PD}_{hot}$ provides the function to describe the overall percentage of dissatisfaction, shown in Equation 13 and plotted in Figure 2.4. From the curve, the minimum of PD occurs at T=22.7°C and has the value of 0.1567, which means there are always more than 15.67% of people not

satisfied at any temperature. This result deviates from the lowest value (5%) in the PMV-PPD graph developed by Fanger and widely used in many standards. Nevertheless, "no more than 20% of people dissatisfied" is used as the criterion for defining the acceptable temperature band, which is consistent with the passing criteria in the evaluation of the acceptable thermal environment in existing space [4]. Fictitiously, if all the office workers selected from the database are sitting in the same room, the acceptable temperature band for this room will be from 21.5°C to 24.0°C.

$$\widehat{PD}_{tot} = 1 + \frac{1}{2}\left[-erf\left(\frac{T_i - \mu_c}{\sigma_c\sqrt{2}}\right) + erf\left(\frac{T_i - \mu_h}{\sigma_h\sqrt{2}}\right)\right] \quad (13)$$

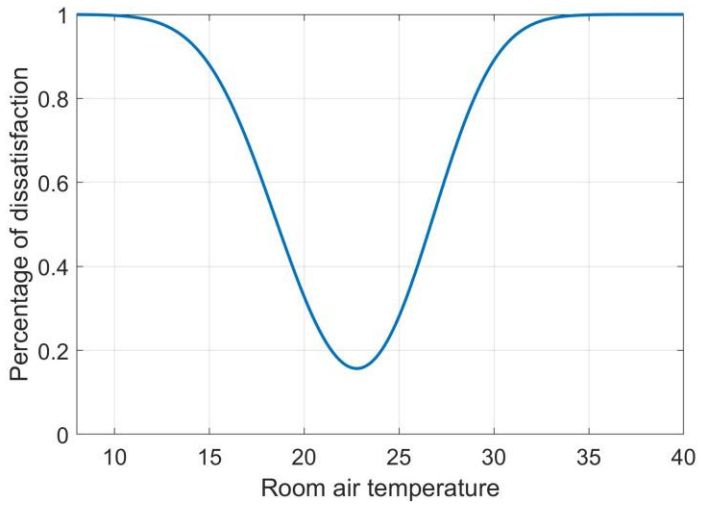

Figure 2.4 Overall percentage of dissatisfaction vs. room air temperature

7) To acquire the acceptable band of the occupants in a specific zone, the lower and upper bound of each occupant are sampled from the distributions described by Pr_{lb} and Pr_{ub}, respectively. A constraint is set to each sample as $T_{ub,individual}$>

$T_{lb,individual}$. Even though this constraint affects the fundamental assumption for i.i.d. sampling, the consequential error is trivial and ignored in this study.

8) At last, the zonal band is defined at the temperature interval that the zonal PD is smaller or equal to 20%. As the acceptable band for each individual has a binary and discrete form, the zonal PD may be in a non-convex or "W" shape. In this situation, the widest interval that satisfies the requirement is selected as the zonal acceptable band. Furthermore, the mean value of the upper and lower bound is taken as the zonal desired temperature.

2.1.2 Results and analysis

To intuitively understand the influence of the number of occupants on the zonal acceptable band, a series of scenarios are inspected, in which the occupant number is set to be 1, 5, 10, 20, 50, and 100. The sampling in each scenario is repeated 200 times to provide the results for statistical analysis. Figure 2.5 shows the raw result of the PD-Temperature curve for all zones in different scenarios; Figure 2.6-2.9 shows the frequency distributions of the desired temperature, lower bound, upper bound, and bandwidth over 200 cases in each scenario, where the bandwidth is defined as the temperature difference between the upper and lower bound. Table 2.1 summarizes the mean and standard deviation* in each category, and the reference values for "a large group of people" derived from the last section is also listed for comparison. (*assuming the normal distribution, explained below)

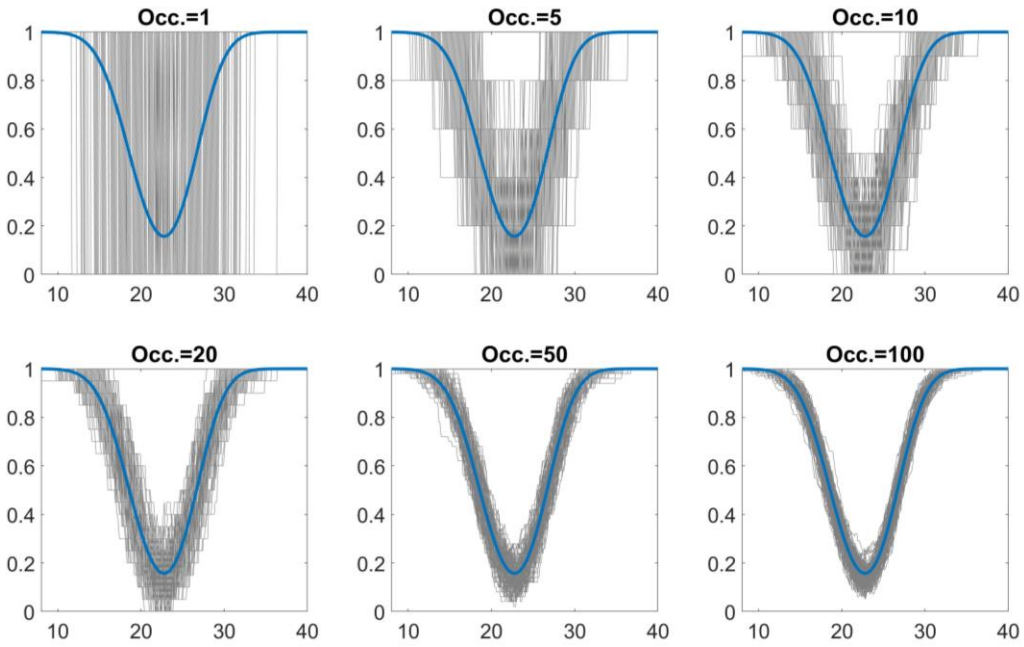

Figure 2.5 Percentage of dissatisfaction-Temperature for all zones in 6 scenarios, the reference curve is shown in blue line for comparison.
(x-axis temperature, y-axis PD)

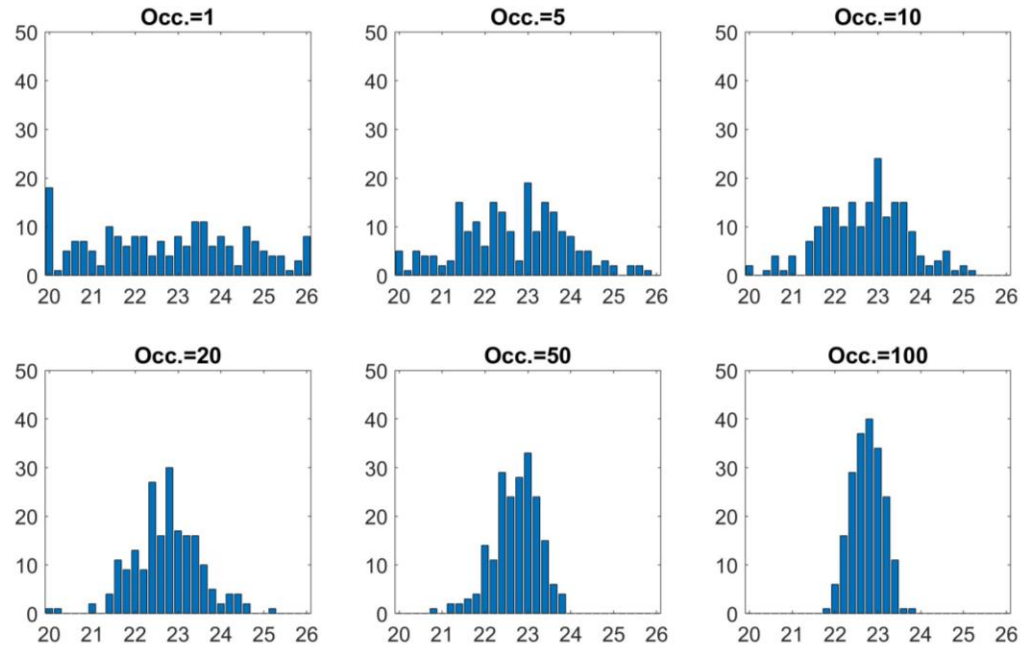

Figure 2.6 Frequency distribution of zonal desired temperature in scenarios
(x-axis temperature, y-axis zone counts)

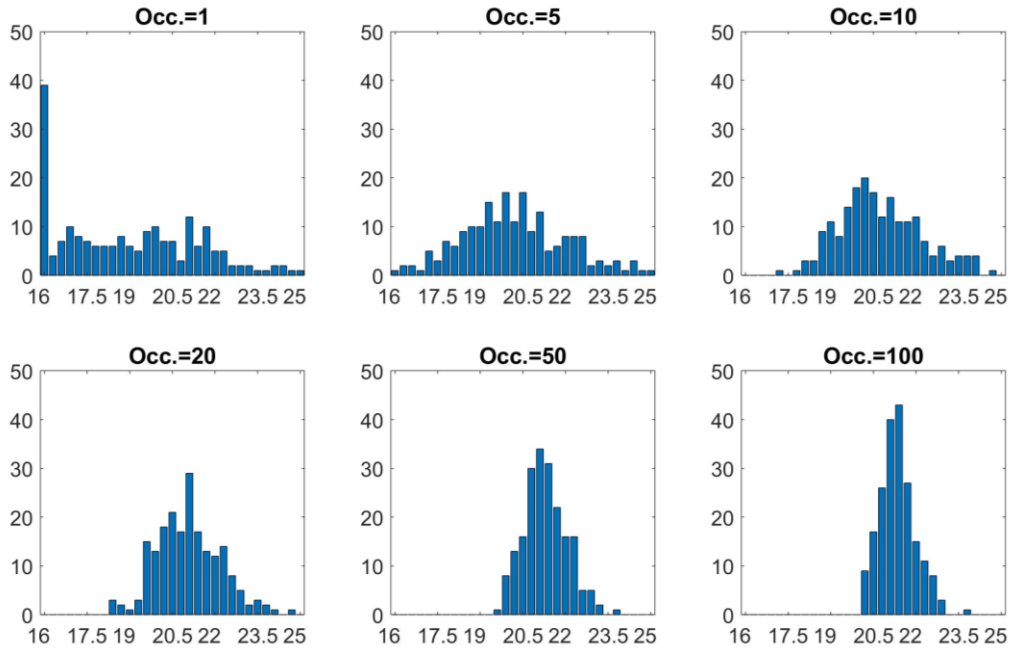

Figure 2.7 Frequency distribution of zonal lower temperature bound in scenarios (x-axis temperature, y-axis zone counts)

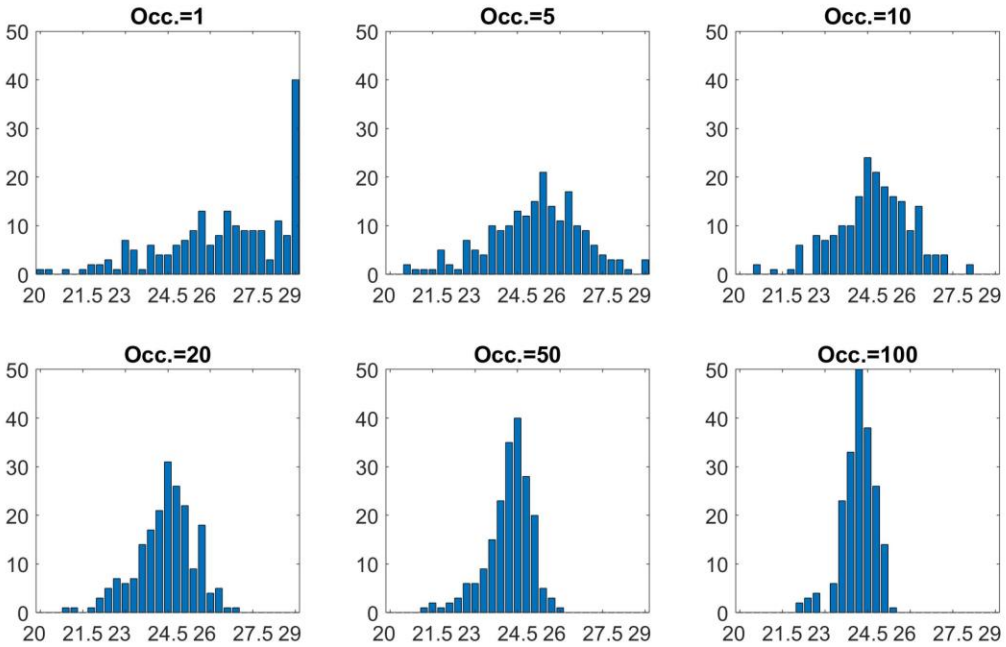

Figure 2.8 Frequency distribution of zonal upper temperature bound in scenarios (x-axis temperature, y-axis zone counts)

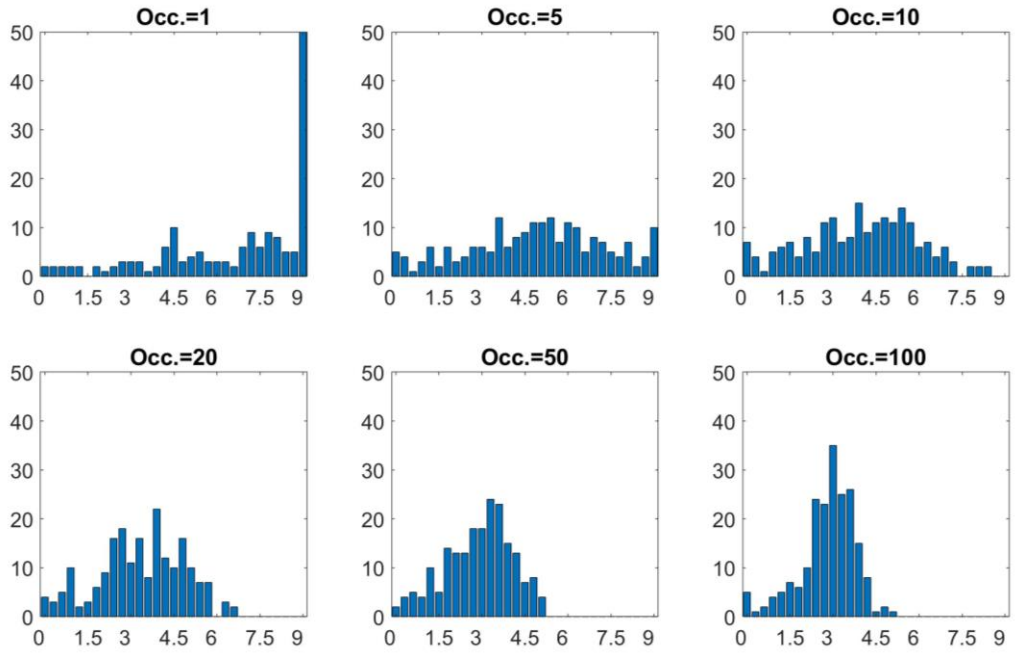

Figure 2.9 Frequency distribution of zonal temperature bandwidth in scenarios (x-axis temperature, y-axis zone counts)

Table 2.1 Summary of temperature band in scenarios

Scenarios	**Desired Temperature**		**Lower bound**		**Upper bound**		**Bandwidth**	
Occupants number	Mean	Std.*	Mean	Std.*	Mean	Std.*	Mean	Std.*
1	22.7	2.0	18.7	2.8	26.8	2.7	8.1	3.7
5	22.7	1.2	20.2	1.8	25.1	1.6	4.9	2.4
10	22.7	1.0	20.8	1.5	24.7	1.3	4.0	2.0
20	22.7	0.8	21.1	1.1	24.4	1.0	3.4	1.5
50	22.7	0.5	21.3	0.8	24.2	0.8	2.9	1.2
100	22.8	0.4	21.3	0.6	24.2	0.6	2.8	1.0
Reference	22.7	-	21.5	-	24.0	-	2.5	-

* Assuming normal distribution

From Table 2.1, the mean values of desired temperature keep identically at the same level as the reference, which proves that the sample size of 200 zones in each scenario is adequate for this study. The desired temperature of the single-occupant zone (Occ.=1) has the highest variability among all scenarios. Even though the variance of the desired

temperature has the trend to converge to 0 as zonal occupants increase, a nontrivial variation from 22 to 24 ^{o}C is observed at Occ=100 (Figure 2.6).

The scenarios of the single-occupant zone (Occ=1) and multi-occupant zone (Occ=5, 10, 20, 50, 100) are discussed separately in analyzing the temperature bands. For multi-occupant zones, the wider temperature bands (mean value) are observed in the scenarios with lower occupant numbers. This is mainly because of the inclusiveness of the 20% threshold in defining temperature band, and the temperature band in the scenario of Occ=100 is converging closely to the reference value. However, due to the bias (on the lower and upper bound) caused by the error in sampling, there is always a gap between the mean of the bandwidth from sampling and the reference value. A few zones have bandwidth=0, for which zones even the lowest PD is higher than 20%. Visually, the distributions of lower and upper bound may not follow the shape of the normal distribution; they are more in the shape of Gamma distribution with a softened short end. Unfortunately, categorizing these distributions is outside of the author's knowledge and the scope of this study.

For single-occupant zones, the same criteria used for defining the band have a different meaning. Since there is only one occupant in the zone, his/her temperature acceptance is dominant to the zonal band. Therefore, the mean values of the lower and upper bound in these zones automatically follow the temperature where the maximum of the PDFs $\Pr_{lb}$ and $\Pr_{ub}$ occurs. Even though it is exaggerated to set up such a wide band in reality, the implication from this result should be perceived that the thermal comfort requirements for the zones with one or a few occupants have a huge variation and may theoretically differ from the requirements for "a large group of people". An ideal way to

derive the control band of this type of zones is to use a quantified expression for the acceptance of each occupant, and PD will be accordingly defined as the averaged percentage of dissatisfaction of all individuals. As the definition of thermal acceptance is still in the academic debate, there is no such data to support the development of this method.

In addition, controlling a specific zone with the reference temperature band may result in a violation of thermal comfort, which happens when the zonal lower or upper temperature bound exceeds the reference ones. Table 2.2 summarizes the violation instances and percentage if the thermal zones are controlled using the reference band or the mean value of the corresponding scenario. Within 200 zones in each scenario, 30-50% of which will experience thermal discomfort at the temperature set in the reference band. For the scenario mean band, dissatisfied zones will increase to around 75%. Assuming the zonal lower and upper bound follows normal distribution ($T_{mean} = T_{median}$), the violation percentage in both categories will theoretically converge to 75%, as E(%)=1-0.5*0.5=0.75.

Table 2.2 The violation instances and percentage

Scenarios	**Reference Band**		**Scenario Mean Band**	
Occupants number	violation counts	violation percentage	violation counts	violation percentage
1	60	30%	154	77%
5	83	42%	150	75%
10	89	45%	143	72%
20	97	49%	138	69%
50	104	52%	141	71%
100	101	51%	136	68%

2.2 Productivity (loss) function

Serving as the most crucial component in the multi-objective optimization as Equation 5, the productivity loss function holds the link between the influence of building thermal environment on worker productivity and the operation cost of the HVAC system. As discussed in the literature review, the general form of the productivity function has been developed in [67] by synthesizing past studies, shown in Equation 6. To clarify, "productivity" discussed in this chapter are in the relative form, where productivity loss = 1 – productivity.

From a mathematical point of view, the third-order term in this equation is not very friendly for optimization since its convexity is not ensured along with the temperature. From an intuitive point of view, this function should be strongly convex (concave in the formulation in [67]) near the point of maximum productivity. In other words, if the room air temperature is increasingly going apart near the point of maximum productivity, the ratio of productivity loss increases. Thus, a second-order equation is proposed in this study to represent the original third-order one. In addition, as the maximum productivity is normalized to 1, only two parameters are required for defining the second-order function. The general form of this function is shown in Equation 14, where a is negative, the value of a could be defined as the "specific acceleration of relative-productivity loss" in the unit of %/K^2; b is the temperature where the maximum productivity occurs, since $P_{(T)} = 1$ when $T = b$.

$$P_{(T)} = a(T - b)^2 + 1 \tag{14}$$

By curve fitting, a second-order function is used to represent the original one, shown in Equation 15. From the comparison in Figure 2.10, this fitted productivity function performs almost identically as the original function between the temperature interval between 18 to 26 ^{o}C, which covers most of the operation conditions in office buildings. Furthermore, the second-order form of this function enables fast and accurate optimization in analyzing the potentials of MPC, later in chapter 3.

$$P_{(T)} = -0.0016817(T - 21.8079)^2 + 1 \tag{15}$$

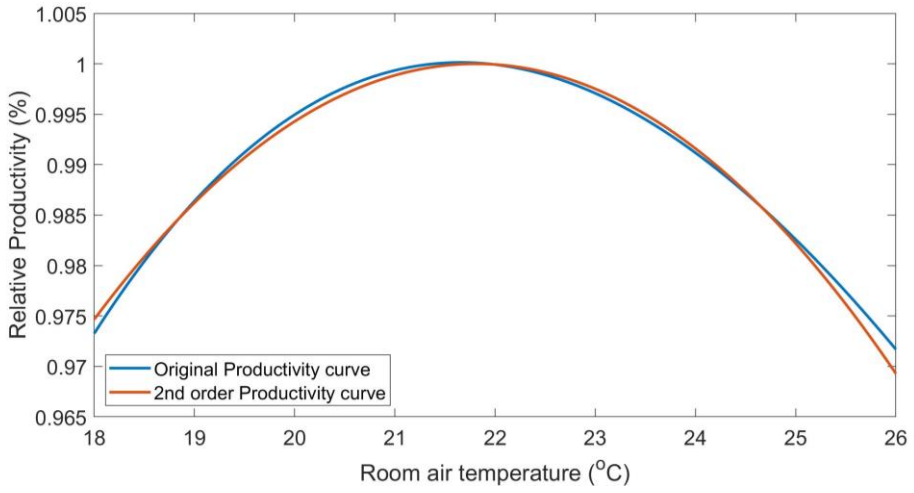

Figure 2.10 Original and fitted productivity curve

2.2.1 Methodology and Approach

Given the fact that there is not enough data which directly spotlights the influence of temperature on individual productivity, an additional step is required to derive the zonal productivity function. The percentage of dissatisfaction (PD) curve is proposed in this case. Thus, an ambitious assumption is made that: there is a strong correlation between the PD curve and productivity curve, and this correlation remains the same for any group of workers. If so, a linkage is created by the inverse of the PD function. Since $\widehat{PD}_{tot}$ in

Equation 13 is not monotonic, $\widehat{PD}_{cold}$ and $\widehat{PD}_{hot}$ (in Equation 9 and 10) are used to give the only solution from each function, as shown in Equation 16-19.

$$T_c = \sqrt{2}\sigma_c erf^{-1}(-2PD_{cold} + 1) + \mu_c \tag{16}$$

$$T_h = \sqrt{2}\sigma_h erf^{-1}(2PD_{hot} - 1) + \mu_h \tag{17}$$

$$P_c = P_{(T_c)} \tag{18}$$

$$P_h = P_{(T_h)} \tag{19}$$

Where PD_{cold} and PD_{hot} are the known percentage of dissatisfaction curves, erf^{-1} represents the inverse-erf function, T_c and T_h are the inverse function of $\widehat{PD}_{cold}$ and $\widehat{PD}_{hot}$, P_c and P_h are the productivity curve calculated from PD_{cold} and PD_{hot}. If PD_{cold} = $\widehat{PD}_{cold}$ and $PD_{hot} = \widehat{PD}_{hot}$, P_c and P_h share the same profile. But for each individual zone, the result of P_c and P_h may be different. Since the inverse-erf function is defined at (-1<x<1), this method does not apply to those single-occupant zones. This limitation actually confirms the conclusion made in the last section that the single-occupant and multi-occupant zones do not share the same thermal requirement. To be noticed, since the accuracy of Equation 15 is only examined in the domain of 18 to 26 ^{o}C, in which both the $\widehat{PD}_{cold}$ and $\widehat{PD}_{hot}$ are less than 40%, the result of P_c and P_h might not be correct when PD exceeds this limit on either side.

At last, the productivity curve for every zone ($\hat{P}_z$) is fitted from P_c and P_h by a second-order function keeping the same form of Equation 14, which is continuous and smooth for mathematical evaluation. And the productivity loss function is defined as $1 - \hat{P}_z$. To clarify, Figure 2.11 shows the derived and fitted curves for an example zone.

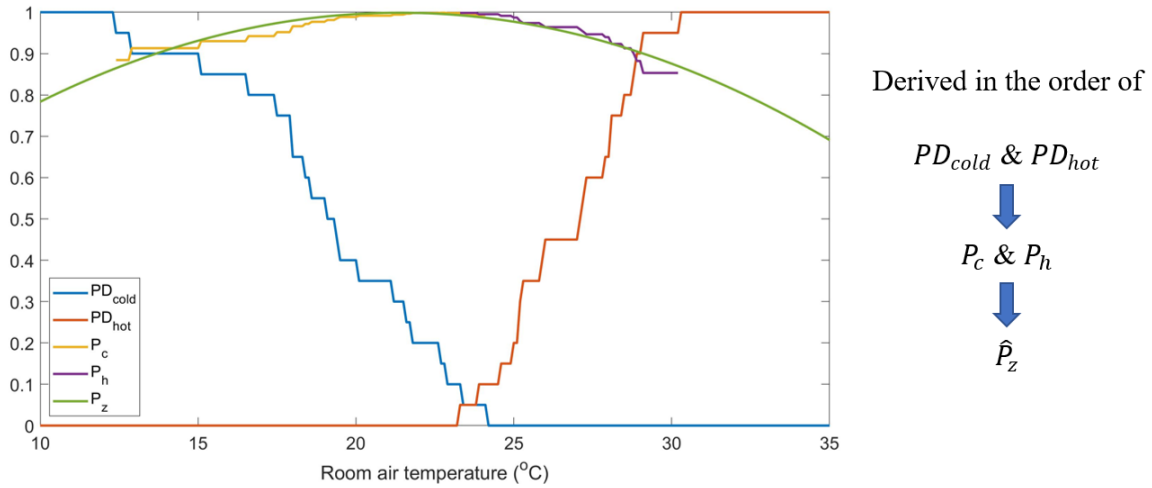

Figure 2.11 Derived and fitted curves for an example zone

2.2.2 Result and analysis

This approach is applied to all the multi-occupant zones in scenarios 2 to 5. The productivity curves in each zone are plotted in Figure 2.12 for an intuitive understanding. The frequency distribution of a and b for each zone is shown in Figure 2.13 and Figure 2.14. A statistical summary is made in Table 2.3.

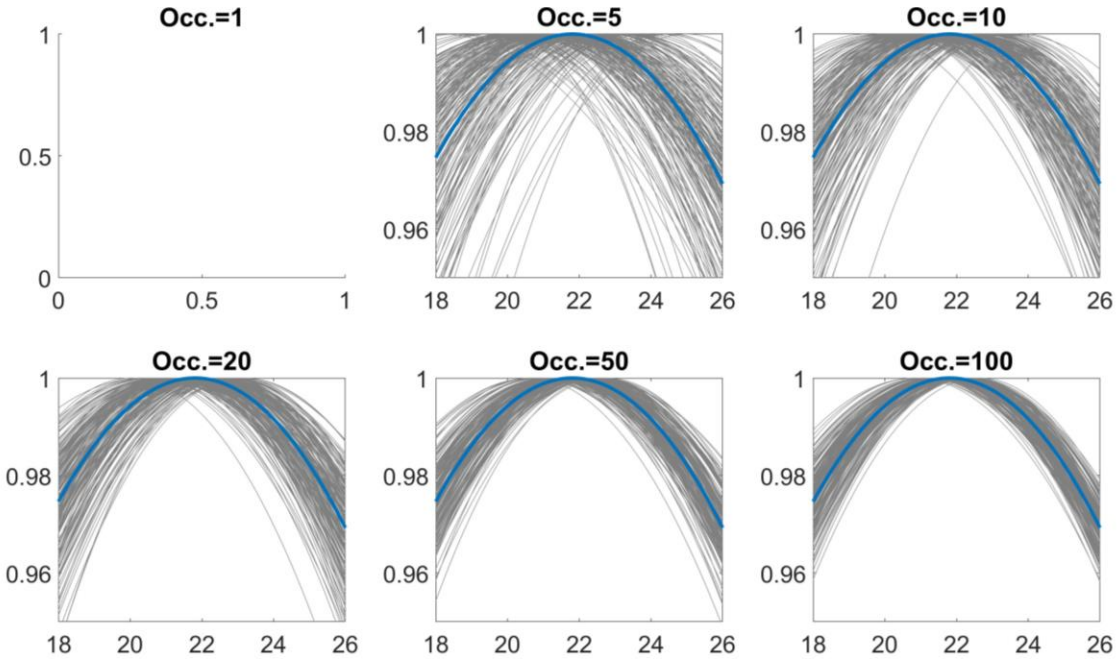

Figure 2.12 Fitted productivity curve for all zones in multi-occupant scenarios compared with the reference curve (blue) in Equation 15 (x-axis temperature, y-axis productivity)

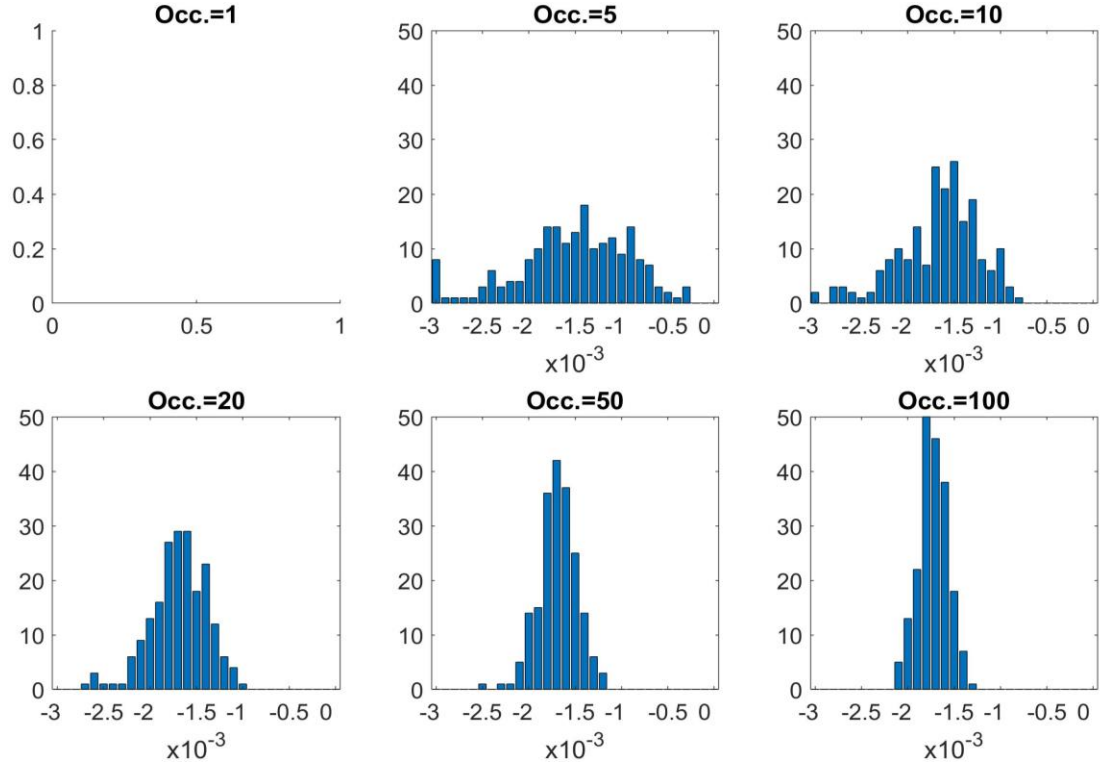

Figure 2.13 Frequency distributions of specific acceleration of relative productivity loss (x-axis specific acceleration, y-axis zone counts)

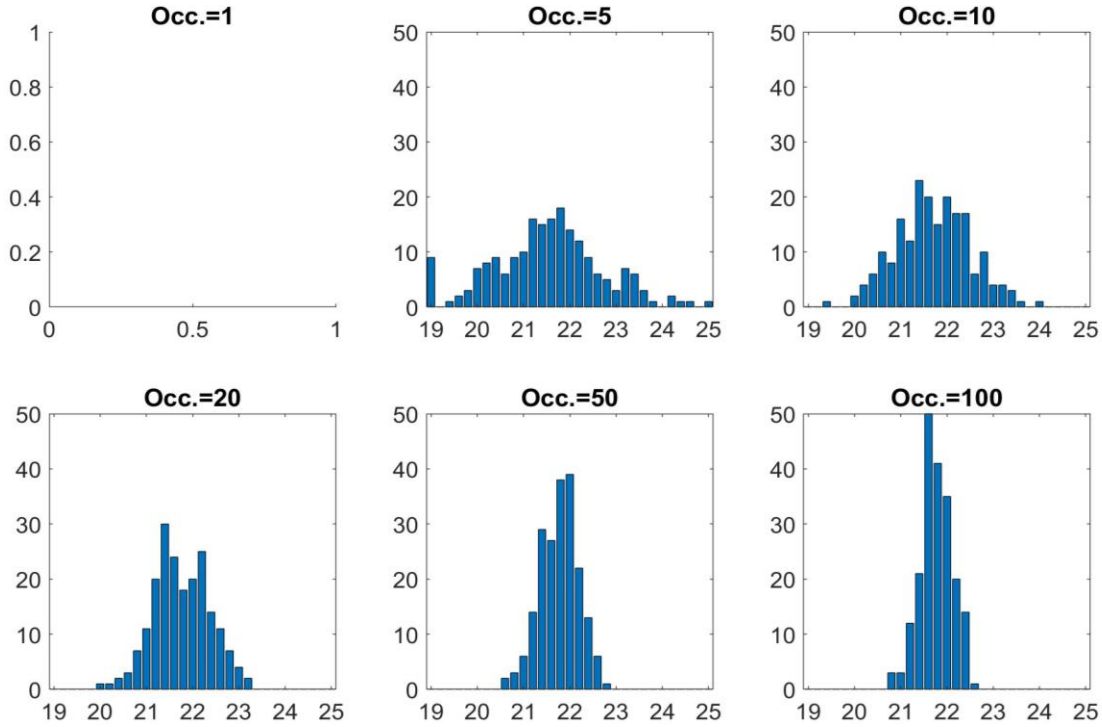

Figure 2.14 Frequency distributions of temperature with maximum productivity (x-axis temperature, y-axis zone counts)

Table 2.3 Summary of productivity in scenarios

Scenarios	**Specific Acceleration $\times 10^{-3}$**		**Temp. for max. Productivity**	
Occupants number	Mean	Std.	Mean	Std.
5	-1.522	0.600	21.4	1.6
10	-1.662	0.432	21.7	0.8
20	-1.690	0.305	21.8	0.6
50	-1.691	0.202	21.8	0.4
100	-1.726	0.158	21.8	0.3
Reference	-1.682		21.8	

From Table 2.3, the mean values of the specific acceleration keep at the same level of the reference value, and the mean value of the temperature with maximum productivity shows an even better convergence to the reference value. Without having a significant bias, the correctness of this method for deriving zonal productivity is confirmed. Unsurprisingly, the variation of both the acceleration and temperature reduce as zone occupancy increases, which can also be observed from Figure 2.13 and Figure 2.14. Comparing the temperature columns in Table 2.3 with the desired temperature in Table 2.2, the variation of temperature

for max productivity is smaller than the variation of zonal desired temperature when Occ.≥10.

Throughout the results in all scenarios, the scenario of Occ.=5 performs a relatively higher bias in both acceleration and temperature categories. This phenomenon is mainly because of the mathematical formulation, which naturally rejects 2 nodes where PD=0 and PD=1 in both PD_{cold} and PD_{hot} curve. The influence is especially obvious and exaggerates the variation in Occ.=5 scenario, since only 4 effective values are left in each curve. Even though it is not wrong that a second-order curve could be defined by 3 given nodes, the result for this scenario will not be used later in this study.

2.3 Conclusion

In this chapter, two studies address the zonal control flexibility form different perspectives, and the results lead to the same conclusion that:

1) The range of zonal control flexibility is significant if driven by an occupant satisfaction model
2) More divergence is observed in the zones with fewer occupants.
3) Single-occupant zone and multi-occupant zone do not share the same thermal requirement for defining control flexibility.
4) The control flexibility of each thermal zone should be defined separately.

For office buildings, a large open space usually has more than one HVAC terminal unit serving the space. If independent control is available for each terminal unit, very few

thermal zones will practically have more than 10 occupants. Based on the result, the necessity of zone-specified control flexibility is further amplified.

The result from this chapter can be potentially used for uncertainty quantification and risk analysis in building performance simulation. (Chapter 10 in [58] and [74]) In addition, the results could also serve as a prior for the calibration of existing buildings when the data is not sufficient from field surveys [75]. Since the results in this chapter are derived from subject-based static-measured data and should not be categorized in scenario uncertainty, using the results as time-varying thermal comfort requirement in stochastic optimization is NOT recommended by the author.

In order to improve this study, several aspects need to be realized and further proved. Firstly, the adaptability of occupants to the thermal environment needs to be considered, which includes both the weather-influenced thermal comfort preference and the occupants' adaptation to a given indoor thermal environment. This study may potentially be combined with the research outcomes from [76]. Secondly, the connection between thermal comfort (i.e., PD) to productivity should be consolidated, for which a possible way is to collect both thermal comfort indicators and productivity-related data from the same group of subjects. Last but not least, the consistency of the thermal requirements between the static and temperature-varying environment needs to be further proved. Even though the room air temperature under MPC does not violate the "static thermal environment" defined in [4], the control flexibility may still be different.

CHAPTER 3. POTENTIAL BENEFITS OF BUILDING THERMAL LOAD CONTROL

For the adaptive building thermal load control, the potential can be defined as the savings of HVAC operation cost or the increment of organizational benefit (OB), compared with the reference case, by controlling building thermal load in the manners of load shifting and/or peak shaving. Current work on MPC is deficient in the sense that MPC savings are often overstated. The stated savings are the result of improved or relaxed comfort requirements in combination with the forward-looking optimal control of the heating and cooling supply. By not separating the two mechanisms, the actual contribution of MPC is misrepresented. The study in this chapter makes a clear separation between the two, thus isolating the benefit of implementing MPC. The saving potential analyzed by the method developed in this chapter will serve as a benchmark for uncertainty analysis and model development, which are performed later in this dissertation.

A dedicated method is proposed in this chapter. Firstly, a clear-box high fidelity, finite element based, linear building model is established as the prediction model to optimally capture the building dynamics. Secondly, this building model is translated into a state-space representation, and a linear transformation is used to realize the interrelation over iterations in the optimizations performed by linear and quadratic programming. After the first two steps, the control strategies of load shifting and peak shaving are separately and jointly applied to the building for the examination of their individual and combined contributions, in which both the general and zonal control flexibility are applied for

comparative results. The detailed methodology and approach are shown in the following sections.

Several assumptions and setups used in this study:

1) This study is based on the subject of a five-zone small office building in Atlanta, GA, USA. The building information is drawn from the EnergyPlus IDF file of DOE Reference building (climate zone 3A), which the information includes building geometry, construction, material, zonal internal gain (except occupants).
2) A Unitary heat pump unit is assumed in each zone with individual control. The HVAC system COP curve is calculated form a multi-linear regression model trained from EnergyPlus simulation result (R^2=0.91)
3) The electricity TOU rate is based on the Georgia Power company [78], and the peak to valley ratio is 2.06. The detailed TOU schedule is shown in Table 3.1.

Table 3.1 Electricity time of use rate form Georgia Power

Seasons	Schedule		Unit Price (per kWh)
June - September	Mon-Fri	2p.m. to 7p.m.	0.16923
	Sat, Sun		0.08198
Other	All days		0.08198

4) Zonal control flexibility is assumed to be well known for every individual zone. The theoretical control potentials are examined deterministically. Scenario uncertainties in weather prediction, internal heat gain, and occupants' thermal requirements are assumed to be "zero".
5) The revenue generated from each occupant is assumed at 300,000 USD per year [53], which is about 150 USD per office hour.

6) Since this study serves only as an analysis of potentials, the energy flow rate is directly used as the control variable in optimization. In reality, this control variable needs to be translated for actuation.

3.1 Methodology

3.1.1 Prediction Model

Serving as a research method, a clear-box model is fundamentally a white-box model but allows modelers to maximumly manipulate the simulation process and extract the information needed. With this property, the concerns [15] applied to the white-box models could be easily resolved. The clear-box model constructed in this section is an application of the modeling method presented in [78] and [79].

The model is based on a finite element approach, which results in a nodal network, in which the building is broken down into components and relations, where each component is represented by a node. Energy conservation law applies to every node, as in Equation 20.

$$\frac{dE_{sys}}{dt} = \sum \dot{E}_{in} - \sum \dot{E}_{out} \tag{20}$$

Where E_{sys} is the embedded energy in a single node, $\dot{E}_{in}$ and $\dot{E}_{out}$ are the inward and outward energy flow. Regarding the internal and solar heat gain as in heat generation term, Equation 20 is expanded to a heat balance equation for each node, shown in Equation 21.

$$mc\frac{dT}{dt} = \sum \dot{Q}_{cond} + \sum \dot{Q}_{conv} + \sum \dot{Q}_{rad} + \sum \dot{Q}_{gen} + \sum \dot{m}c(T_{in} - T_{out}) \quad (21)$$

Where $\dot{Q}_{cond}$, $\dot{Q}_{conv}$, $\dot{Q}_{rad}$, $\dot{Q}_{gen}$ are the heat transfer by conduction, convection, longwave radiation, and generation respectively, $\dot{m}$ is the mass flow rate of infiltration, which is assumed to be 0.5 ACH interzonal and to the exterior. The mass term m for every room node is multiplied by a factor calibrated with the original EnergyPlus model, which factor represents the room-contained thermal mass like furniture, etc. The formula and parameters used for calculating $\dot{Q}_{cond}$, $\dot{Q}_{conv}$, $\dot{Q}_{rad}$, $\dot{Q}_{gen}$ are given in Equation 22 – 27, which describes the heat transfer process in the relation of node m and node n, evaluated at node m.

$$\dot{Q}_{cond} = -kA\frac{(T_m - T_n)}{l} \quad (22)$$

$$\dot{Q}_{conv} = -h_{conv}A(T_m - T_n) \quad (23)$$

$$\dot{Q}_{rad} = -h_{rad}AF_{mn}\varepsilon_{mn}(T_m - T_n) \quad (24)$$

where

$$h_{rad} = \sigma\,(T_m + T_n)(T_m^2 + T_n^2) \quad (25)$$

$$\dot{Q}_{gen,sol} = A\varepsilon_m\dot{q}_{sol,i} \quad (26)$$

$$\dot{Q}_{gen,room} = \dot{Q}_{int} + \sum_n A_n\tau_n\dot{q}_{sol,i} \quad (27)$$

Where k, h_{conv}, h_{rad} are the conductivity, convective heat transfer coefficient, and linearized radiative heat transfer coefficient. l is the thickness of the material, A is the area of the component m. ε and τ are the emissivity and transparency, F_{mn} is the pre-calculated view factor from face m to face n. $\dot{q}_{sol,i}$ is the solar radiation intensity on the direction i

that component m is facing upon, and σ is the Stefan-Boltzmann constant. $\dot{Q}_{int}$ is the energy flow rate from internal heat gain. Equation 26 applies to all the surfaces which receive solar radiation, and the second term in Equation 27 describes the heat generated in the room node from the sunlight through windows.

Overall, there are 174 nodes in total throughout the five-zone office building (6 zones, including the unconditioned attic). By applying heat balance equations evaluated at every node, a nodal network is established to maximumly secure the building dynamics. Figure 3.1 shows a schematic diagram of PART of the nodal network, where attic and soil nodes are omitted. Furthermore, the heat balance equations can be written in a matrix form as in Equation 28. To ensure accuracy in modeling, this nodal network is generated by a customized MATLAB program, which is similar to a mesh generation tool.

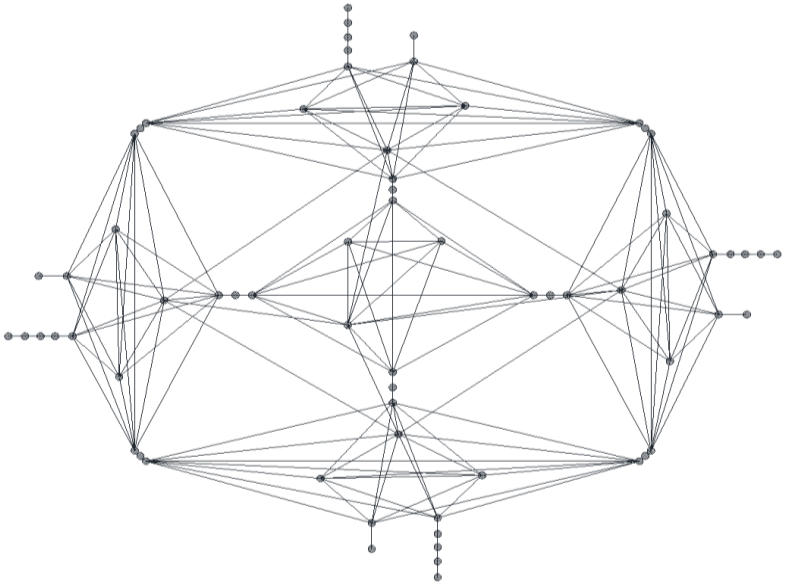

Figure 3.1 Schematic diagram of part of the nodal network

$$M\frac{dT}{dt} = ST + E_H Q_H + E_T T_a + E_S Q_S + E_I Q_I \tag{28}$$

Where $T \in \mathbb{R}^{\lambda}$ is the temperature state of every node, for this building $\lambda = 174$. $M \in \mathbb{R}^{diag\ \lambda}$ represents the thermal storage properties of each node, $S \in \mathbb{R}^{\lambda \times \lambda}$ represents the heat transfer process between nodes. $E_H \in \mathbb{R}^{\lambda \times 10}$ is the indicator of the 5 HVAC conditioned nodes for both cooling and heating, $Q_H \in \mathbb{R}^{10}$ is the cooling and heating flow rate for the 5 conditioned nodes. $E_T \in \mathbb{R}^{\lambda \times 2}$, $E_S \in \mathbb{R}^{\lambda \times 9}$, and $E_I \in \mathbb{R}^{\lambda \times 5}$ represents the heat transfer properties for prescribed temperatures, solar heat gain, and internal heat gain. And $T_a \in \mathbb{R}^2$, $Q_s \in \mathbb{R}^9$, $Q_I \in \mathbb{R}^5$ are the prescribed boundary conditions in the categories of temperature, solar radiation intensity, and internal heat gain. Figure 3.2 illustrates the values in matrix S in a contour plot for a visual understanding.

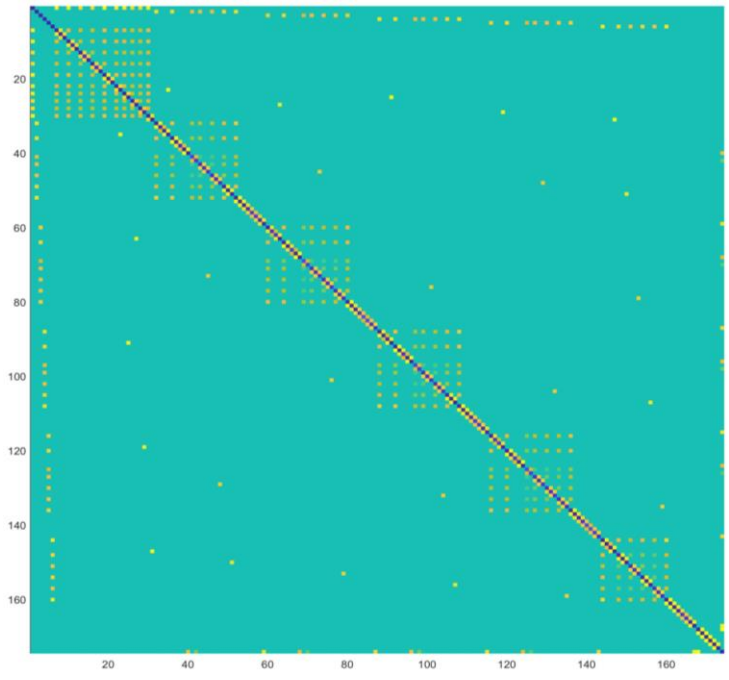

Figure 3.2 The connections between nodes in the nodal network

Equation 28 is numerically solved using explicit Euler, shown in Equation 29. The simulation time step is set to 10 mins to ensure the prediction accuracy. The HVAC energy consumption rate (ω) is expressed as in Equation 30, in which HVAC system COP for both heating and cooling are determined from multi-linear regression models (Equation 31 and 32) using outdoor air temperature, relative humidity (RH), and wind speed (V). Thus, the nodal network model is adequately established to predict room air temperature and HVAC energy consumption in iterations. In both Equation 29 and 30, the only control input is the energy flow rate of the HVAC system, $Q_{H,i}$, which will be determined in later sections.

$$T_{i+1} = T_i + M^{-1}\left(ST_i + E_H Q_{H,i} + E_T T_{a,i} + E_S Q_{S,i} + E_I Q_{I,i}\right)\Delta t \tag{29}$$

$$\omega_i = COP_i^{-1} Q_{H,i} \Delta t \tag{30}$$

where $$COP_{Heating,i} = \chi_i \beta_{Heating}, \qquad COP_{cooling,i} = \chi_i \beta_{cooling} \tag{31}$$

and $$\chi_i = \{T_{a,i}, RH_i, V_i, 1\} \tag{32}$$

3.1.2 Linear system and optimization

Back to the objective function shown in Equation 2, 3, and 5 (copied below), the optimizations aim to minimize the summation of a series of control variable sets.

$$\min_{u_i} \sum_{i=1}^{n} C_{i(u_i)} \tag{2}$$

Subj.to $$T_{lb,i,j} \le T_{i,j} \le T_{ub,i,j}, \qquad \forall i = 1 \dots n, \forall j = 1 \dots m \tag{3}$$

$$\min_{u_i} \sum_{i=1}^{n} (C_{i(u_i)} + vr_i p_{i(T_i)}) \tag{5}$$

However, these control variables are not only interrelated within a set (time step) but also non-orthogonal over time steps. The interrelationship within a set can be addressed in the nodal network, but the dependency over time needs to be resolved in a robust linear system. This section demonstrates the establishment and transformation of the linear system in realizing control sequence optimization. The procedure used in this section highly refers to [25, 26] and [80].

Firstly, Equation 29 is re-written in a state-space form in Equation 33, and the components are translated through Equation 34-39. Still, full observability is assumed in this state-space system.

$$x_{i+1} = Ax_i + Bu_i + Dw_i \tag{33}$$

Where

$$x_i = T_i \tag{34}$$

$$u_i = Q_{H,i} \tag{35}$$

$$w_i = \{T_{a,i};\ Q_{S,i};\ Q_{I,i}\} \tag{36}$$

$$A = I + M^{-1}S\Delta t \tag{37}$$

$$B = M^{-1}E_H\Delta t \tag{38}$$

$$D = M^{-1}\{E_T, E_S, E_I\}\Delta t \tag{39}$$

Equation 33 describes the recursive formula of the nodal-network evaluated at time step i. Then for time step $i+1$, the recursive formula can be written in Equation 40.

$$x_{i+2} = Ax_{i+1} + Bu_{i+1} + Dw_{i+1} \tag{40}$$

Taking Equation 33 into Equation 40, Equation 41 is acquired, which is a non-recursive formula evaluated at the state x_i.

$$x_{i+2} = A^2 x_i + ABu_i + Bu_{i+1} + ADw_i + Dw_{i+1} \tag{41}$$

Accordingly, given the prediction length of n, the state at n^{th} step follows:

$$x_{i+n} = A^n x_i + A^{n-1}Bu_i + A^{n-2}Bu_{i+1} + \cdots + ABu_{i+n-1} + A^{n-1}Dw_i + A^{n-2}Dw_i + \cdots + ADw_{i+n-1} \tag{42}$$

Where the right-hand side of the equation includes three components:

1) $$A^n x_i$$

2) $$A^{n-1}Bu_i + A^{n-2}Bu_{i+1} + \cdots + ABu_{i+n-1}$$

3) $$A^{n-1}Dw_i + A^{n-2}Dw_i + \cdots + ADw_{i+n-1}$$

Given the constant matrix A, B, D, and the known vector w for every time step, the non-recursive formulas for all states x_{i+1} to x_{i+n} remain the linear formulation. Accordingly, all the stats in the prediction horizon n can be expressed in a new linear system as in Equation 43-49.

$$X = \Psi x_i + \Phi U + \Theta W \tag{43}$$

Where

$$X = \{x_{i+1};\ x_{i+2};\ x_{i+3};\ \cdots;\ x_{i+n}\} \tag{44}$$

$$U = \{u_i;\ u_{i+1};\ u_{i+2};\cdots;\ u_{i+n-1}\} \tag{45}$$

$$W = \{w_i;\ w_{i+1};\ w_{i+2};\cdots;\ w_{i+n-1}\} \tag{46}$$

$$\Psi = \{A;\ A^2;\ A^3;\ \cdots; A^n\} \tag{47}$$

$$\Phi = \begin{Bmatrix} B & 0 & 0 & \cdots & 0 \\ AB & B & 0 & \cdots & 0 \\ A^2B & AB & B & \cdots & 0 \\ \vdots & \vdots & \vdots & \ddots & \vdots \\ A^{n-1}B & A^{n-2}B & A^{n-3}B & \cdots & B \end{Bmatrix} \tag{48}$$

$$\Theta = \begin{Bmatrix} D & 0 & 0 & \cdots & 0 \\ AD & D & 0 & \cdots & 0 \\ A^2D & AD & D & \cdots & 0 \\ \vdots & \vdots & \vdots & \ddots & \vdots \\ A^{n-1}D & A^{n-2}D & A^{n-3}D & \cdots & D \end{Bmatrix} \quad (49)$$

Thus, this transformation realizes the interrelation over steps, and the new linear system fits linear and quadratic programming methods, which ensure the global optimum. Then at every MPC control interval i, Equation 2, 3 and Equation 5 can be re-written in Equation 50, 51 and Equation 52.

$$\min_{U_i} R_i \Omega_{i(U_i)} \quad (50)$$

Subj.to $$X_{lb,i} \leq X_i \leq X_{ub,i} \quad (51)$$

$$\min_{U_i} R_i \Omega_i + \mathrm{P}_{i(X_i)} \quad (52)$$

Where the subscript i denotes the optimization is run at the i^{th} control interval of MPC. $\Omega_i = \{\omega_i;\ \omega_{i+1};\ \cdots;\ \omega_{i+n-1}\}$ where $\omega_i$as given in Equation 30, $R_i \in \mathbb{R}^{10 \cdot n}$ is the electricity price at every time step in prediction, $\mathrm{P}_i \in \mathbb{R}$ is the overall productivity loss in the capital unit, which is a second-order term derived from Equation 5 and 14.

The modeling and optimization methods introduced in these two sections serve as the foundation for analyzing the potentials. The detailed simulation setups are illustrated in the following section.

3.1.3 Experiment setups

In order to comprehensively inspect and understand the control potentials, three research questions need to be properly addressed:

1) What is the baseline control scenarios?

2) What are the potentials from load shifting and peak shaving?

3) What is the difference in potentials by traditional and adaptive control?

To answer these questions, 12 control scenarios are designed and experimented with for comparison, summarized in Table 3.2. To narrow down the question, 10 occupants are assumed in each zone of the building. All simulations are run from June to September to reflect the seasonal performance. The detailed case specifications are shown below.

Table 3.2 List of scenarios in the analysis of potentials

Scenario Number*	Control flexibility	Objective	Control strategy
T1	Traditional	N/A	Desired Temperature
T2		N/A	Max Productivity
T3		Min. Cost	Load Shifting
T4		Min. Cost	Peak Shaving
T5		Min. Cost	Load Shifting + Peak Shaving
T6		Max. OB	Load Shifting + Peak Shaving
A1	Adaptive	N/A	Desired Temperature
A2		N/A	Max Productivity
A3		Min. Cost	Load Shifting
A4		Min. Cost	Peak Shaving
A5		Min. Cost	Load Shifting + Peak Shaving
A6		Max. OB	Load Shifting + Peak Shaving

*It is highly recommended for readers to refer to this table, as the following of this chapter will use the Scenario Number to represent the detailed setup.

Firstly, 36 buildings with 180 zones are used to represent the randomness of the adaptive control scenarios. In each zone, 10 people are sampled from the distribution in Figure 2.3, and the zonal control flexibilities for temperature band and productivity loss curves are derived for each zone. As discussed in previous chapters, the desired temperature is defined as the average value of the upper and lower bound. Comparatively, the traditional control scenario has only one building with 5 zones, in which the mean value of the 180 control bands is used, as same as the mean curve.

Secondly, the scenarios T1 and A1 are the comparison groups for T2-T5 and A2-A5, and the scenarios T2 and A2 are the comparison groups for T6 and A6. The setpoint temperature during office hours is statically set at the zonal desired temperature for T1 and A1, and the setpoint temperature for T2 and A2 during office hours are set at the temperature that the maximum zonal productivity occurs. These baseline scenarios adopt the idealized control, which is also known as the one-step predictive control, given in Equation 53-55.

Given
$$x_{i+1} = Ax_i + Bu_i + Dw_i$$
$$u_i = \{u_{i,cool}; u_{i,heat}\} \quad (53)$$

Where
$$u_{i,cool} = B^{-1}\left(T_{set,cool,i+1} - Ax_i - Dw_i\right), \qquad u_{cap,cool} < u_{i,cool} < 0 \quad (54)$$
$$u_{i,heat} = B^{-1}(T_{set,heat,i+1} - Ax_i - Dw_i), \qquad 0 < u_{i,heat} < u_{cap,heat} \quad (55)$$

Thirdly, all baseline cases (T1, T2, A1, A2) and pure peak shaving cases (T4, A4) act 1 hour precooling in every workday before office hour starts. Since the MPC strives to satisfy temperature constraints all the time, it naturally optimizes the timing for precooling before office hours. These scenarios with one-hour precooling are considered to provide a fair comparison and separate the contribution of load shifting and peak shaving. Actually, the "setpoint temperature band" in baseline scenarios and the "temperature constraint band" in MPC are fundamentally in different definitions, but the discrepancy resulted from them could be categorized as system errors.

Fourthly, the flexibility for load shifting is defined in the band of the desired temperature and lower bound. Peak shaving allows the temperature to go to the upper

bound, and this control boundary offset only happens in peak hours. (14:00-19:00) The scenarios which contain load shifting are realized by MPC algorithms illustrated in the previous section. The pure peak shaving scenarios (T4, A4) require no MPC and can be realized by the idealized control algorithm. In addition, if a specific room does not have control flexibility (width of control band = 0), this room is treated in MPC without load shifting nor peak shaving but with optimized precooling, and the mean of the temperatures with the lowest percentage of dissatisfaction rate is used as the desired temperature during office hours.

Last but not least, the temperature constraints used in T5 and A5 are also applied in T6 and A6. This is mainly because of an ethical question: for whom does the indoor environment serve? There are essentially 3 stakeholders of an office building: 1) the occupants, 2) the company of employment, and 3) the building manager who pays the electricity bill. There may be some deep and indirect relations among these stakeholders, but the interests of these stakeholders are distinct: 1) occupants require comfort, 2) the company needs profit, and 3) the building manager wants to lower the cost. Eventually, the distinct interests need to be reflected in the objective function in MPC control. The multi-objective optimization (T6 and A6) applies when the company and the building manager are the same entity, or say the company is paying for the electricity bill. Thus, the temperature constraints from occupants have to be in the optimization formulation, as the building is for people.

In the preparation of the simulation, the building with constant heating and cooling setpoints is used for the system sizing and warming-up for all scenarios. Even with a 1.2 sizing factor applied, the system size might not fit the operation condition for all scenarios,

but it follows the principle that the HVAC designer is not able to know the specific thermal requirement of the actual user. A 5.5-year (until May 31st of the 6th year) warming-up is performed to ensure the periodical quasi-equilibrium of the system.

For the MPC controlled cases, the prediction horizon is 24 hours, in which 144 prediction intervals are iterated with 10 mins of one interval. The optimization in MPC is repeated every hour, and the optimized control variables of the first 6 prediction interval are applied for actuation. Thus, 2928 optimization runs are performed in each building covering the period from June to September.

3.2 Results

3.2.1 Inspection

Before analyzing the potential, the results are inspected to ensure the correctness. The simulation result of a typical zone in 3 continuous days is selected to show the MPC performance, shown in Figure 3.3. In the plot, the baseline (T1), pure load shifting (T3), pure peak shaving (T4), and load shifting and peak shaving combined (T5) scenarios of traditional control flexibility are inspected in terms of the profiles of 1) zone temperature, 2) HVAC power consumption, and 3) HVAC electricity cost. From the plots, the temperature is reduced before the peak hours in T3 and T5 scenarios, which could be attributed to the activation of load shifting. This effect could also be observed in the power and cost plots, in which both of the values increase at 1-3 hours before the peak hours.

As for peak shaving, the control logic in T4 and T5 scenarios allows the temperature to increase to the upper bound, which is reflected in the temperature plot. Accordingly, the

HVAC power cost keeps at a lower level during the peak hours, compared to T1 and T3 scenarios. To be noticed, the activation of load shifting is reduced and postponed by peak shaving, which can be observed in the temperature plot that the downward "spikes" of T5 always appear smaller and later than the ones in T3.

Besides, the starting times of precooling are very close in all cases, which validates the simulation setup of 1-hour precooling for non-MPC-controlled scenarios. To repeat, there is no feasible method, by the author's knowledge, to completely fix this gap without a predictive control. From another perspective, it can be regarded as an embedded advantage of MPC.

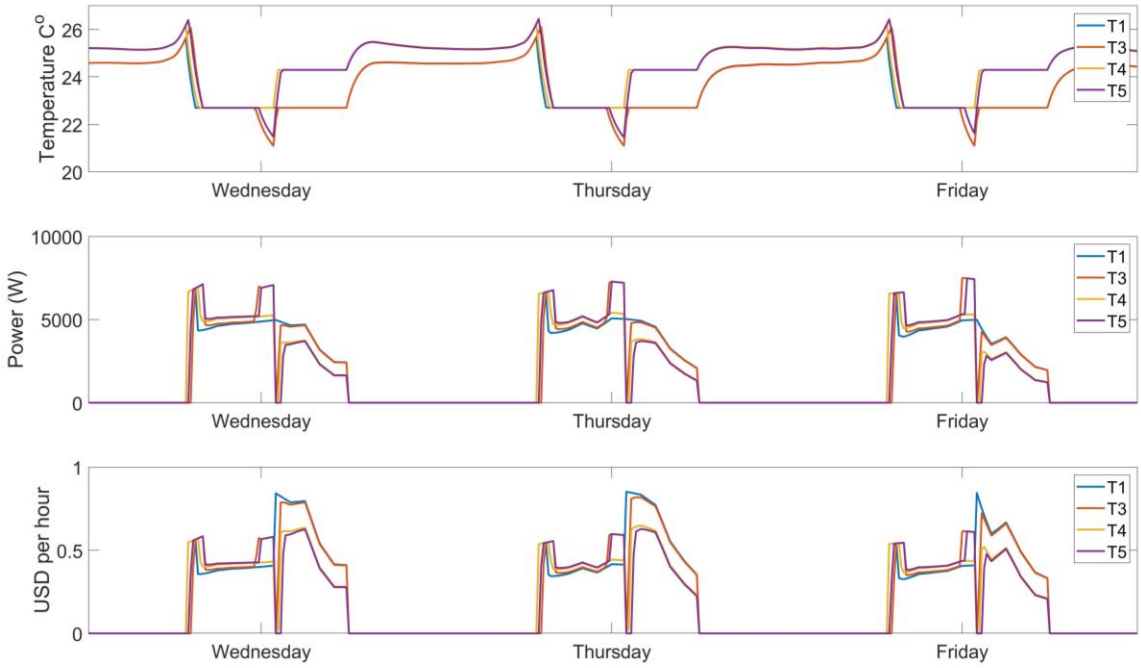

Figure 3.3 Temperature, power, and cost in 3 consecutive days

Figure 3.4 shows the daily zonal OB increase of all the zones in scenarios A6 compared to their baseline scenario A2, in which the weekends are excluded. From the histogram, all samples have the value greater or equal to 0, which is a strong proof of the

correctness of the optimization. The same results are also seen in the scenarios of minimizing operation costs.

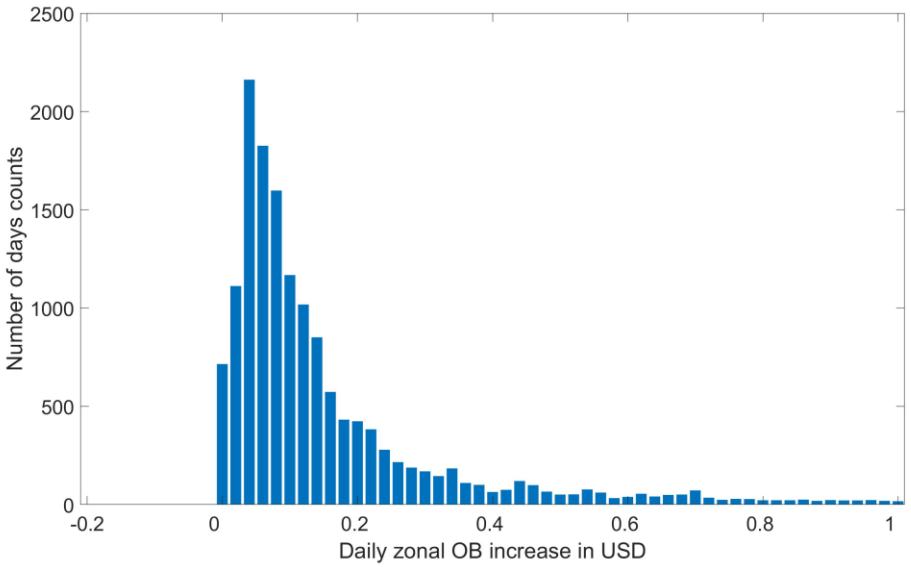

Figure 3.4 Daily zonal OB increase in USD

3.2.2 Potential cost-saving

To reflect the saving potentials based on the traditional control flexibility, a summary of building-level HVAC electricity cost over scenarios are shown in Table 3.3, and the same content is also plotted in Figure 3.5 for a visual presentation.

Table 3.3 Building HVAC operation cost in scenarios (T1, T3-T5)

	Baseline	Load Shifting		Peak Shaving		Load Shifting + Peak Shaving	
	COST (USD)	COST (USD)	Saving (%)	COST (USD)	Saving (%)	COST (USD)	Saving (%)
June	386.29	375.76	2.7%	293.41	24.0%	289.67	25.0%
July	469.47	457.71	2.5%	376.67	19.8%	371.89	20.8%
Auguest	542.65	529.63	2.4%	442.71	18.4%	437.14	19.4%
September	342.39	330.72	3.4%	266.91	22.0%	261.28	23.7%
Total	1740.80	1693.82	2.7%	1379.71	20.7%	1359.98	21.9%

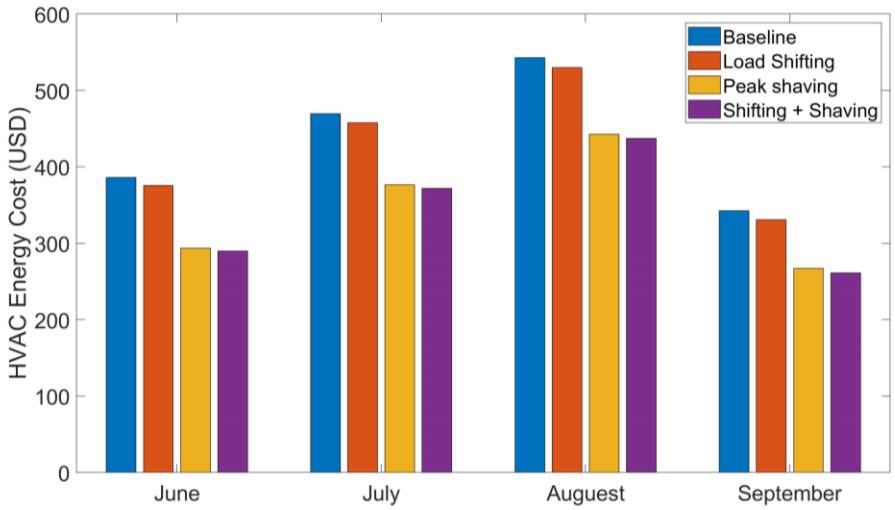

Figure 3.5 Building HVAC cost in scenarios with traditional control flexibilities

From the results, the cost-saving potential from load shifting is very limited, showing only 2.7% over the entire summer months. The amount of cost-saving is considerable for peak shaving, in which 20.7% of the HVAC electricity cost is reduced, being more than 7 times that of the saving from load shifting. The lowest cost occurs when these two aforementioned methods are combined (L+P), but the total saving amount is smaller than the sum of the individual effects. As discussed earlier, the reduction of saving is mainly because of the depressed activation of load shifting by the following peak shaving. In other words, the activation of load shifting is dominated by the flexibility for peak shaving. For example, if a zone has a very high upper bound of acceptance, and the room air temperature never reaches the upper bound during the peak hours, then there is no energy consumed for cooling in this peak period, and no load shifting is needed anymore. In reality, this situation may not happen, but the later the cooling starts in peak hours, the less load shifting is needed. This phenomenon may explain that in some existing studies, load shifting is never found in the optimized control.

Even though June and September are not in the transition season, the net cost-saving and cost-saving percentages are indeed higher in these “less hot” seasons. There is enough reason to believe that load shifting and peak shaving may have higher potentials in transition seasons if the pricing plan of the TOU rate extends. If the normalized values are considered, the cost-saving per person will be 0.94 from load shifting, 7.22 from peak shaving, 7.62 from the L&P combined strategy; and the cost-saving per square meter will be 0.09, 0.71, and 0.75 from the scenarios, respectively.

The cost-saving performance of using adaptive control flexibility is very similar to the ones of using traditional flexibility. A plot of seasonal cost-saving performance of the three control strategies in each building is shown in Figure 3.6. The buildings are identified by the colors, which are ranked by the cost-saving percentage of the L&P combined scenario (from light-yellow to dark-blue). The grey box in the background in each plot represents the saving percentage under traditional control flexibility in the respective category. From the result, the ranking pattern of peak shaving is almost identical to the L&P combined scenario, which indicates that the contribution from load shifting to cost-saving is very minimal in the L&P combined scenario. Depending on the control flexibility of each zone, the cost-saving potential at the building level (5 zones) may vary from 13% to 32%.

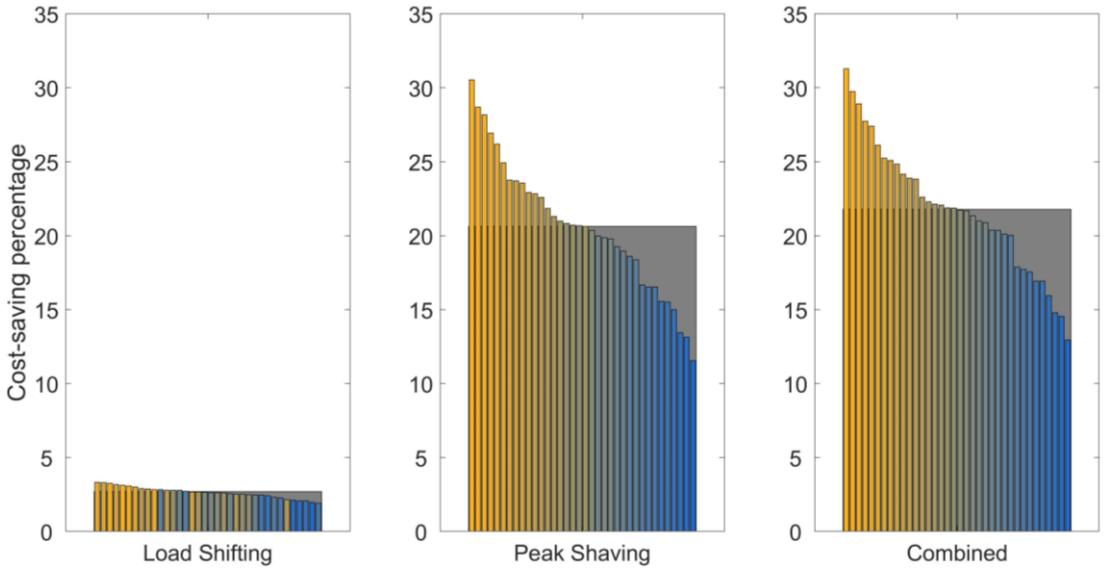

Figure 3.6 Cost-saving percentage at the building level

In addition, the zonal cost-saving percentage is plotted in Figure 3.7. The color bars represent the cost-saving percentage of all individual zones, and the grey box represents the zone under traditional control flexibility. From the result, the cost-saving percentage between zone-categories shares a very similar value and profile. Even though this study is based on a small office building, it is reasonable to believe that the cost-saving potential based on the center zone is extendable to reflect the potentials of medium and large office buildings, since the building size is defined by its form factor, which can also be interpreted as the relative size of its center zones (see 3.2.4.1)

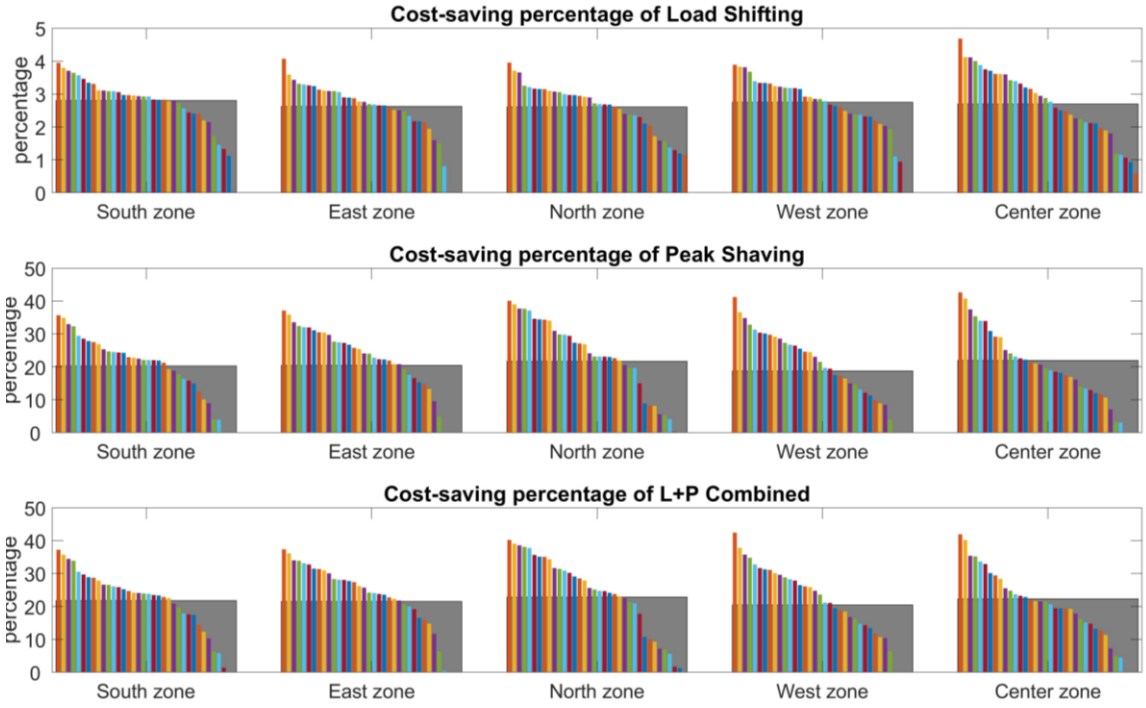

Figure 3.7 Cost-saving percentage of individual zone

3.2.3 Potential of organizational benefit increase

Since in baseline scenarios (T2, A2) the temperature is maintained at the value where the maximum productivity occurs, the OB increased from optimized control is minimal. Table 3.4 summarizes the comparative result from the scenarios with traditional control flexibility (T2, T6). Throughout the 4 months, there are only 14 USD increased from the baseline scenarios.

Nevertheless, the distribution of the total OB increase over 180 zones is shown in Figure 3.8, in which a more sparse distribution is observed comparing with the cost-saving potential. This distribution is concentrated at the same level as the OB increased from the traditional control flexibility. Since the increase of OB is marginal, there is no necessity for further analysis.

Table 3.4 OB in scenarios (T2 & T6)

	Baseline	Load Shifting + Peak Shaving	
	OB (USD)	OB (USD)	OB increase (USD)
June	1216634	1216639	5
July	1216549	1216552	3
August	1263284	1263287	4
September	1216681	1216684	2
Total	4913149	4913162	14

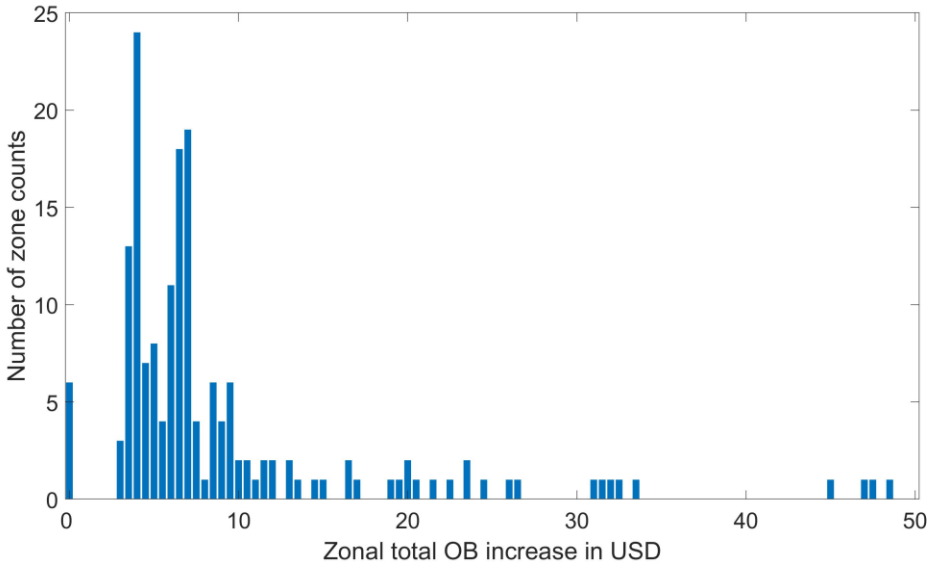

Figure 3.8 Zonal total OB increase by L&P control

3.2.4 Extensions

3.2.4.1 The cost-saving potential for medium and large office buildings

Due to the versatility of the MATLAB-based clear-box model, an experiment is further established to explore the cost-saving potential of the zones in medium and large office buildings. In the developed nodal-network, several connections represent the conductive heat transfer between the ceilings of office zones to the floor of the attic and between the floor of the office zones to the soil. Cutting off these connections makes this building to have adiabatic boundary conditions at the top and bottom and essentially to be

representable of an intermediate floor in medium or large office buildings. Other scenario configurations are kept the same as in T1, T3-T5. The result of cost-saving potentials in each zone category is shown in Figure 3.9.

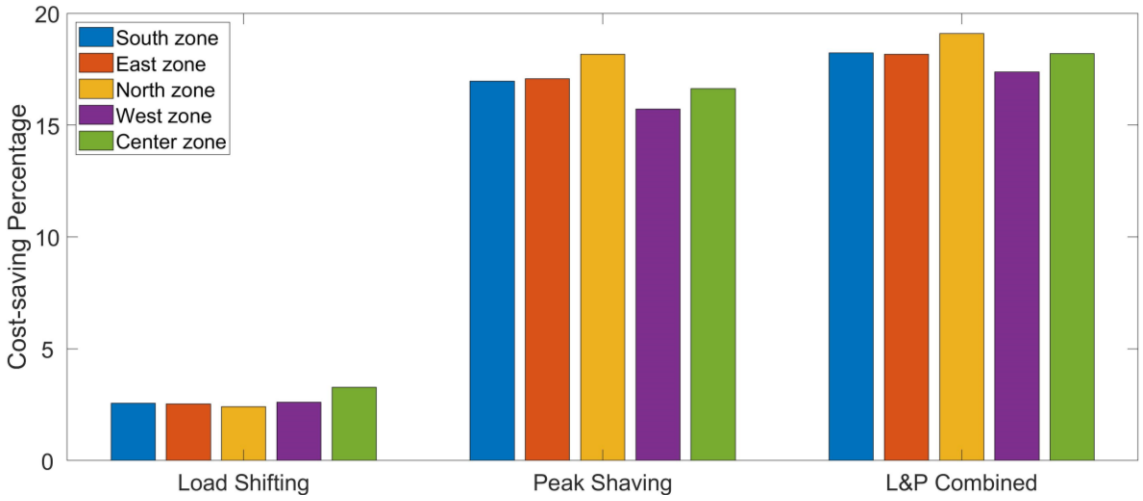

Figure 3.9 Cost-saving potentials in the zones of medium and large office buildings

From the result, the cost-saving potentials are very similar to the ones in the small office building. A touch of increased saving is observed at the center zone, but it is very subtle and case dependent.

3.2.4.2 OB at the condition of the zonal desired temperature

The results of this study can be further used to understand the OB profile under the condition of the zonal desired temperature. A comparison is made between the A1 and A2 scenarios, in which the zonal temperature profiles of scenario A1 are evaluated by the zonal productivity loss function. A summary is shown in Table 3.5, and the distribution of the OB loss of each zone is shown in Figure 3.10.

Table 3.5 Zonal OB comparison between A2 and A1 scenarios over 4 months

Mean OB of A2 (thousand USD)	Mean OB of A1 (thousand USD)	OB loss (thousand USD)
981.9	980.1	1.8

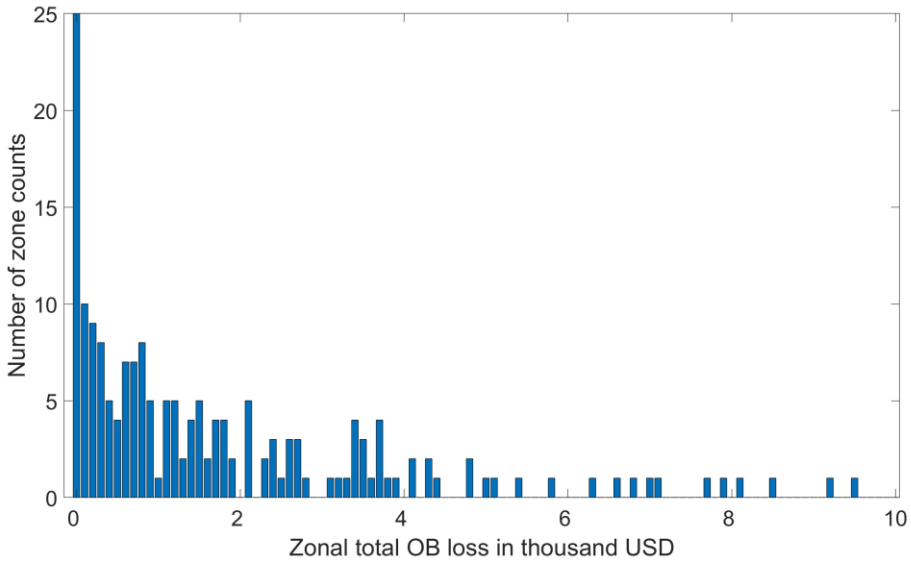

Figure 3.10 Zonal total OB loss in zonal desired temperature control

From the result, the zonal OB loss is not trivial if the zone temperature is not set to maximize productivity. Even though this result itself is irrelevant to the topic of building thermal load control, it shows the significance (weight) of the zone thermal environment to the occupants' productivity and OB, from which the minimal contribution of using L+P strategies in maximizing OB is explained.

3.3 Conclusion

Throughout this chapter, the individual & compounded contribution from load shifting and peak shaving are examined for their seasonal performance in cost-saving and maximizing OB. The methodology used in this chapter, a clear-box high fidelity model with linear or quadratic programming, proved to be effective and efficient in the MPC studies, especially for the analysis of potentials. The result shows that about 13%-32%

HVAC electricity cost can be reduced by combining adaptive load shifting and peak shaving strategies for typical small office buildings, but the contribution from pure load shifting by using passive thermal mass is very limited (1%-5%). The result is further proved to have the extendibility to reflect the control potential of medium and large office buildings. To be noticed, the embedded assumptions of the TOU rate and weather conditions limit the results to be applicable to buildings in similar circumstances. More analysis is performed in Chapter 4, which specifically discusses the performance of building thermal load control for varying climate zones and construction types.

Several lessons may be learned from this study. Firstly, the functionality of passive building thermal mass may be overestimated in the existing studies. The actual contribution of passive thermal mass in building thermal load control reflects only in the cost-saving potential of load shifting and "part" of the potential of peak shaving, when the room air temperature has not reached the upper bound. Secondly, the importance of zonal thermal condition is whelming the purpose of cost-saving under the evaluation by OB. It reflects the general observation that the purpose of using HVAC is not energy saving. Thirdly, it is crucial to know the zonal control flexibility before the implementation of dynamic control. Following the reference or standardized thermal requirement may be counterproductive for both cost-saving and maximizing OB, as illustrated in Figure 3.7 and Figure 3.10.

According to the conclusions mentioned above, the following chapters only focus on the cost-saving performance of building thermal load control. The reference control band used in the T3-5 scenarios in this chapter is exemplified in the studies that follow.

CHAPTER 4. COST-SAVING POTENTIAL ACROSS BUILDING TYPES AND CLIMATES

The study in this chapter is highly motivated by a recent literature review [85]. The authors point out that there exists a gap in the current studies in understanding the dominant disturbances of MPC. There is a need to gain a fundamental understanding, for a wide range of building types, climate zones, and building functions. Due to the fast run-speed of the clear-box model along with linear programming optimization illustrated in chapter 3, it is feasible and responsible for expanding the analysis of potentials to a much broader scale. Even though the outcomes in this chapter do not fill all of the gaps pointed out in [85], the performed theoretical analysis will nevertheless add to a better understanding of the underlying issues.

It has been proved in section 3.2.4 that the performance of building thermal load control derived for the small office building is very similar to, and hence representative of, the control performance for medium or large buildings. Thus, taking the small office building as the leading case, the saving potentials of building thermal load control will be examined for multiple variants of climates and building constructions. Three main research questions are proposed:

1) How is the variation in cost saving potentials influenced by climate?
2) How is the variation in cost saving potentials influenced by construction type?
3) What are the influential factors?

To answer these questions, 13 climates and 3 construction types are selected to construct all combinations of climate, construction type, and scenario. An in-depth analysis is then performed based on the simulation result to understand the influential factors, which leads to conclusions at the end of this chapter.

4.1 Climate conditions

4.1.1 Climate zones and selected cities

ASHRAE standard 169 [86] provides a zoning method based on heating/cooling degree days, month and season average temperature, and precipitation. The climate zones derived according to this method are broadly accepted and implemented in building codes and government guidelines for building design, construction, and system sizing [87] [88]. In order to provide a comprehensive analysis, this study covers most regions in the USA, which extends over 13 climate zones from 1A to 6B. One major city is selected in each climate zone as representative of its weather. The list of cities is shown in Table 4.1. The TMY3 files of the chosen cities are used in the following analysis.

Table 4.1 The list of cities in climate zone 1A to 6B

Climate Zone	City	State
1A	Miami	Florida
2A	Houston	Texas
2B	Phoenix	Arizona
3A	Atlanta	Georgia
3B	Las Vegas	Nevada
3C	San Francisco	California
4A	Baltimore	Maryland
4B	Albuquerque	New Mexico
4C	Seattle	Washington
5A	Chicago	Illinois
5B	Boulder	Colorado
6A	Minneapolis	Minnesota
6B	Helena	Montana

4.1.2 Time of use rate in cities

Due to the different state regulations, utility company strategies with different compositions of the energy sources, and the operation strategies of the electricity providers, designated on-peak/off-peak hours and time of use rates (TOU) differ in each city. A survey is conducted to summarize the schedule and unit price of the TOU rate for small office buildings in each selected city [89-98], listed in Table 4.2

Table 4.2 TOU rate plans in selected cities

City	Peak Months	Peak Hours	Unit Price (USD per kWh)	
			On-Peak	Off-Peak
Miami	April - October	12:00-21:00	0.11022	0.03774
Houston	June - September	13:00-19:00	0.116209	0.037379
Phoenix	May - October	14:00-19:00	0.1357	0.0529
Atlanta	June - September	14:00-19:00	0.16923	0.08198
Las Vegas	June - September	13:00-19:00	0.2194	0.05115
San Francisco	June - September	12:00-18:00	varies	
Baltimore	July - September	10:00-12:00	0.08316	0.05337
Albuquerque	All Year		0.17951	0.036767
Seattle	Flat Rate Only			
Chicago	Dynamic Hourly Price		varies	
Boulder	June - September	14:00-18:00	0.18	0.08
Minneapolis	June - September	09:00-21:00	0.1488	0.07919
Helena	June - September	12:00-18:00	varies	

The survey shows that the electricity companies in most cities provide TOU rate plans with two exceptions, Seattle and Chicago. From the reviewed information sources, the city of Seattle adapts a flat electricity rate at 0.19 USD per kWh, while Chicago is using the dynamic hourly price, which has a similar schedule to the TOU rate but with fluctuating rates in every hour.

For the cities where a TOU rate is implemented, the peak months are concentrated in summer, mostly from June to September, and the peak hours are mainly from 14:00-

19:00. The mean value of the on-peak and off-peak unit price is at 0.149 and 0.057 USD per kWh. Although the dollar amount of unit price in each city varies, the ratio of on-peak to off-peak unit price is similar, around 3.

Thus, to isolate the influence of weather conditions and construction type on the cost-saving potential, all the cities are assumed to have a uniform TOU schedule and rate, in which the peak months are from June to September, the peak hours are from 14:00 to 19:00, and the unit price for on-peak and off-peak hours are assumed at 0.15 and 0.05 USD per kWh, respectively.

4.2 Construction types

As many different types of envelope assemblies are being implemented in modern building design and constructions, it is hardly possible to include all construction types in this analysis. Thus, this study uses three typical exterior wall constructions based on their heat transfer properties, i.e., 1) light-weight exterior wall, 2) heavy-weight exterior wall with insulation on the inside ("heavy-in"), and 3) heavy-weight exterior wall with insulation on the outside ("heavy-out"). Conceptually, the heavy-out wall can store the most amount of energy and has a direct thermal connection to the thermal zone; the heavy-in wall has the same overall thermal capacity, but the heat transfer between the major thermal capacitor and the conditioned space is drastically reduced by the insulation layer; in contrast, the light-weight wall has low thermal capacity compared to both heavy-weight walls.

To reflect the realistic wall assemblies, the interior and exterior finishings are represented by a 20mm gypsum board and a 30mm stucco layers, respectively. The

thickness of the insulation layers in envelopes (including the wall, roof, ground slab, etc.) and the U-factor of windows are adjusted in each climate zone in compliance with the International Energy Conservation Code (IECC 2018) [99]. To be noticed, the wood-frame wall is required by the code to have higher overall insulation than the heavy-weight walls. The detailed wall assemblies are shown in Figure 4.1- 4.3.

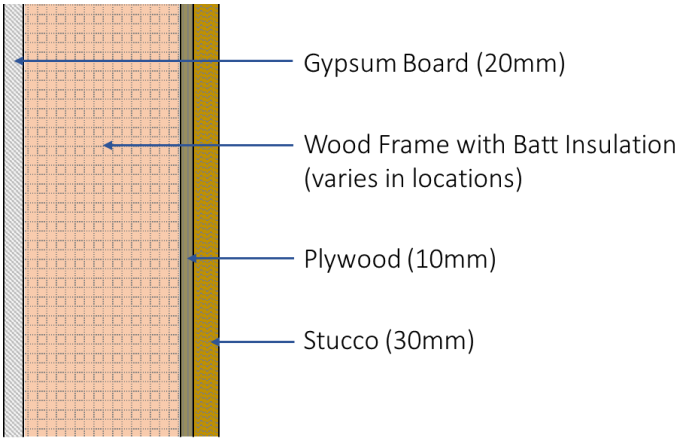

Figure 4.1 Construction of the light-weight exterior wall

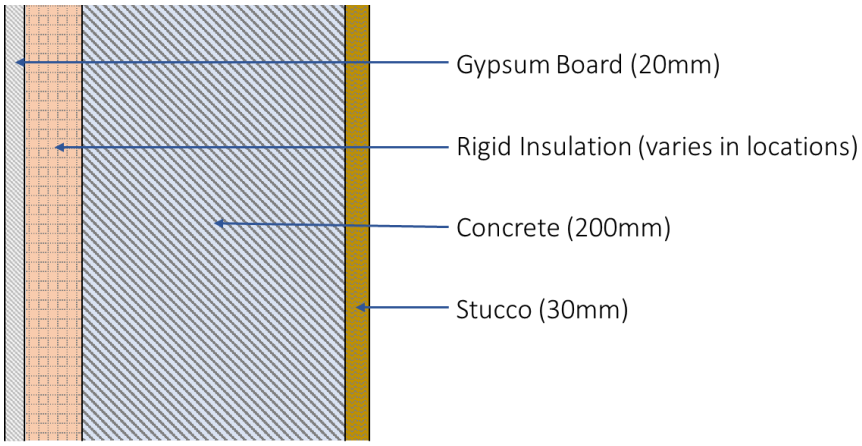

Figure 4.2 Construction of the heavy-weight exterior wall with insulation inside

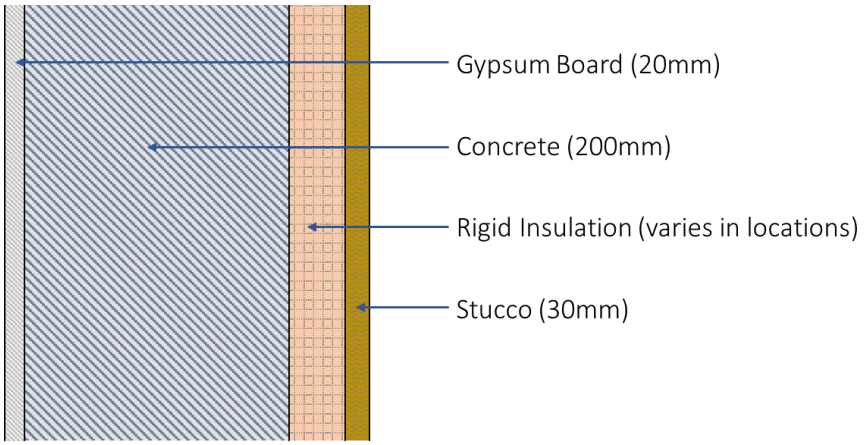

Figure 4.3 Construction of the heavy-weight exterior wall with insulation outside

4.3 Experiment results

The simulation scenarios adapted in this study are kept the same as the T1 and T3-5 scenarios established in Section 3.1.3, including the original temperature setpoint control ("original"), MPC with load shifting only ("load shifting"), peak shaving temperature setpoint control ("peak shaving"), and MPC with load shifting and peak shaving ("L+P"). Still, the original scenarios will serve as the baseline cases in calculating the cost-saving performance. The four scenarios are repeatedly applied to every building within the full combination of the 13 climate zones (cities) and 3 construction types. Therefore, 39 sets of simulations with 4 variant runs for each zone-construction combination are performed. The HVAC operation cost and the saving percentage (June to September) in all scenarios are listed in Table 4.3 and plotted in Figures 4.4 and 4.5. The cases are inspected in the same way as explained in section 3.2.1, which is omitted here.

Table 4.3 The seasonal HVAC energy cost, cost savings, and cost-saving percentage of all simulated scenarios

Climate zone	City	Construction Type	Seasonal HVAC Energy Cost (USD)				Cost Savings (USD)			Cost-saving Percentage		
			Original	Load Shifting	Peak Shaving	L+P	Load Shifting	Peak Shaving	L+P	Load Shifting	Peak Shaving	L+P
1A	Miami	Light	1697.90	1592.31	1339.57	1258.85	105.60	358.33	439.05	6.22%	21.10%	25.86%
		Heavy-in	1751.25	1648.50	1389.12	1310.16	102.75	362.13	441.09	5.87%	20.68%	25.19%
		Heavy-out	1771.46	1682.63	1404.36	1338.66	88.82	367.10	432.79	5.01%	20.72%	24.43%
2A	Houston	Light	1593.50	1481.77	1237.46	1152.58	111.73	356.04	440.92	7.01%	22.34%	27.67%
		Heavy-in	1643.50	1535.50	1282.94	1200.86	108.00	360.56	442.64	6.57%	21.94%	26.93%
		Heavy-out	1661.31	1567.75	1296.82	1228.58	93.57	364.50	432.74	5.63%	21.94%	26.05%
2B	Phoenix	Light	1887.27	1781.37	1574.72	1479.84	105.90	312.55	407.42	5.61%	16.56%	21.59%
		Heavy-in	1971.43	1868.35	1659.65	1568.42	103.08	311.78	403.01	5.23%	15.81%	20.44%
		Heavy-out	1995.27	1904.20	1673.96	1594.11	91.08	321.31	401.16	4.56%	16.10%	20.11%
3A	Atlanta	Light	1219.88	1114.47	901.94	829.01	105.41	317.94	390.87	8.64%	26.06%	32.04%
		Heavy-in	1246.87	1145.11	926.13	855.10	101.76	320.74	391.77	8.16%	25.72%	31.42%
		Heavy-out	1258.45	1171.91	935.26	876.48	86.54	323.19	381.97	6.88%	25.68%	30.35%
3B	Las Vegas	Light	1389.58	1294.20	1120.40	1043.87	95.38	269.18	345.71	6.86%	19.37%	24.88%
		Heavy-in	1435.39	1344.55	1164.94	1089.68	90.84	270.45	345.70	6.33%	18.84%	24.08%
		Heavy-out	1451.82	1374.03	1176.94	1114.72	77.79	274.88	337.11	5.36%	18.93%	23.22%
3C	San Francisco	Light	380.30	325.36	202.04	194.45	54.95	178.26	185.86	14.45%	46.87%	48.87%
		Heavy-in	367.01	313.93	191.69	184.59	53.08	175.32	182.42	14.46%	47.77%	49.71%
		Heavy-out	361.70	314.95	190.25	184.40	46.75	171.45	177.31	12.93%	47.40%	49.02%
4A	Baltimore	Light	937.16	838.30	644.00	592.21	98.86	293.15	344.94	10.55%	31.28%	36.81%
		Heavy-in	948.45	851.89	653.72	602.10	96.57	294.73	346.35	10.18%	31.08%	36.52%
		Heavy-out	952.72	871.58	656.95	614.81	81.14	295.77	337.92	8.52%	31.04%	35.47%

Table 4.3 The seasonal HVAC energy cost, cost savings, and cost-saving percentage of all simulated scenarios (cont.)

Climate zone	City	Construction Type	Seasonal HVAC Energy Cost (USD)				Cost Savings (USD)			Cost-saving Percentage		
			Original	Load Shifting	Peak Shaving	L+P	Load Shifting	Peak Shaving	L+P	Load Shifting	Peak Shaving	L+P
4B	Albuquerque	Light	821.70	744.68	581.65	536.71	77.02	240.05	284.99	9.37%	29.21%	34.68%
		Heavy-in	831.28	755.63	589.82	545.27	75.64	241.45	286.01	9.10%	29.05%	34.41%
		Heavy-out	835.13	771.21	592.61	556.18	63.92	242.52	278.95	7.65%	29.04%	33.40%
4C	Seattle	Light	394.25	327.82	203.58	192.02	66.43	190.67	202.23	16.85%	48.36%	51.29%
		Heavy-in	389.10	324.04	199.79	188.54	65.06	189.31	200.56	16.72%	48.65%	51.54%
		Heavy-out	383.52	328.53	197.70	189.37	54.99	185.81	194.14	14.34%	48.45%	50.62%
5A	Chicago	Light	830.25	735.26	560.16	513.78	94.99	270.09	316.47	11.44%	32.53%	38.12%
		Heavy-in	837.23	743.98	566.19	519.68	93.26	271.04	317.55	11.14%	32.37%	37.93%
		Heavy-out	838.59	761.38	566.97	529.39	77.21	271.62	309.19	9.21%	32.39%	36.87%
5B	Boulder	Light	544.39	474.33	337.32	313.56	70.06	207.07	230.83	12.87%	38.04%	42.40%
		Heavy-in	544.91	475.91	337.60	313.92	68.99	207.31	230.99	12.66%	38.04%	42.39%
		Heavy-out	542.20	484.37	335.66	317.29	57.83	206.54	224.92	10.67%	38.09%	41.48%
6A	Minneapolis	Light	613.34	522.30	373.23	343.42	91.04	240.11	269.92	14.84%	39.15%	44.01%
		Heavy-in	614.99	525.03	374.61	344.93	89.96	240.39	270.06	14.63%	39.09%	43.91%
		Heavy-out	612.04	537.88	372.85	349.96	74.16	239.19	262.08	12.12%	39.08%	42.82%
6B	Helena	Light	395.44	331.32	215.46	200.72	64.11	179.98	194.72	16.21%	45.51%	49.24%
		Heavy-in	394.32	330.94	214.75	200.20	63.38	179.57	194.12	16.07%	45.54%	49.23%
		Heavy-out	388.56	335.68	211.88	201.13	52.88	176.68	187.43	13.61%	45.47%	48.24%

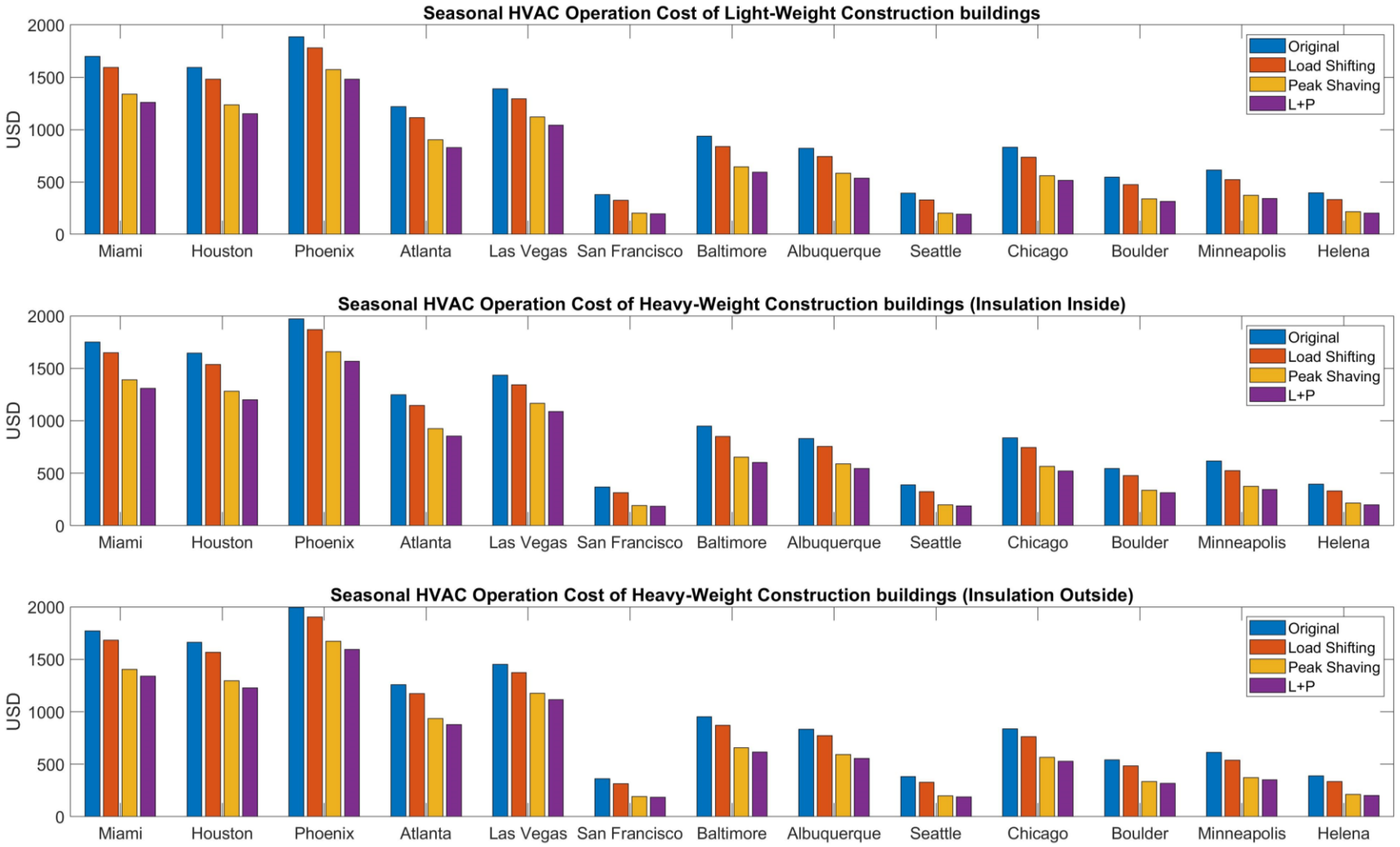

Figure 4.4 Seasonal HVAC operation cost of all simulated scenarios

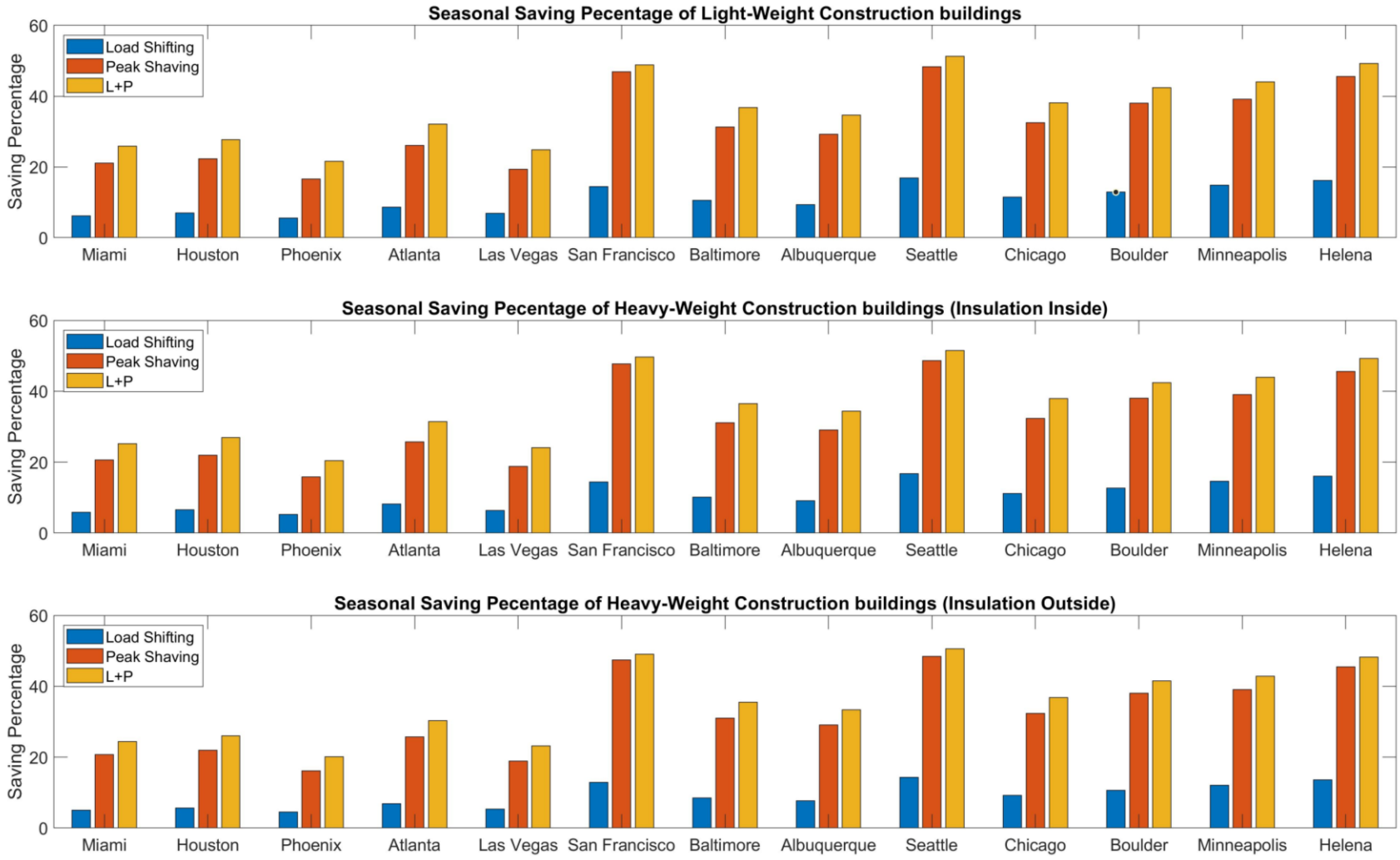

Figure 4.5 Seasonal cost-saving percentages of all simulated scenarios

The results show that all climate zones can benefit from building thermal load control in terms of reducing HVAC operation costs. Higher absolute cost savings are seen in the hot climates, i.e., Miami, Phoenix, etc., and higher cost-saving percentages occur in the marine and cold climates, i.e., San Francisco, Seattle, Minneapolis, etc. It has been proved in chapter 3 that the strategy of peak shaving reduces the contribution of load shifting in L+P scenarios. This effect is more evident in the result of the marine climates, as the extra cost-saving amount from peak shaving as part of L+P scenarios is much less than the cost-saving from load shifting alone.

The difference in cost-saving performance caused by construction type is less significant than the variation of the performance resulting across climate zones. Among all the construction types in all climates, the light-weight construction leads to the lowest energy cost and the highest cost-saving percentage in all scenarios. The heavy-in construction is observed to have a higher cost-saving percentage than the heavy-out construction in both load shifting and L+P scenarios in all climates. The buildings with the heavy-out construction turn out to have the highest energy cost and the lowest saving percentage in most of the cases. This result is virtually contrary to the expectation introduced in section 4.2. A possible reason could be that the three construction types have the same inside layer (20mm gypsum board) on the exterior walls, and the building thermal load control can only utilize a thin layer of the constructions for thermal energy storage. Hence, the different constructions beneath the gypsum board would have very little influence on the control performance. In the light-weight and heavy-in constructions, the cooling energy stored in the gypsum board layer is maintained by the adjacent insulation,

while the concrete layer in the heavy-out construction absorbs this storage, which results in the cases with heavy-out wall to have the worst performance.

4.4 Analysis of influential factors on cost saving potential

In order to understand the influence of climate, the correlation table and scatter plots are adopted to show the relationship between the saving performances and characteristic weather inputs. From this, a regression model is established to provide quick evaluations of the saving in other locations.

Since the influence of climate on seasonal (yearly) saving is fundamentally the cumulative effects of daily weather conditions, the analysis in this section is performed based on daily simulation results. To further expand the sample size, different construction types are also included in the analysis. Thus 3 sets of samples representing the daily saving percentage of load shifting (S_L), peak shaving (S_P), and both L+P (S_B) scenarios are constructed respectively, containing 3393 samples in each set.

The weather parameters used as the simulation inputs include dry bulb temperature of outdoor air (T_a), sky temperature (T_s), and global horizontal radiation intensity (Q_s). The daily mean ($\bar{T}_a$, $\bar{T}_s$, $\bar{Q}_s$) and variation ($\tilde{T}_a$, $\tilde{T}_s$, $\tilde{Q}_s$) of these variables are considered as the independent variables of parameterized weather conditions. The daily mean values of the variables are calculated as the algebraic average of the values over 24 hours. The daily variation of each variable is defined as the amplitude of the daily harmonic (f=1/86400Hz) in the frequency domain through the Discrete Fourier Transform of the daily profile (24 data points included), shown in Equation 56-57.

The Discrete Fourier Transform can be formulated as:

$$\hat{f}_k = \sum_{j=0}^{n-1} f_j \mathrm{e}^{-\mathrm{i}2\pi\frac{jk}{n}}, for\ k = 0,1,2,\ldots,23 \tag{56}$$

Where f_j is the weather data at jth hour in a day ($n = 24$). $\hat{f}_k$ is the Fourier coefficient at kth frequency, and the daily frequency is at k=1 in this study. Denoting the T_a, T_s, Q_s as f, the amplitude λ_1 representing $\tilde{T}_a$, $\tilde{T}_s$, $\tilde{Q}_s$ is written as:

$$\lambda_1 = \frac{\hat{f}_1^2}{24} \tag{57}$$

Thus, the characteristics of the weather are parameterized, and the correlation matrix is calculated as:

$$\rho_{X,Y} = \frac{\mathrm{E}[(X - \mu_X)(Y - \mu_Y)]}{\sigma_X \sigma_Y} \tag{58}$$

Where $\rho_{X,Y}$ is the sample correlation coefficient between random variables X and Y, which has expected values μ_X and μ_Y and standard deviations σ_X and σ_Y. The correlation matrix is shown in Table 4.4, and a scatter plot of weather parameters and performance measures is shown in Figure 4.6.

Table 4.4 Correlation matrix of cost-saving percentage and weather parameters

	S_L	S_P	S_B	$\bar{T}_a$	$\tilde{T}_a$	$\bar{T}_s$	$\tilde{T}_s$	$\bar{Q}_s$	$\tilde{Q}_s$
S_L		0.791	0.827	-0.763	-0.110	-0.730	-0.134	-0.367	-0.443
S_P	0.791		0.991	-0.808	-0.056	-0.777	-0.092	-0.231	-0.312
S_B	0.827	0.991		-0.797	-0.052	-0.763	-0.084	-0.249	-0.330
$\bar{T}_a$	-0.763	-0.808	-0.797		0.185	0.927	0.207	0.405	0.451
$\tilde{T}_a$	-0.110	-0.056	-0.052	0.185		-0.093	0.906	0.603	0.533
$\bar{T}_s$	-0.730	-0.777	-0.763	0.927	-0.093		-0.019	0.157	0.236
$\tilde{T}_s$	-0.134	-0.092	-0.084	0.207	0.906	-0.019		0.466	0.411
$\bar{Q}_s$	-0.367	-0.231	-0.249	0.405	0.603	0.157	0.466		0.903
$\tilde{Q}_s$	-0.443	-0.312	-0.330	0.451	0.533	0.236	0.411	0.903	

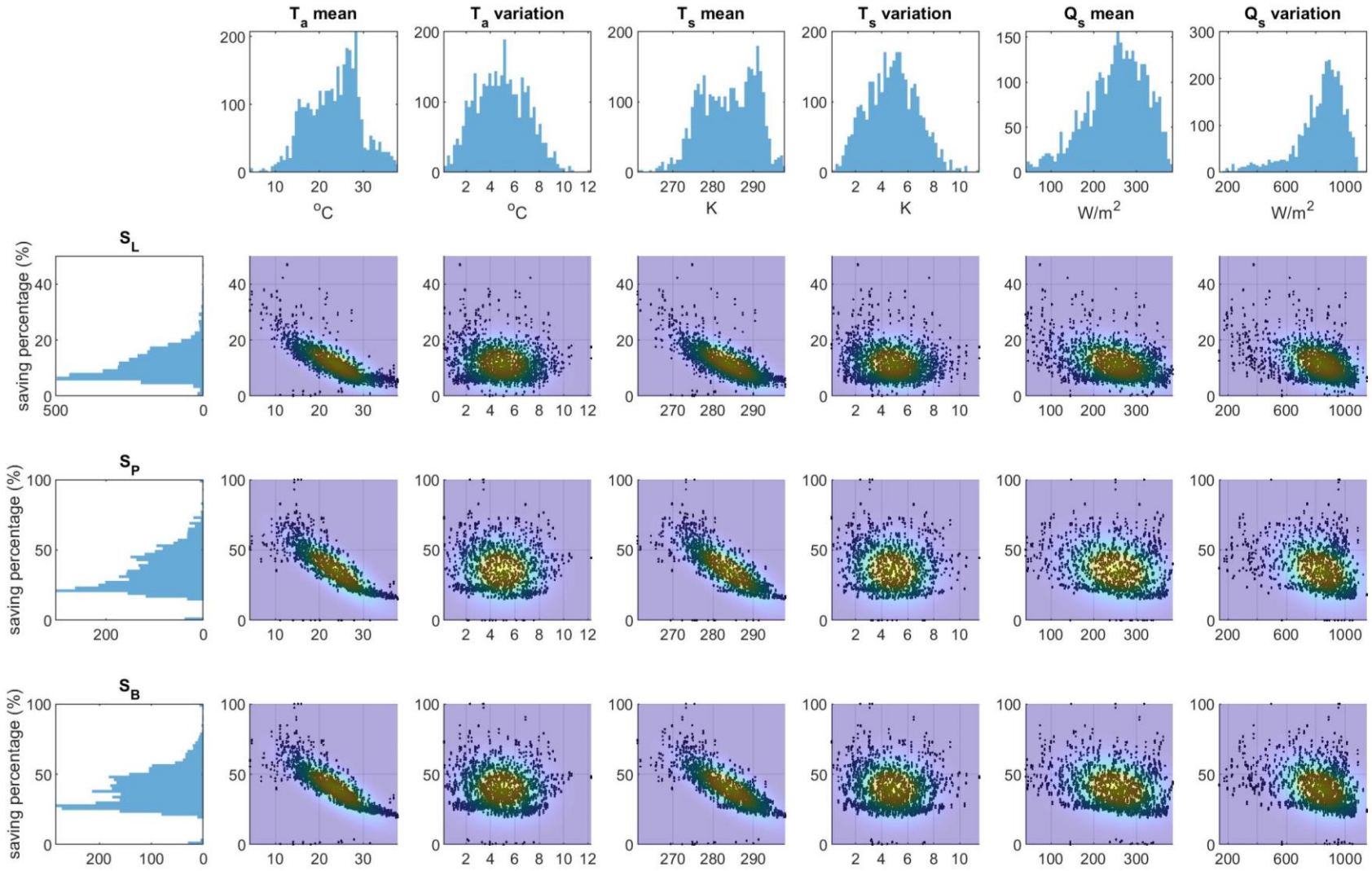

Figure 4.6 Scatter plots of weather parameters v.s. the cost-saving percentage in scenarios

The correlation table reveals that the performance of all control strategies is most correlated to the daily mean air temperature ($\bar{T}_a$), having a coefficient of about -0.8. The mean sky temperature ($\bar{T}_s$) is also showing a strong correlation with performance. This correlation, however, could mainly result from the dependency of sky temperature on air temperature since the effective sky temperature is suggested in multiple sources to be calculated from air temperature, relative humidity, and infrared radiation [100-102]. The variation of both air and sky temperatures ($\tilde{T}_a$, $\tilde{T}_s$) are observed to have insignificant correlations with performance, while the variation of solar radiation ($\tilde{Q}_s$) is more significant than its mean value ($\bar{Q}_s$), even though these two categories are highly correlated.

To be noticed, all weather parameters are showing negative-correlations to the saving percentage. This result is somewhat understandable in terms of the mean values. The cooler the outdoor condition is, the more gradually the room air temperature rises during the free-floating time; thus, more cost is saved in the peak hours. But more importantly, this result also proves that the building thermal load control is NOT, essentially, utilizing the fluctuation of weather conditions to reduce operation costs since the higher variation decreases the cost-saving percentage in all scenarios.

An emulator is built based on the analysis above. The goal of this emulator is to provide a deliverable and quick access method to evaluate the seasonal saving potential for a given location (climate) with tolerable accuracy. The same model form with different parameters is considered to predict the saving performance of load shifting, peak shaving, and L+P scenarios, respectively. Since the influence of construction type on saving is

minimal, the characteristic of building thermal mass is not included as an input parameter in this emulator.

To increase the degree of freedom hence accuracy, the emulator is constructed in a bottom-up form. In which the saving percentage of each workday is predicted in the first place. Then the seasonal saving percentage of all workdays is acquired as the average of the daily saving weighted by original energy cost. Finally, a coefficient is applied to the seasonal-workday saving to calculate the overall seasonal saving performance. The general form is shown in Equation 59-60

$$S_{season} = c \sum_{d} w_d S_d \tag{59}$$

$$w_d = \frac{C_d}{\sum_d C_d} \tag{60}$$

Where S_{season} is the seasonal saving percentage, S_d is the daily saving percentage, and w_d is the weighting factor, which is calculated from the daily energy cost in the original scenario (C_d). c is the coefficient that indicates the ratio of the energy cost between all workdays and the whole season.

Inspecting Figure 4.6 shows that nonlinearity exists between the weather parameters and the saving. In order to capture the nonlinear correlations while keeping the simple form of the model, the second-order polynomial regression models are employed to calculate S_d of each scenario and C_d, in the form as

$$Y = X\beta \tag{61}$$

Where Y represents the S_d in scenarios and C_d, X is the input variables which contains 13 parameter categories as $\{\bar{T}_a^2, \tilde{T}_a^2, \bar{T}_s^2, \tilde{T}_s^2, \bar{Q}_s^2, \tilde{Q}_s^2, \bar{T}_a, \tilde{T}_a, \bar{T}_s, \tilde{T}_s, \bar{Q}_s, \tilde{Q}_s, 1\}$, where β is the regression coefficient. The daily saving percentage over 13 climate zones, including 3393 samples in each scenario, is used as the training data sets. The developed emulator is then tested based on the saving percentage in the climate conditions of 3 other locations (3A – New Orleans, 3C – Los Angeles, and 5A – Boston). The training error of the regression models are shown in Table 4.5 and plotted in Figure 4.7, and the training error of the emulator is shown in Table 4.6 and plotted in Figure 4.8.

Table 4.5 Training error of the regression models

Regression model	R-squared	Residual mean	Residual std. deviation*
Saving Load shifting (%)	0.6747	-2.95E-15	3.3%
Saving Peak shaving (%)	0.7754	-1.24E-14	6.7%
Saving L+P (%)	0.6747	-8.21E-15	7.7%
Original Cost (USD)	0.9118	1.94E-13	1.81 USD

*Assuming normal distribution

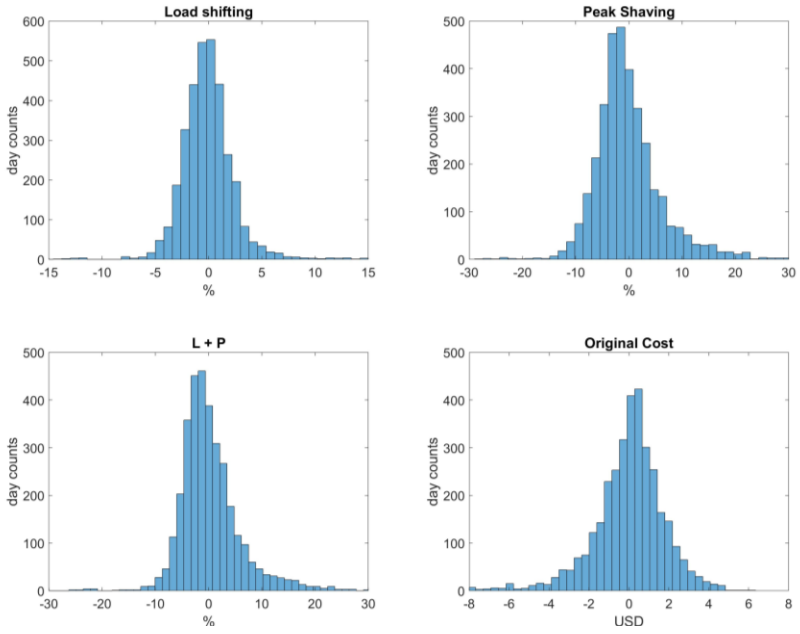

Figure 4.7 The distributions of the training error of the regression models

Table 4.6 Summary of the emulator's training error

Emulator to predict seasonal savings	R-squared	Residual mean	Residual std. deviation
Load shifting (%)	0.8482	0.03%	1.49%
Peak shaving (%)	0.9409	-0.47%	2.57%
L+P (%)	0.9461	-0.10%	2.50%

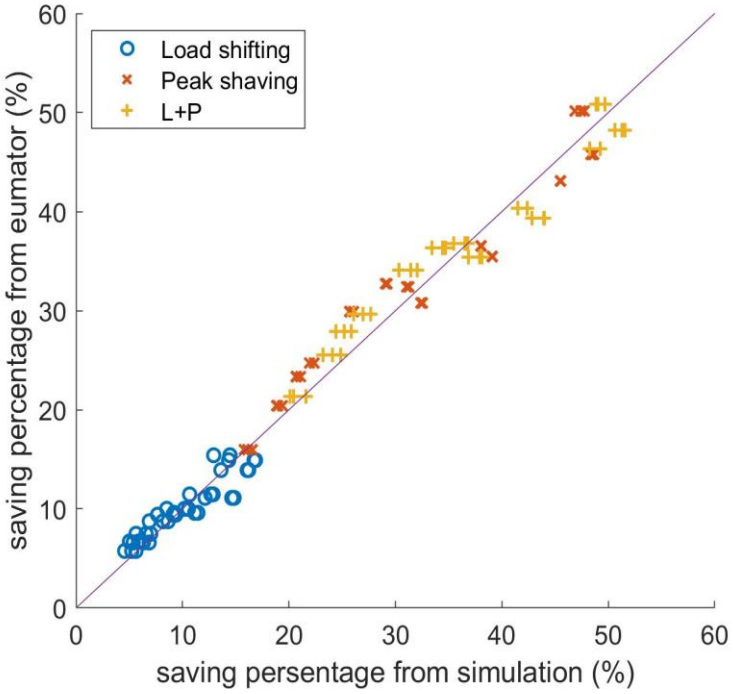

Figure 4.8 Q-Q plot based on the training dataset of the emulators

Even though the regression models are not providing very accurate results, the residual of the predictions of daily saving and original energy cost neutralize in the summation to seasonal performance. Taking this into account, the accuracy of the emulator is acceptable for preliminary analysis, having the R-squared value at around 0.9. The testing result of the emulator is shown in Table 4.7, 4.8.

Table 4.7 Testing result of the emulator

Climate Zone	City	Strategy	Actual Saving			Predicted saving	Abs.Error (mean)
			Light Weight	Heavy In	Heavy Out		
2A	New Orleans	Load Shifting	7.14%	6.67%	5.71%	7.49%	0.98%
		Peak Shaving	22.89%	22.50%	22.48%	25.28%	2.66%
		L+P	28.22%	27.48%	26.60%	30.01%	2.57%
3C	Los Angeles	Load Shifting	11.77%	11.47%	9.96%	11.58%	0.64%
		Peak Shaving	37.06%	37.35%	37.33%	42.35%	5.10%
		L+P	40.63%	40.91%	40.18%	43.65%	3.08%
5A	Boston	Load Shifting	12.72%	12.51%	10.64%	11.04%	1.18%
		Peak Shaving	37.84%	37.79%	37.69%	36.21%	1.56%
		L+P	41.63%	41.60%	40.74%	39.82%	1.50%

Table 4.8 Summary of the emulator's testing error

Emulator to predict seasonal performance	R-squared	Residual mean	Residual std. deviation
Saving Load shifting (%)	0.7929	-0.19%	1.14%
Saving Peak shaving (%)	0.7594	-2.07%	3.44%
Saving L+P (%)	0.8445	-1.39%	2.52%

The test results confirm that the emulator can provide accurate predictions in most cases. An exception is observed at the peak shaving scenarios in the Los Angeles climate, having a prediction error of 5% (which is however still within the prediction interval). Additionally, the standard deviation of the residual remains at the same level as the training result, which proves that the emulator is not overfitted to the training data set. Thus, the effectiveness of this emulator is confirmed, and the detailed model form and parameters are shown in Appendix A.

4.5 Conclusion

This chapter provides a comprehensive analysis of the cost-saving potential of building thermal load control in different climates and wall construction types. The analysis reveals that climate conditions have a substantial influence on cost-saving percentage.

Depending on the climate, the seasonal cost-saving percentage can vary from 5%-20% in load shifting, 15%-45% in peak shaving, and 18%-48% in L+P scenarios. The in-depth analysis performed in 4.4 shows that the higher variation of daily weather conditions does not result in a higher saving percentage, which proves that the optimum strategy of building thermal load control does not rely on the fluctuation of weather conditions. Based on the outcomes, an emulator is developed to provide a quick estimation of the saving percentages in any given location.

In contrast, the construction types are observed to have minimal influences on cost-saving performance, showing 1%-3% discrepancies throughout all simulated scenarios. Among the construction types, the light-weight and heavy-in constructions can lead to higher cost savings than the heavy-out construction. A possible guess is that the building thermal load control can only utilize a thin layer of construction for load shifting, and the different construction layers behind are only serving as insulation of the internal finishing, i.e., without adding a capacity effect.

Back to the assumptions suggested at the beginning of this chapter that the unified TOU rate is used for all cities with 0.15/0.05 USD on/off peak. The validity of the simulation result and analysis highly rely on this assumption. The constructed emulator is effective to provide a quick estimation of the cost-saving potential for the new locations, if the TOU rate at this location have similar schedule and on/off peak price ratio as the assumption.

CHAPTER 5. COST-SAVING PERFORMANCE UNDER SCENARIO UNCERTAINTY

This chapter takes the discussion of building thermal load control in a direction that has practical significance. It addresses the influence of scenario uncertainties on cost-saving performance. This is important since in any real forward-looking optimal control, it is unavoidable to make guesses about building usage and other scenarios within the prediction time horizon of the control.

Scenario parameters are introduced to capture the inherent variability of internal and external scenarios that the building is subjected to [74]. This considers occupants as part of the (internal) environment. A "scenario parameter" is viewed as a "disturbance" that affects the building control system, which sees disturbances as non-controllable input that influences building behavior [85]. Following this reasoning, the scenario uncertainties in this study are defined as the discrepancy between the true environment of the building system and the predicted scenario parameters that are the inputs in the simulation model.

Due to the nature of MPC, which counts on knowing the future values of scenario parameters in the optimization, their uncertainty may affect the performance of MPC in the three consecutive steps of the procedure: 1) decreasing the accuracy of prediction models, 2) leading to suboptimal control sequences, and 3) reducing thermal comfort and cost-saving. To be noticed, the consequences in these three steps may not necessarily be magnified during the process. For example, a certain MPC may have inaccurate predictions

of the building states but can capture the increase/decrease trend of the states correctly, then the generated control sequence of cooling/heating is still acceptable.

Very few studies have directly investigated the influence of scenario uncertainty on MPC performance. In [103], the impact of the weather forecast on predictive optimal control of active and passive building thermal storage is evaluated. Five weather prediction models are analyzed in four geographic locations, and the simulation is performed on a 3-story office building model. With the predictive control outcome under the perfect predicted weather serving as the benchmark, the best weather prediction mode analyzed in this literature leads to only a marginal increase in the total HVAC energy cost. In contrast, the authors of [37] examine the potential applications of MPC on the combination of multiple building features, including the HVAC system, electric lighting, natural ventilation, etc., and compare the energy usage of the theoretical optimal scenario and the ones based on imperfect weather predictions. A single-zone RC model is employed as the building/prediction model in the experiment, in which 18 cases over 4 geographic locations are included. The result shows that the imperfect weather prediction can heavily influence the performance of MPC, resulting in the violation of thermal comfort and the increase of energy usage, and in some cases, the MPC is affected to have even worse performance than the original rule-based control. In [104], the effect of weather forecast uncertainty on MPC is inspected based on zones in different orientations and with varying types of construction. The normalized energy use is chosen as the outcome measure in the evaluations. The conclusion the authors draw from this study is that the uncertainties in weather forecasts have less influence on the MPC performance in scenarios with heavy thermal mass, and

the performance of the controls in case of light thermal mass is more sensitive to the accuracy of solar irradiance forecast.

The influence of occupancy and internal heat gain on building climate control is investigated in [105], in which the performance of MPC with perfect occupancy prediction is compared with the ones using a presumed standard profile. Similar to the study performed in [37], the control variables configured in this study include HVAC operation, blind position, electrical lighting, etc. From the results, compared to the scenarios that use assumed occupancy profiles, up to 15% extra energy savings are realized in scenarios with (hypothetically) full-knowledge of future occupancy. An analogous study is done in [106], which inspects the performance of different control strategies with different levels of knowledge in occupancy profiles. The zonal simulation is performed on a 10-node RC model, and the supply air temperature and mass flow rate of the HVAC terminal unit are used as control variables. From the result, up to 55% of energy saving is realized if the future occupancy profile is assumed to be known, and at least 45% of energy saving is observed if only the occupant number is measured.

Inconsistent or even incomparable results are seen in the reviewed literature, mainly due to the difference in 1) representations of the building, 2) boundary of controllability, and 3) definition of the contribution of MPC. The details of these 3 aspects are discussed in Chapter 1. Despite the differences, two things are common across all studies. Firstly, the passive building thermal mass is utilized as an energy capacitor or a “buffer” to facilitate MPC. Secondly, the HVAC system is the energy and hence cost “consumer”, which eventually enables the thermal comfort of the zone. In other words, no matter what add-on features of control are applied to the building, the passive thermal mass and HVAC system

are the core components of MPC. Thus, it is crucial and fundamental to investigate the influence of scenario uncertainties on the performance of MPC based solely on utilizing the passive thermal mass and HVAC system in the first place. The following research questions are intended to be answered in this study.

1) What is the influence of scenario uncertainties on the performance of MPC?
2) How big is the range of scenario uncertainty?
3) How significant is its influence?

5.1 Methodology

5.1.1 Definitions and Attributes

The sources, types, and influences of uncertainties in building energy performance prediction are extensively discussed in two dissertations in [107, 108] and in the review article in [74]. In order to fully understand the influence of scenario uncertainty in MPC, it is necessary to revisit these studies and properly allocate the research questions.

Considering a building as a complicated thermodynamic system, the status of all the components are evolving over time due to the interventions of environments (including occupants) and building equipment. Given x^* represents the status, u^* and w^* represent the influence of building equipment and environments, the true building state at the next time step is an unknown function f, in discrete form as

$$x_{i+1}^* = f(x_i^*, u_i^*, w_i^*) \tag{62}$$

A building model is established to interpret this system to mathematical equations and intended to reflect the dynamics of the system in certain degrees. The state-space form of a building model is shown in Equation 63.

$$x_{i+1} = Ax_i + Bu_i + Dw_i \tag{63}$$

Where x, u, and w are the believed representation of x^*, u^*, and w^*; A, B, and D are the state space, control space, and disturbance space operators, respectively. For a building model, even if all the required input parameters can be assigned the true value, the predicted states will not equal the actual state. The discrepancy between the two is referred to as model inadequacy or model form uncertainty. Theoretically, the model form uncertainty (ϵ_m) is quantified as

$$\epsilon_{m,i} = x^*_{i+1} - x_{i+1} = f(x^*_i, u^*_i, w^*_i) - (Ax_i + Bu_i + Dw_i) \tag{64}$$

Given a certain model form, the true value of the model parameters is hardly available, and the A, B, and D space yield to $A°$, $B°$, and $D°$ in the building model in Equation 65. The state x_i and control u_i are assumed to be the true values in Equation 65-67. The unsureness of the model parameters is defined as the parameter uncertainty, in which the prediction error (ϵ_p) is quantified in Equation 66.

$$x^o_{i+1} = A°x_i + B°u_i + D°w_i \tag{65}$$

$$\epsilon_{p,i} = x_{i+1} - x^o_{i+1} = (A - A°)x_i + (B - B°)u_i + (D - D°)w_i \tag{66}$$

As defined earlier in this chapter, the scenario parameters are considered with prediction error, which is defined as the scenario uncertainty. Therefore, the w term in

Equation 63 yields to $\widehat{w}$ in Equation 67. And the prediction error (ϵ_s), given x_i and u_i, is quantified in Equation 68.

$$\hat{x}_{i+1} = Ax_i + Bu_i + D\widehat{w}_i \tag{67}$$

$$\epsilon_{s,i} = x_{i+1} - \hat{x}_{i+1} = D(w_i - \widehat{w}_i) \tag{68}$$

In some situations, the control input u_i is also influenced by scenario uncertainties, i.e., the solar heat gain blocked by controllable window blinds or the energy flow rate from the HVAC system based on on/off control. The control inputs u_i in these two cases are dependent on the scenario parameters, hence uncertain. But in this study, it is more reasonable to assume u_i to be exact, and the influence of scenario uncertainty on control variables is migrated in the estimation of the energy consumption of the HVAC system, given in Equation 69. Where the $\widehat{\omega}_i$ is the predicted energy consumption, and the $\widehat{COP_i}$ is estimated based on future weather parameters, given in Equation 31 in Chapter 3.

$$\widehat{\omega}_i = \widehat{COP_i}^{-1} u_i \Delta t \tag{69}$$

Since the influence of scenario uncertainty is the only focus in this chapter, it is reasonable to assume 1) the building model can fully represent the building system, and 2) all parameters in the building model are exact. Which means there is no model form nor parameter uncertainties ($\epsilon_m = 0$, $\epsilon_s = 0$). Therefore, the prediction model with scenario uncertainty can be written in Equation 70.

$$x_{i+1} = Ax_i + Bu_i + D\widehat{w}_i + \epsilon_{s,i} \tag{70}$$

5.1.2 Definition of the influence of scenario uncertainties on MPC

According to Equation 67, the non-recurrent linear system is rewritten as in equation 71-72. The U, Ψ, Φ, and Θ are kept the same formulation as in Equation 44-49 in Chapter 3.

$$\hat{X} = \Psi \hat{x}_i + \Phi U + \Theta \widehat{W} \tag{71}$$

Where

$$\widehat{W} = \{\widehat{w}_i;\ \widehat{w}_{i+1};\ \widehat{w}_{i+2};\cdots;\ \widehat{w}_{i+n-1}\} \tag{72}$$

The $\hat{x}_i$ is the initial state as an input in the MPC controller. The optimum control input $\widehat{U}$ under scenario uncertainty can then be derived with the usual LP formulation, shown in Equation 73-74. To be noticed, the $\hat{x}_i$, $\widehat{U}$, and $\widehat{W}$ are all estimated values but from different predictors, $\hat{x}_i$ is from the state estimator, $\widehat{W}$ is from scenario parameter predictor, and $\widehat{U}$ is from MPC optimization.

$$\widehat{U}_i = \underset{U_i}{argmin}\, R_i \widehat{\Omega}_{i(U_i)} \tag{73}$$

$$X_{lb,i} \leq \hat{X}_i \leq X_{ub,i} \tag{74}$$

Where the subscript i denotes that the optimization is run at the i^{th} control interval, $\widehat{\Omega}_i = \{\widehat{\omega}_i;\ \widehat{\omega}_{i+1};\ \cdots;\widehat{\omega}_{i+n-1}\}$ where $\widehat{\omega}_i$ as given in Equation 69, and R_i is the electricity price over the prediction horizon.

Due to the prediction error resulting from scenario uncertainties, it is undoubtedly possible that the room air temperature can go beyond the comfort band. Therefore, the influences of scenario uncertainties have to be evaluated from both ends by energy cost

and thermal comfort measures. To avoid this twofold evaluation and also to reflect the reality, one control logic is added on top of the control sequences provided by MPC ($\widehat{U}_i$), namely an "insurance" control. Assuming the lower and upper temperature band (x_{lb}, x_{ub}) is known, the HVAC system follows the MPC as long as the room air temperature is within the comfort band. If the room air temperature exceeds the upper or lower bound in a certain timestep, the thermostat will overwrite the control sequence from MPC by temperature setpoint control until the end of the timestep, shown in Equation 75.

$$u_{j,k}^{*} = \begin{cases} \hat{u}_{j,k}, & if \quad x_{lb,j+1} \le \hat{x}_{j+1,k} \le x_{ub,j+1} \\ B_k^{-1}(x_{ub,j+1} - (A_k x_j + D_k w_j)), & if \quad \hat{x}_{j+1,k} \ge x_{ub,j+1} \\ 0, & if \quad \hat{x}_{j+1,k} \le x_{lb,j+1} \end{cases} \tag{75}$$

Where j is the time step in the building model rather than the MPC model, k represents a specific thermal zone, $\hat{u}_{j,k}$ is the control input predicted by MPC, and $u_{j,k}^{*}$ is the control input applied in the zone. A_k, B_k, and D_k are the rows which relate to zone k in the spaces A, B, and D. From the equation, this insurance control is implemented as a one-step predictive control in the simulation, which is coincidentally very similar to the control logic used in standard EnergyPlus runs. But in reality, the insurance control has the same logic as the temperature setpoint control currently implemented in the thermostats, which is a feedback control and does not require predictions. Thus, the insurance control is not influenced by scenario uncertainties. To the author's belief, using the combination of MPC and this so-called insurance control is more realistic in implementations than letting the MPC running "free".

Two scenarios are in comparison, 1) a building with the HVAC system controlled by MPC using the exact scenario parameters, and 2) the same building, HVAC system, and

MPC controller but with uncertain scenario parameters. And the difference in HVAC operation cost between these two scenarios is defined as the influence of scenario uncertainty on MPC (ΔC), given in Equation 76.

$$\Delta C = R(\Omega - \widehat{\Omega}) \tag{76}$$

To be noticed, the peak shaving strategy in building thermal load control is simply a schedule-based control that does not require MPC. Deliberately using MPC only to realize peak shaving is counterproductive as it results in the amplification of the influence of scenario uncertainty. Thus, the load shifting and L+P strategies are investigated individually, and the peak shaving strategy is removed from consideration in this chapter.

5.2 Uncertainty range

As the prerequisite to investigate the influence of scenario uncertainties, a plausible range of uncertainties has to be available. Assuming the building and MPC model are kept the same as in previous chapters, there are five categories of scenario parameters considered uncertain in this study: 1) ambient temperature (T_a), 2) sky temperature (T_s), 3) global horizontal radiation (q_{GH}), 4) occupancy heat gain (q_{Occ}), and 5) lighting and equipment heat gain (q_{LP}). T_a, T_s, and q_{GH} are considered as weather parameters, whereas q_{Occ} and q_{LP} are considered as internal heat gain parameters. The acquisition and prediction of these two sets of parameters are discussed in the following.

5.2.1 Literature review on prediction methods

5.2.1.1 Weather prediction

The most convenient way to obtain predicted weather parameters is from online weather forecast services, which provides forecasts based on advanced climate models [85]. [109] and [110] are two analysis reports, from a weather forecast monitoring company, that investigate the forecast accuracy of several commercial weather forecast providers. In the reports, the comparison is made in terms of the errors in one-day-ahead air temperature prediction. The most accurate forecast model can manage the prediction error (RMSE) below 1.5 ℃ in summer months and about 1.8 ℃ during winter. Nowadays, most commercial weather forecast providers offer an API to users at an affordable cost, and obtaining the weather forecast online does not require any installation and maintenance of the instrument on-site. These two advantages make it an easy-to-use method for obtaining predicted weather parameters from online forecast services. But this method has two drawbacks. Firstly, the online weather forecast is generated based on the weather station data that can be far away from the building itself. The prediction error is enlarged, resulting in not only more variation but also biased prediction. Secondly, since the online weather forecast is designed for accommodating routine daily use, the data categories provided by the online weather forecast may not fulfill the input categories of building models. For example, the solar radiation intensity is a commonly used input parameter in building models, but this parameter is usually represented by the sunshine index or UV index in weather forecasts. Thus, extra calculations are required in most situations.

On the other hand, local weather forecast methods are extensively studied throughout the past 50 years. The literature reviews in [111-115] reflect on a clear road map of the evolution of the methods in addressing this topic. Mainly due to the computational power, the deterministic and analytical models are prevalent in the early

stages, and the stochastic and adaptive models based on machine learning techniques are currently in the mainstream. Along with more applications of PV systems in recent years, localized weather forecast models are under development, which aims to provide short-term high-resolution predictions [116]. Presumably, a local forecast model can provide unbiased on-site predictions based on the locally installed weather station's data. With denoising algorithms, it can outperform online weather forecasts with higher prediction accuracy. But still, this method has its drawbacks in two aspects when applying to building simulations. Firstly, the locally installed weather stations, in most cases, have higher measurement errors compared to the data from commercial-use weather stations. Secondly, local weather stations require extra efforts of maintenance to ensure its functionality and accuracy. For example, the hourly weather data are drawn from the weather stations installed in Georgia Tech typically have up to 500 missing points in a one-year profile. It is feasible to fill the missing points by interpolation if the gap is relatively small. But for the gaps greater than the period of days, a reasonable weather forecast by solely using the weather station data is not possible.

5.2.1.2 Internal heat gain prediction

There is hardly any literature that suggests a consolidated method to predict internal heat gain. The reason is that the internal heat gain is such an imaginary quantity that has no explicit way to measure it. One specific study addressing this question is offered in [117], in which the authors use a recurrent neural network (RNN, long short-term memory to be exact) to predict the internal heat gain profile with 24 hours. The miscellaneous electricity load (MEL), lighting load, and occupant count profiles from the past are taken as the model input to predict the internal heat gain profiles in the future. The prediction

error (relative rooted mean square error or rRMSE) is around to be 7-9% for the case study building with lower internal gain fluctuations and 12-18% for the building with higher fluctuations, which outperforms the prediction based on the ASHRAE reference profile (uncalibrated) for internal heat gain. But as mentioned earlier, the training of the prediction model does require the measured internal heat gain. In this study, it is calculated by a deterministic equation taking MEL, lighting loads, and occupants count as inputs. It must be recognized that the functionality of this RNN is fundamentally to predict the future MEL, lighting, and occupancy based on past profiles.

Except for the methods that generate an independent prediction on future internal heat gains, some studies also provide the methods to estimate the lighting and plug load based on occupancy and reveal the interrelations between these parameters. In [118], an analytical model is formulated to estimate the energy consumption of office equipment based on predetermined parameters such as working time, on-duty and off-duty time, and computer input power. In fact, most of these parameters are hardly measurable in daily building operations, but since it is an analytical model, it does not require actual measurement. The study presented in [119] investigates the relationship between the presence of occupants and the plug-load. The result shows that the personal plug load fraction can be very well estimated by a linear regression model taking the presence probability as the input when the regression model is personalized. If one regression model is employed to explain the same relationship for a group of 8 people, the accuracy drops drastically (from mean R^2>0.95 to R^2=0.7). A similar study is seen in [108], in which the author finds out that the correlation of the variation of the occupancy ratio and the lighting & plug load ratio can be explained by an AR(1) autoregression model.

Indeed, most of the estimation and prediction methods of internal heat gains are based on occupancy information, but occupants are hardly predictable in real life. As for building modeling and simulation purposes, the historical occupancy profile is essential in generating an unbiased mean profile serving as the simulation input. The historical profile is usually estimated from multiple types of sensors, including occupancy sensors, motion sensors, and AI-based vision sensors. A review of occupancy sensing techniques is seen in [120]. Alternatively, for experimental purposes, the occupancy profiles can be generated based on occupant behavior models. The details of various types of models are thoroughly discussed in the literature review in [121].

5.2.2 Experiment setups

Back to the discussion on MPC, the following assumptions are made in order to define the range of uncertainties properly. The assumption term with a hash sign (#) means this assumption only applies to certain setups discussed later in this section.

1) As used in previous chapters, the same 5-zone small office building is considered as the objective building. This building is located in Atlanta, GA. The building is assumed to have lightweight constructions, see Chapter 4. All the building models discussed below have the same model form, and all model parameters are exact.
2) #There is a weather station installed right at the location of the building. All data recorded by the weather station has no measurement error, and the measured data in the weather station does represent the external environment of the building, which means no measurement bias either. This is a very ambitious assumption and not possible to realize in actual settings.

3) The online weather forecast is always available, and the historical weather forecast is documented.
4) #The online forecast can be calibrated and modified based on the data recorded at the local weather station to produce local weather forecasts.
5) #There exists a certain type of "omnipotent sensor" to detect the exact internal heat gain from the past. Of course, this assumption is never reachable in reality. Nevertheless, by combining the read-outs from multiple sensors such as the electricity meter and occupancy sensor, a close estimation is possible.
6) #The mean profile of internal heat gain is derived from the "omnipotent sensor", which is used as the prediction of future internal heat gain profiles.
7) #The Kalman filter is used to estimate the full states of the building.

Depending on the different instruments installed on-site, the range of scenario uncertainties are different. Three setups of scenario parameters are defined at either scenario uncertainty source (weather prediction and internal heat gain prediction).

1) **The all-true setup.** In this configuration, the scenario parameters from the past and for the future are assumed to be exact and known, which sets up the baseline for analysis. The flow chart is shown in Figure 5.1.
2) **The best possible setup.** The scenario parameters from the past are known from the read-outs either in the weather station or the "omnipotent sensor", or both. Thus, there is no uncertainty in the past. And the prediction of the scenario parameters is modified based on historical data. (Figure 5.2)
3) **The current reality setup.** There has no recorded scenario parameter available. The weather parameters from the past are from historical online weather prediction,

and the past internal heat gain is from the ASHRAE reference profile with a good estimation. The online weather forecast and the ASHRAE reference internal heat gain profiles are also used for prediction. The errorless thermostat in each zone is the only direct measure of the building state. The full states that serve as the initial conditions for MPC are estimated from the Kalman filter. (Figure5.3)

In figure 5.1-5.3, the negative sign (-) indicates the states or parameters from the past steps, and the positive sign (+) indicates the scenario parameters for future steps. The star sign (*) indicates the variables that are exact or the same as the exact variables in the building system. The only purpose of the incidental model is to calculate or estimate the current states as the initial condition in MPC. Since the scenario parameters from the past are the same between the incidental and the building & HVAC models in the configurations in Figure 5.1 and 5.2, it is the same to initialize MPC using the building & HVAC model. In which the functionality of the incidental model is equal to having the direct measure of full states.

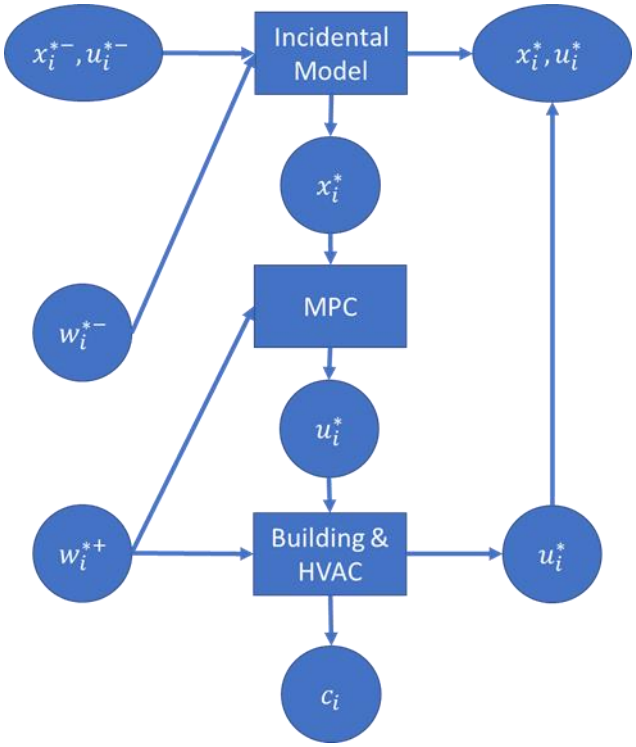

Figure 5.1 Control workflow of the "all-true" scenario setup

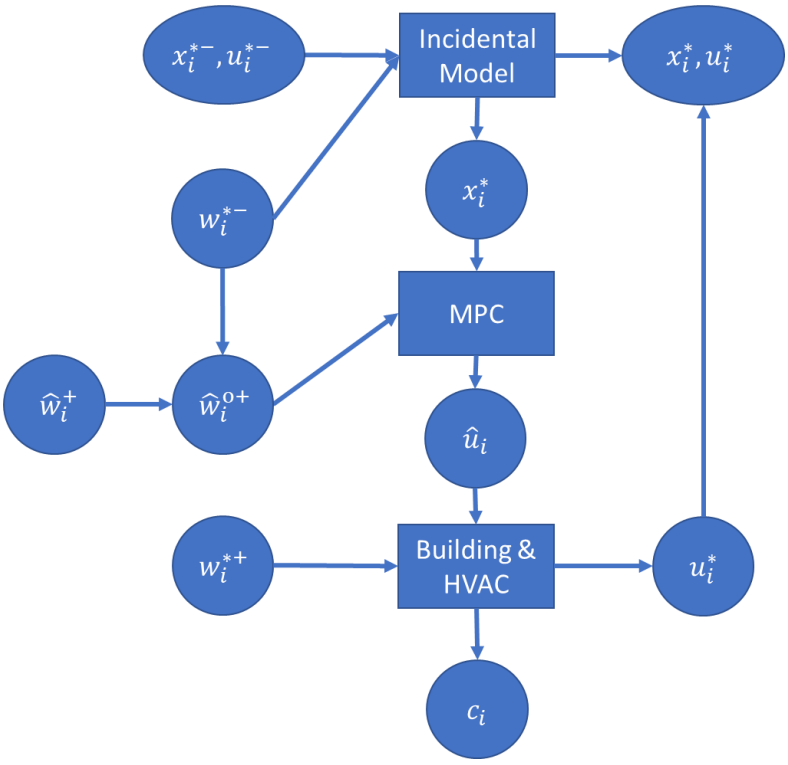

Figure 5.2 Control workflow of the "best possible" scenario setup

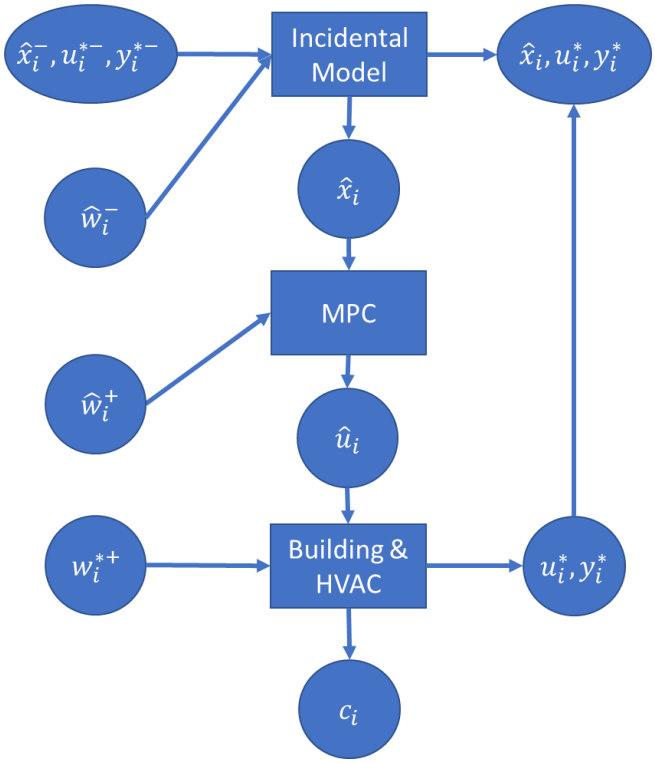

Figure 5.3 Control workflow of the "current reality" scenario setup

To thoroughly investigate the influence of scenario uncertainty on MPC, the full-combination of the three setups for both scenario uncertainty sources is adopted for the load shifting and peak shaving strategies, respectively. Thus, 18 simulation runs are performed in total. The full-combination is shown in Table 5.1. In which the weather parameters are in green, the internal heat gain parameters are in orange, and the case code is in blue. Later in this study, a particular case with the uncertainty configuration and the control strategy will be identified by a case reference code with the abbreviation of that control strategy. For example, AAL is the case with no weather parameter uncertainty nor internal heat gain uncertainty and controlled by load shifting strategy. LPLP is the case in which the weather parameter uncertainties are based on local prediction, the uncertainty of the internal heat gain parameter is based on reference profile prediction, and the control strategy is by load shifting and peak shaving combined.

Table 5.1 The combinations of levels of uncertainty and representing case code

		Weather Parameters					
		All-True		Local Measure/Prediction		Online Prediction	
Internal Heat Gain Parameters	All-True	AA		LA		PA	
		Past	Future	Past	Future	Past	Future
		Real	Real	Real	Local	Pred.	Pred.
		Real	Real	Real	Real	Real	Real
	Local Measure/Prediction	AL		LL		PL	
		Past	Future	Past	Future	Past	Future
		Real	Real	Real	Local	Pred.	Pred.
		Real	Local	Real	Local	Real	Local
	Reference Profile Prediction	AP		LP		PP	
		Past	Future	Past	Future	Past	Future
		Real	Real	Real	Local	Pred.	Pred.
		Pred.	Pred.	Pred.	Pred.	Pred.	Pred.

5.2.3 Kalman filter

In the investigated configurations, five (with letter P in the case code) are required to use the Kalman filter to estimate the full states, which are PA, PL, AP, LP, and PP cases. Given the state space expressions in Equation 70, the true building state with limited measurements is:

$$\begin{aligned} x_{i+1} &= Ax_i + Bu_i + D\widehat{w}_i + \epsilon_{s,i} \\ y_i &= Cx_i \end{aligned} \tag{77}$$

Where the $y_i \in \mathbb{R}^5$ is the measurement of the room air temperature in the 5 zones at time step i, $C \in \mathbb{R}^{174\times5}$ is the measurement space, assuming no measurement noise in this process. In this study, the Kalman filter is designated to estimate the full state, but it also has the function to reduce process noise based on the assumption that the $\epsilon_{s,i}$ is drawn from a zero-mean multivariate normal distribution, $\mathcal{N}$, with covariance Q, that

$\epsilon_{s,i} \sim \mathcal{N}(0, Q)$. But in reality, at least for the range of scenario uncertainties defined later in this section, $\epsilon_{s,i}$ does not follow this assumption, and the noise reduction function of the Kalman filter will be influenced. However, the noise reduction by the Kalman filter is not the focus of this study, and it is beyond the author's knowledge to analyze or quantify its full ramifications. The Kalman filter is implemented as shown in the equations below.

Predicted state estimate (prior)

$$\hat{x}_{i|i-1} = A\hat{x}_{i-1|i-1} + Bu_{i-1} + D\hat{w}_{i-1} \tag{78}$$

Predicted estimate covariance (prior)

$$P_{i|i-1} = AP_{i-1|i-1}A^T + Q \tag{79}$$

Where

$$Q = COV(\epsilon_s) \tag{80}$$

Measurement pre-fit residual

$$z_i = y_i - Cx_{i|i-1} \tag{81}$$

Pre-fit residual covariance

$$S_i = CH_iC^T \tag{82}$$

Optimal Kalman gain

$$K_i = P_{i|i-1}C^T S_i^T \tag{83}$$

Updated state estimate (posterior)

$$\hat{x}_{i|i} = \hat{x}_{i|i-1} + K_i z_i \tag{84}$$

Updated estimate covariance (posterior) for the next step

$$P_{i|i} = (I - K_i C)P_{i|i-1} \tag{85}$$

Even though the purpose of using the Kalman filter is because of the lack of actual measurements in the 5 cases mentioned above, the covariance matrix, Q, is assumed to be known in this study. This assumption is, more or less, contradictory to the original assumption of the lack of actual measurements. But a rough estimation of Q can be used in reality since the Kalman filter is employed only to estimate the full states. In the simulation preparation, all cases share the warming-up period for the first five years, and the Kalman filter is enabled, with initial estimate covariance $P_{0|0} \in 0^{174\times174}$, in those 5 cases on the Jan 1st in the sixth year to have a five-month warm-up for the Kalman filter gain.

5.2.4 Uncertainty Range defined in this study

According to Table 5.1 and Figure 5.1-5.3, six sets of scenario parameter profiles need to be defined, which are 1) actual local weather, 2) local weather prediction, 3) online weather prediction, 4) actual internal heat gain, 5) mean profile of sensed internal heat gain, and 6) deterministically defined reference internal heat gain profile. The detailed definition is shown below.

5.2.4.1 Actual local weather

As assumed in Section 5.2.2, the objective building is located in Atlanta, GA. There is a weather station installed at Bobby Dodd Stadium. The recorded local weather data in 2018 and 2019 can be used to represent the actual local weather. The relevant data categories are air temperature, GH solar radiation, dewpoint temperature, and relative humidity. The only missing data category is the sky temperature, but it can be estimated by the method illustrated in [102]. More information about the weather station and the raw data can be found in [122].

5.2.4.2 Online weather prediction

The historical forecast weather data (HFW) for Atlanta can be found from the commercial weather forecast company World Weather Online, as detailed in [123]. To be noticed, this company does not provide the most accurate forecast online, but it is the only company that provides HFW data.

The available and relevant data categories are air temperature, cloud coverage, dewpoint temperature, and relative humidity. The required sky temperature is also estimated using the same method in [102], and the GH solar radiation, $\hat{q}_{GH,i}$, is calculated based on a linear ANN model shown in Equation 86 and 87

$$\hat{q}_{GH,i} = ANN(\psi_i) q_{EH,i} \tag{86}$$

$$ANN(\psi_i) = \alpha_2(\alpha_1 \psi_i + \beta_1) + \beta_2 \tag{87}$$

$$\psi_i = \{T_{a,i};\ T_{d,i};\ \phi_{cl,i};\ \phi_{RH,i};\ q_{EH,i}\} \tag{88}$$

Where ψ_i is the input for the ANN model, which consists of air temperature ($T_{a,i}$), dewpoint temperature ($T_{d,i}$), cloud coverage ($\phi_{cl,i}$), relative humidity ($\phi_{RH,i}$), and extraterrestrial horizontal radiation ($q_{EH,i}$). $\alpha_1 \in \mathbb{R}^{5\times5}$, $\alpha_2 \in \mathbb{R}^{1\times5}$, $\beta_1 \in \mathbb{R}^{5\times1}$, $\beta_2 \in \mathbb{R}$ are the weights and bias in the ANN model, which has one intermediate layer with five nodes. Essentially, this ANN model is merely a linear regression model but can handle the situation when $q_{EH,i} = 0$. Based on the assumptions in Section 5.2.2, this ANN model can only be trained without local measurement. Therefore, the Atlanta TMY3 file (input & output) is used as the training data set, and the model is tested based on the Atlanta 2017 AMY file (input & output) with the combination of online weather prediction (input) and local measurements (output) of 2018. The statistical summary is shown in Table 5.2, and

the Q-Q scatter plots are shown in Figure 5.4-5.6. For the rest of this chapter, the mean bias error (MBE) is defined as (predicted value − actual value). If a positive MBE is shown, it means overprediction.

Table 5.2 Statistical summary of the ANN model

		for All hours			for sunshine hours		
		MBE	RMSE	R^2	MBE	RMSE	R^2
Training	TMY	0.69	55.60	0.96	1.28	75.73	0.93
Testing	AMY	30.53	49.10	0.93	57.20	54.70	0.87
	2018	57.04	111.33	0.70	107.23	134.64	0.52

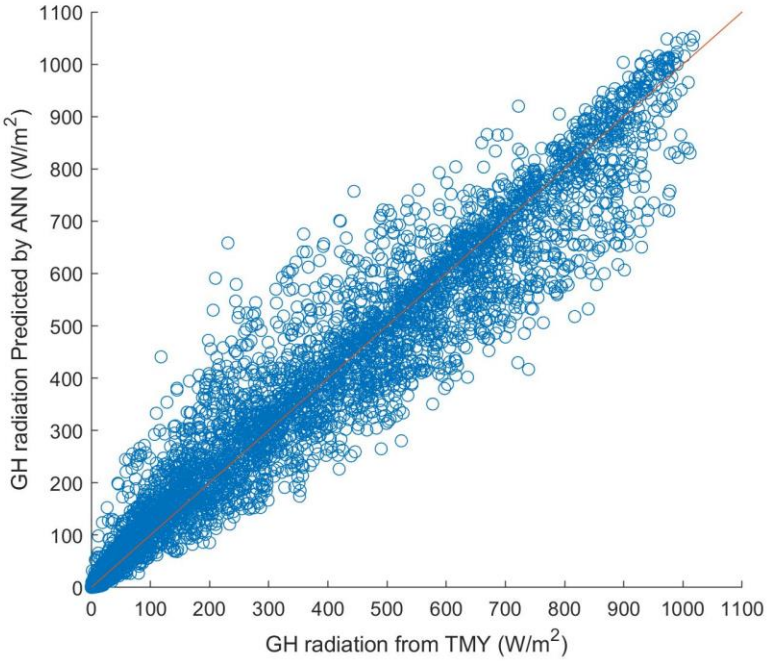

Figure 5.4 Q-Q plot of the training error of the ANN model

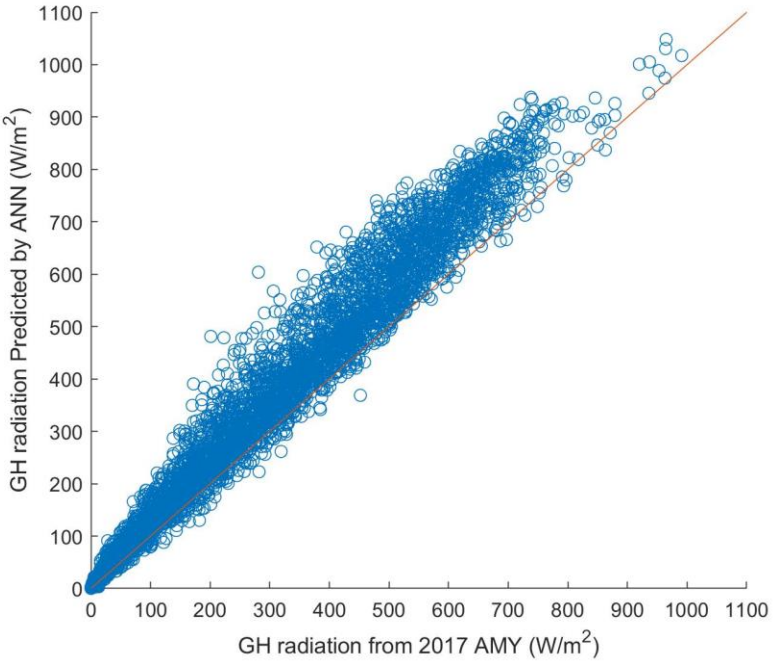

Figure 5.5 Q-Q plot of the testing error of the ANN model based on 2017 AMY

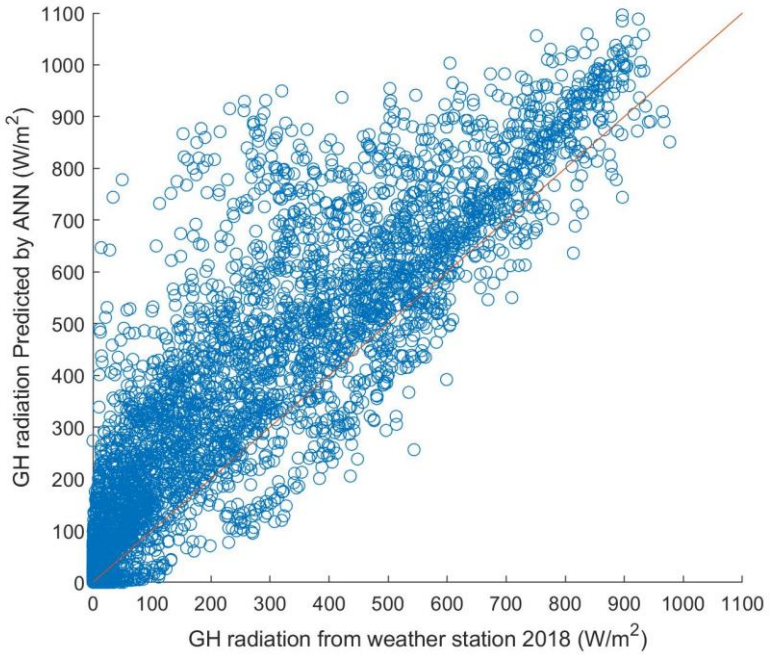

Figure 5.6 Q-Q plot of the testing error of the ANN model based on 2018 weather station recorded data

The results indicate that the model has an excellent fit to the training data set and performs well towards the 2017 AMY data, even when some bias occurs. However, the prediction accuracy drops significantly when the model is tested using the 2018 actual measurement/online weather forecast data. The overfitting problem is tested by reducing the input parameters, but the highest prediction accuracy of the testing data set is still at the situation when all five parameters are used. Hence, the reason for this performance reduction can only be that the GH radiation in TMY/AMY files and in the weather station records are defined or measured differently. However, this prediction error is unavoidable if only the online weather forecast is available.

Despite the error in predicting GH solar radiation, the online weather prediction can yet fulfill the data categories required in the simulation. The prediction error for the year 2019, used in the simulations, is shown in Table 5.3 and Figure 5.7-5.9.

Table 5.3 Statistical summary of online weather forecast

Weather Category	MBE	RMSE
Air Temperature (^oC)	0.66	2.87
Sky Temperature (K)	-1.19	3.23
GH Solar Radiation (W/m^2)	48.53	110.93

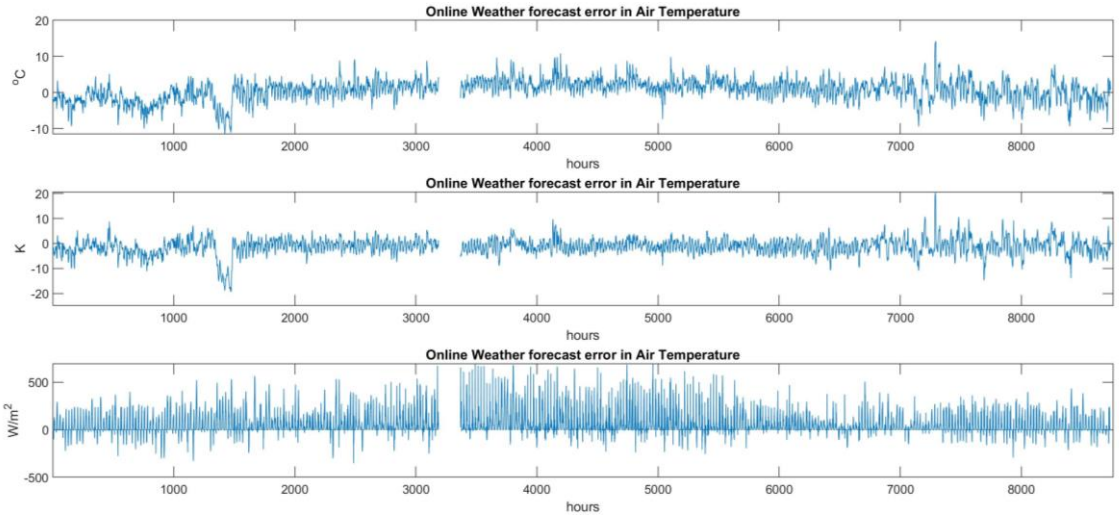

Figure 5.7 Errors of hourly online weather forecast

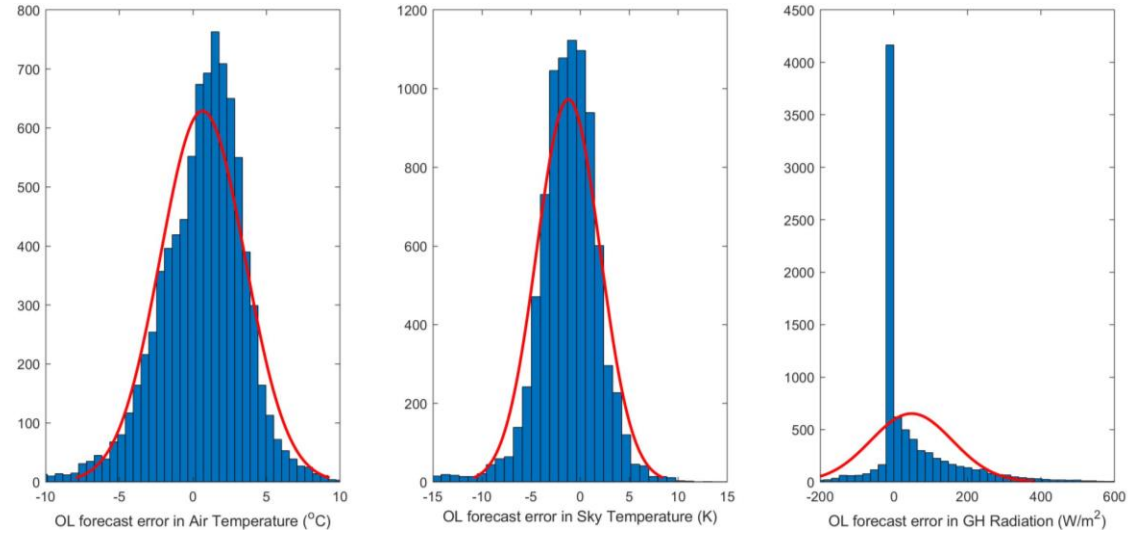

Figure 5.8 Error distribution of the hourly online weather forecast

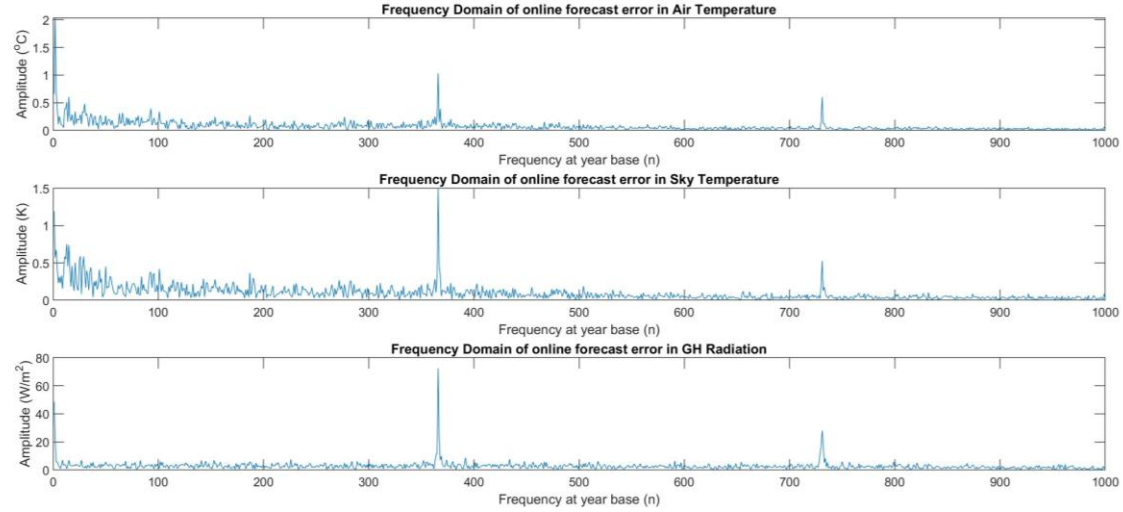

Figure 5.9 Frequency domain of the error of hourly online weather forecast

From the result, the air temperature and GH radiation are overpredicted by the online weather forecast, while the sky temperature is underpredicted. From the distributions of the prediction errors, the residual in each category does not follow a normal distribution, as expected. By Fourier transform, the periodic pattern of the residuals is shown in Figure 5.9. It can be clearly seen that there exist strong signals at yearly, daily, and half-day periods (f=1, f=365, f=730 year based).

5.2.4.3 Local weather prediction

As introduced in Section 5.2.1, there are various methods for local weather prediction. Since the purpose of this study is not to discover the most accurate method, the local weather prediction is generated by simply modifying the online weather forecast based on historical weather station data. As seen previously, there are some long-periods of missing data in the local weather station. This prediction method based on modification may fit better to this study due to its reliability.

Since there is a strong signal at the daily harmonics, the primary purpose of the modification is to eliminate this signal while keeping the overall prediction error lower or at the same level as the online weather forecast. After testing several methods (details omitted), the most effective detrending method is directly deducting the prediction error of the online forecast 24 hours ago from the current online forecast, shown in Equation 89-90

Given

$$\epsilon_i = \widehat{w}_i - w_i^* \tag{89}$$

$$\widehat{w}_i^o = \widehat{w}_i - \epsilon_{i-24h} \tag{90}$$

Where $\widehat{w}_i$ is the online weather forecast, w_i^* is the actual weather condition measured at the weather station, ϵ_i is the prediction error of weather forecast, which is continuously updated once w_i^* is available. $\widehat{w}_i^o$ is the modified weather forecast, which is regarded as the local weather prediction. The prediction error is shown in Table 5.4 and in Figure 5.10-5.12.

Table 5.4 Statistical summary of local weather prediction

Weather Category	MBE	RMSE
Air Temperature (C)	0.01	2.66
Sky Temperature (K)	0.00	3.43
GH Solar Radiation (W/m^2)	1.02	110.98

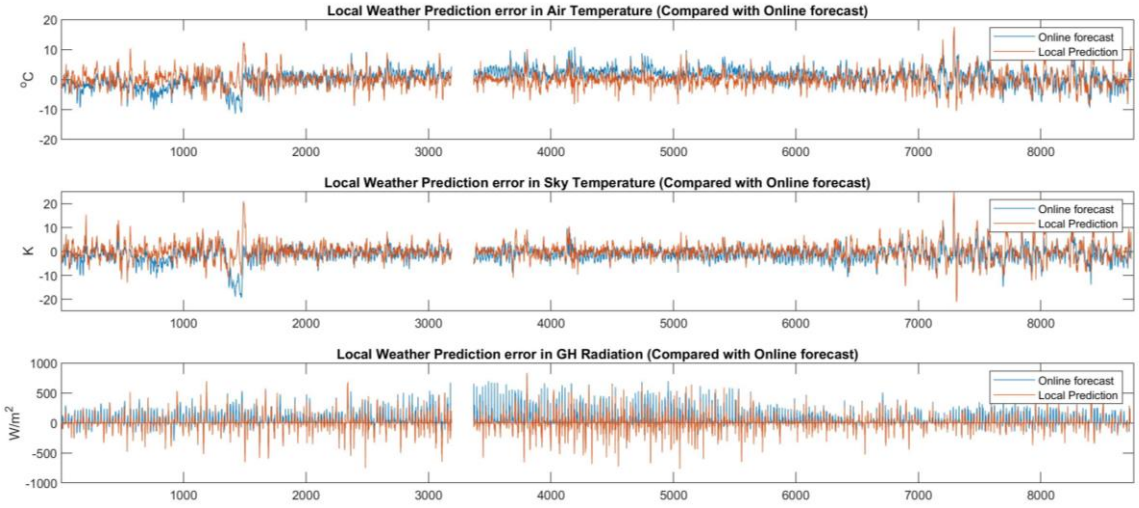

Figure 5.10 Errors of hourly local weather prediction

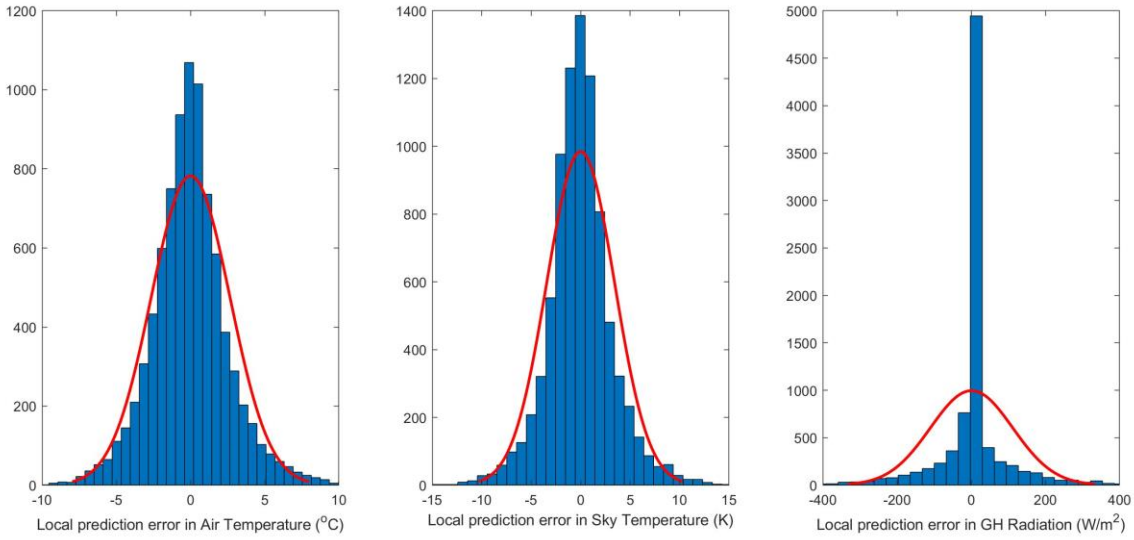

Figure 5.11 Error distribution of the hourly local weather prediction

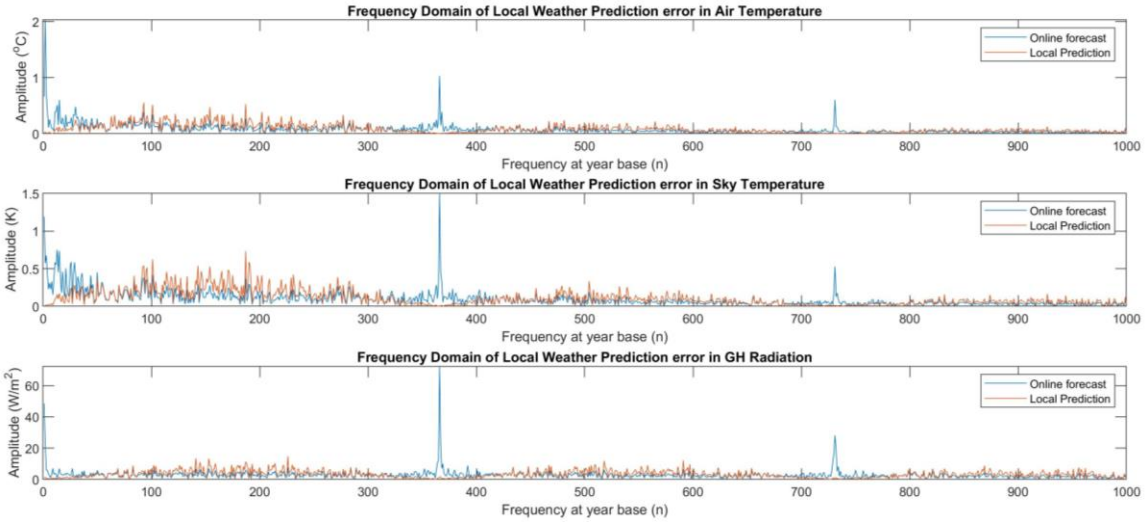

Figure 5.12 Frequency domain of the error of hourly local weather prediction

From the result, two characteristics of using this detrending method can be concluded. Firstly, the prediction error follows a zero-mean distribution, proving that the local weather prediction is overall unbiased. The daily periodic signal is also proved to be removed by examining the frequency domain. Secondly, the RMSE of this model is at the same level as the online weather forecast, which indicates that this method is only

functional as a detrending tool and does not improve the prediction accuracy of the weather forecast. Indeed, more advanced statistical or signal processing tools could be used to acquire the prediction with higher accuracy. Its necessity is discussed later.

5.2.4.4 Actual, local predicted, and reference profiles of internal heat gain

Based on the assumption in Section 5.2.2, the internal heat gain profile of each room is measured by the imaginary "omnipotent" sensor. Since there has no such measured data available, the occupancy behavior model is used to mimic the actual internal heat gain profile in this study.

The occupancy profile is generated from an agent-based occupant behavior modeling tool, Occupancy Simulator [124]. Occupancy generated internal heat gain is calculated accordingly, assuming the heat generation is 120W/person. The hour-to-hour lighting and plug load are generated based on the method developed in [108]. The details of these models are not discussed here. The sum of the two time-series is regarded as the actual internal heat gain profile.

The local prediction of the internal heat gain profile is acquired by simply taking the weekly mean profile of the actual internal heat gain. One assumption behind this method is that the occupancy density and the trend of occupants' behavior, at a weekly interval, are unchanging. In other words, assuming the occupants follow the same pattern over weeks, using the week-period mean profile as the local prediction is unbiased.

The reference profile is generated based on the ASHRAE reference schedule for occupancy, lighting, and plug load [125]. The internal heat gain density and schedule are

modified from the original value at the building level. This modification may be considered a viable option when a control engineer is on-site and has access to the electricity bills.

Thus, all three sets of internal gain profiles are available. The south zone Monday profile is shown in Figure 5.13, the week-based profiles for all five zones are shown in Figure 5.14, and the statistical summary is in Table 5.5. In which, the mean bias relative error (MBrE) and the rooted mean square relative error (RMSrE) are defined in Equation 91-92.

$$MBrE = \frac{\sum_{i=1}^{n} \frac{\hat{y}_i - y_i}{y_i}}{n} \tag{91}$$

$$RMSrE = \sqrt{\frac{\sum_{i=1}^{n} (\frac{\hat{y}_i - y_i}{y_i})^2}{n}} \tag{92}$$

Table 5.5 Statistical summary of internal gain prediction

Zone	Prediction by mean profile				Prediction by reference profile			
	MBE	RMSE	MBrE	RMSrE	MBE	RMSE	MBrE	RMSrE
South	1.52E-14	200.90	0.01	0.08	223.47	309.33	0.18	0.15
East	-1.69E-15	158.43	0.01	0.10	43.04	206.93	0.23	0.23
North	-3.87E-15	193.91	0.01	0.08	254.94	312.01	0.23	0.18
West	7.35E-15	170.69	0.01	0.11	28.70	221.19	0.21	0.23
Center	-1.25E-15	250.16	0.01	0.08	-6.16	356.08	-0.02	0.14

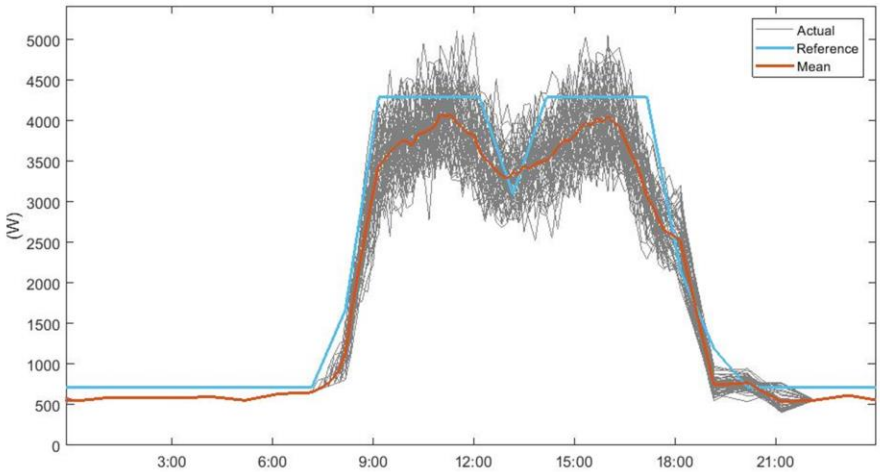

Figure 5.13 Internal gain profiles of south zone on Monday

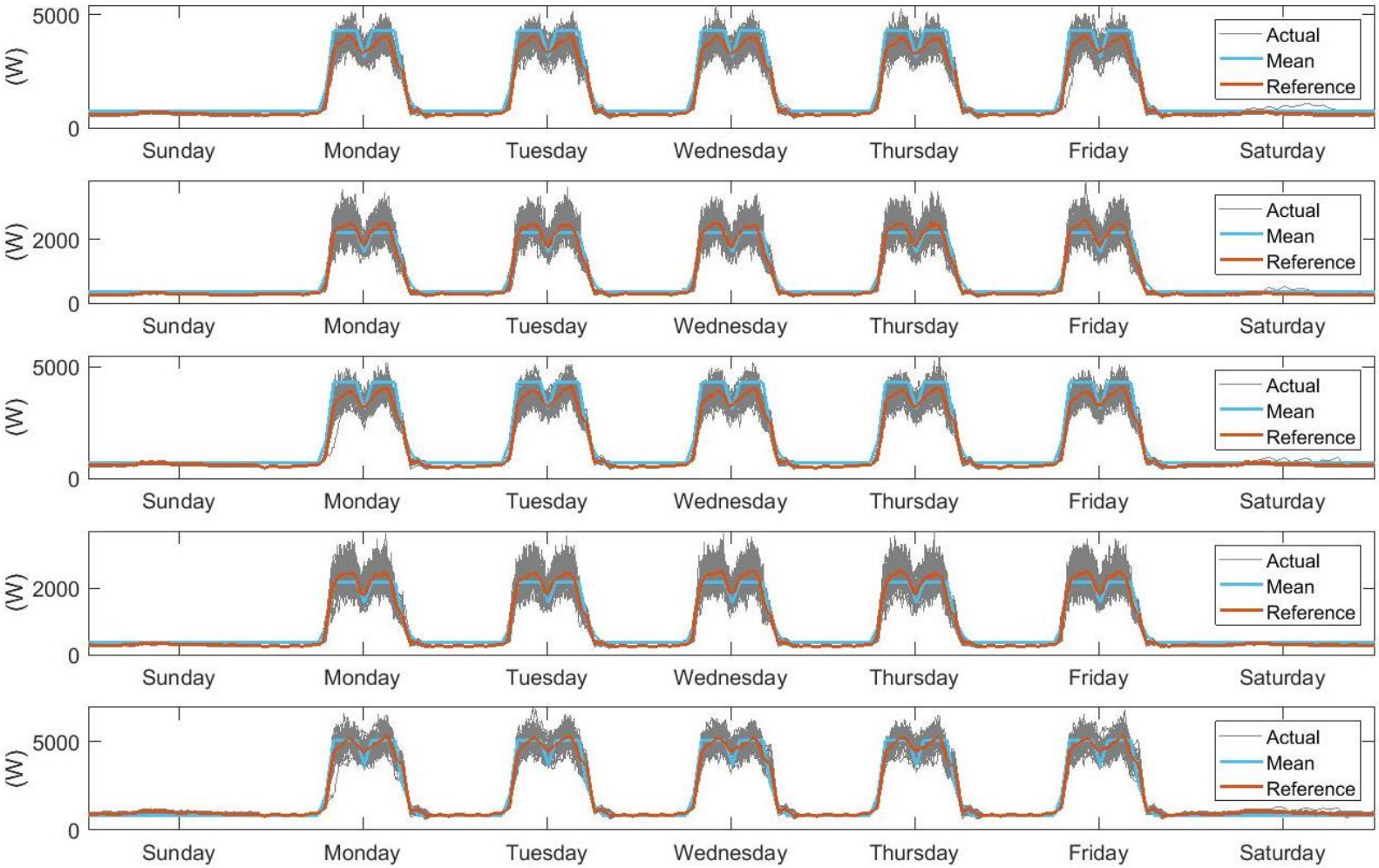

Figure 5.14 Internal gain profiles of all zones in a week

5.3 Result and analysis

For the readers' convenience, Table 5.1 with the case reference codes, is copied below. The letter L or LP following the case code means the load shifting or load shifting + peak shaving strategy is used.

Table 5.1 The combinations of levels of uncertainty and representing case code

		Weather Parameters					
		All-True		Local Measure/Prediction		Online Prediction	
Internal Heat Gain Parameters	All-True	AA		LA		PA	
		Past	Future	Past	Future	Past	Future
		Real	Real	Real	Local	Pred.	Pred.
		Real	Real	Real	Real	Real	Real
	Local Measure/Prediction	AL		LL		PL	
		Past	Future	Past	Future	Past	Future
		Real	Real	Real	Local	Pred.	Pred.
		Real	Local	Real	Local	Real	Local
	Reference Profile Prediction	AP		LP		PP	
		Past	Future	Past	Future	Past	Future
		Real	Real	Real	Local	Pred.	Pred.
		Pred.	Pred.	Pred.	Pred.	Pred.	Pred.

5.3.1 Result inspection

Firstly, the results are inspected in terms of the room air temperature profile in both load shifting and L+P strategies, along with the corresponding scenario parameters. The profiles on a typical day in July are shown in Figure 5.15, in which the room air temperature of the south zone is plotted.

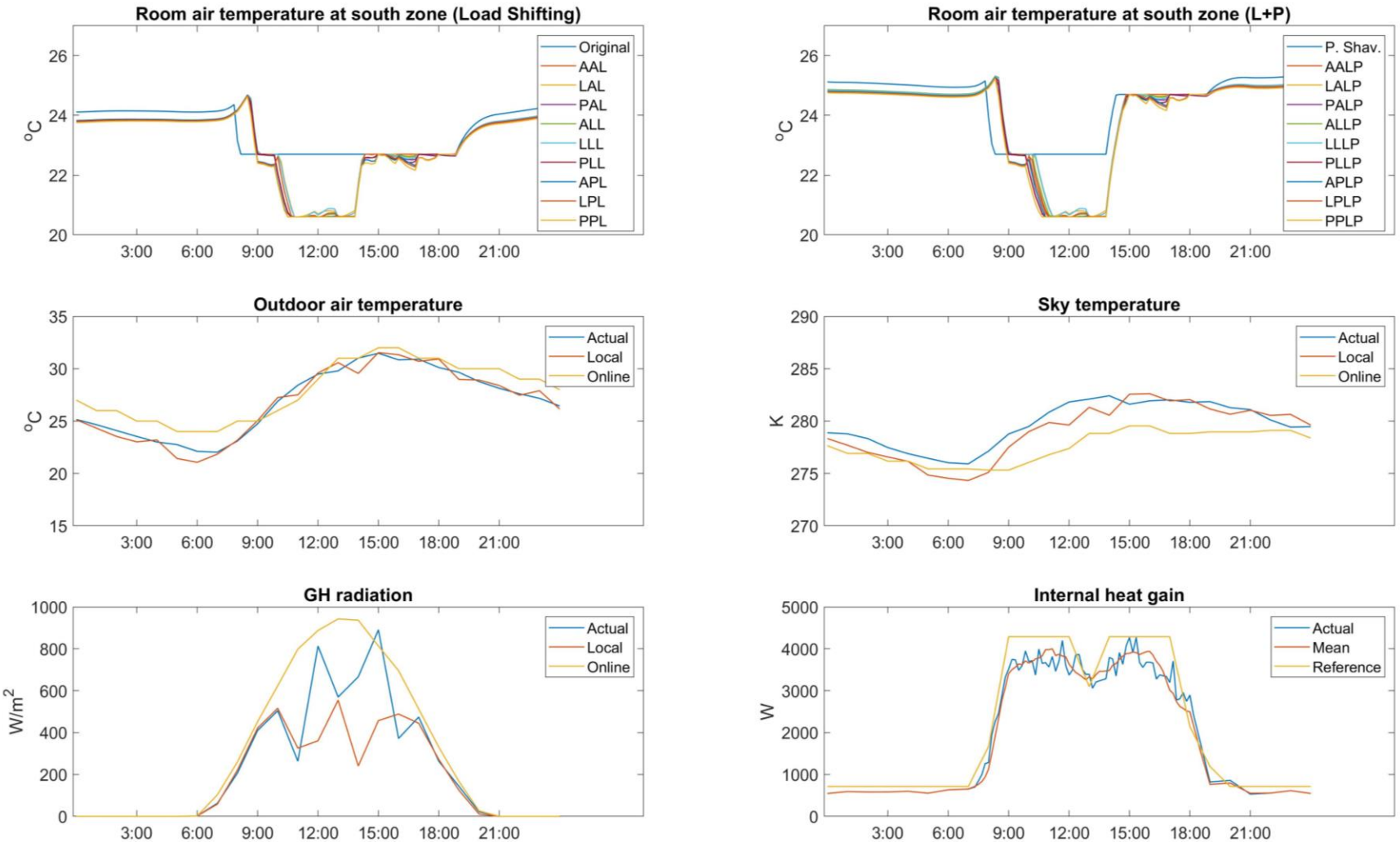

Figure 5.15 Room air temperature and scenario parameter profiles

From the profiles, the room air temperature in all cases is securely bounded within the comfort band, which proves the effectiveness of the insurance control. The starting point of pre-cooling varies in each case due to different levels of uncertainty. More variation of the starting point is observed in the L+P scenarios, which may potentially indicate that the already low saving potential of load shifting is even further diminished in the L+P strategy due to the influence of scenario uncertainties.

5.3.2 The influence of scenario uncertainties on MPC

The seasonal (yearly) performance of MPC in all 18 cases are shown in Table 5.6, and the cost-saving percentage of cases is in Figure 5.16.

Table 5.6 Seasonal performance of MPC in cases with levels of scenario uncertainty

Strategy and uncertainty setups	HVAC operation cost (USD)	Cost savings (USD)	Cost-saving percentage (%)	Cost-saving reduced by scenario uncertainty (USD)	Cost-saving reduced percentage by scenario uncertainty (%)
Original	1354.43	-	-	-	-
AAL	1245.54	108.89	8.0%	-	-
LAL	1253.64	100.79	7.4%	8.10	7.4%
PAL	1261.30	93.14	6.9%	15.76	14.5%
ALL	1253.34	101.09	7.5%	7.80	7.2%
LLL	1257.37	97.06	7.2%	11.83	10.9%
PLL	1264.57	89.86	6.6%	19.03	17.5%
APL	1261.56	92.87	6.9%	16.02	14.7%
LPL	1264.29	90.15	6.7%	18.75	17.2%
PPL	1271.36	83.07	6.1%	25.82	23.7%
Peak Shaving	1027.34	327.09	24.1%	-	-
AALP	949.18	405.26	29.9%	-	-
LALP	956.16	398.28	29.4%	6.98	1.7%
PALP	961.49	392.95	29.0%	12.31	3.0%
ALLP	955.31	399.12	29.5%	6.14	1.5%
LLLP	959.01	395.42	29.2%	9.84	2.4%
PLLP	964.00	390.43	28.8%	14.83	3.7%
APLP	961.89	392.54	29.0%	12.71	3.1%
LPLP	964.61	389.82	28.8%	15.43	3.8%
PPLP	969.76	384.67	28.4%	20.58	5.1%

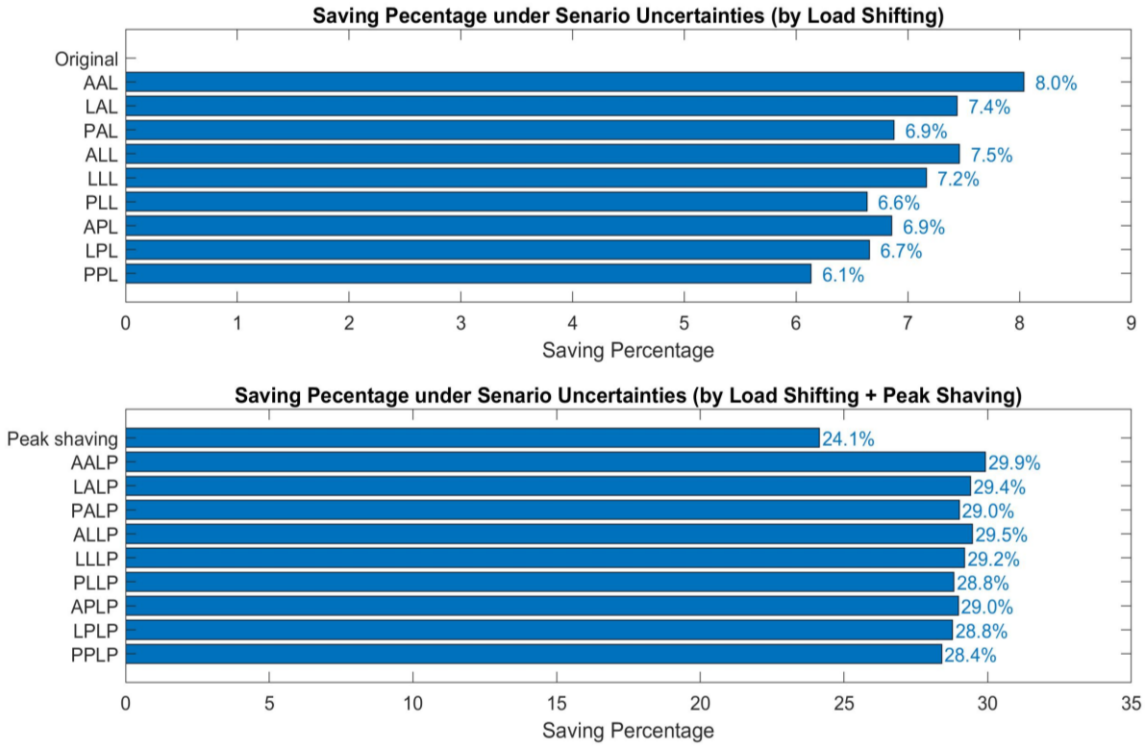

Figure 5.16 Cost-saving percentage under levels of scenario uncertainty

The results indicate that the influence of scenario uncertainty on the performance of MPC is rather small. Even for the PPL and PPLP cases where the predictions are only based on the online weather forecast and a reference internal heat gain profile, there are only 23.7% and 5.1% cost-saving reduced in the load shifting and L+P strategies, compared with the absolute cost-saving amount in AAL and AALP cases, respectively.

The effects of the uncertainties in weather and internal heat gain prediction can be evaluated by comparing the performance reduction in the set of AA, LA, PA cases with the set of AA, AL, AP cases. Since very similar performance reductions are seen between these two case sets, it is evident that the performance of MPC is equivalently sensitive to both uncertainty categories.

There are two remarkable findings by comparing the AA, LL, and PP cases. Firstly, the local installed weather station and multiple types of occupant sensors can improve the accuracy in predicting scenario parameters. However, improved prediction accuracy can only lead to marginally extra cost savings in MPC applications. Secondly, the performance difference of MPCs between using the best possible predictions and perfect predictions is small. To be noticed, this performance gap is theoretically unfixable. Thus, applying advanced methods in local weather prediction may have only a marginal improvement of MPC performance.

5.4 Conclusion and Inference

As shown in Section 5.3, the conclusion of this chapter is simple and straightforward: the influence of scenario uncertainty on the performance of MPC is marginal, and a properly defined MPC controller has adequate robustness for cost saving under scenario uncertainties.

Throughout the study in this chapter, several points are made that need repeating. Firstly, the influence of scenario uncertainty on the performance of MPC should be defined strictly and carefully in the first place. By definition, the only difference between the setups of cases should be that of scenario parameters, and the resulting performance difference should only be restricted to the result of MPC.

Secondly, the concept of MPC is more about an optimizer than an actuator. Adding a readily used “insurance” controller to the MPC can effectively eliminate the risk of violating thermal comfort.

Thirdly, based on the MPC configurations in this study, sophisticated local prediction models are not needed if the local measurement can accurately reflect the environment of the building system, or practically speaking, if the local measurement can accurately reflect the scenario parameters in the building model. This question is principally about the need to theoretically distinguish and characterize the model form, parameter, and scenario uncertainties. In fact, these are all relative definitions. [107]

As more studies are currently focusing on developing stochastic model predictive controllers, the need for a common framework and agreement on the concepts becomes urgent. It is the intention of this chapter to make a contribution in this respect and serve as a reference.

CHAPTER 6. A POSSIBLE ROAD TO REAL APPLICATION

Throughout the former chapters in this dissertation, all the theoretical analyses are performed based on a high fidelity clear-box nodal-network model. However, this model is not realistically applicable, mainly due to 1) thousands of parameters are required in establishing the model, which are sheer impossible to be calibrated, and 2) the optimized control input is in the form of cooling energy flow rate, which is only the control outcome of the optimization and requires further translation to be "interpretable" for actual implementation by local HVAC units.

In this chapter, a simple but effective MPC structure is presented to address these two problems simultaneously. Firstly, the simulation results in Chapter 5 are reinspected to discover the regularities of the control sequences generated by MPC. Then, an MPC structure is suggested and analyzed, followed by the illustration of its significance. At last, a hypothetical case study is presented to further demonstrate the effectiveness of this MPC structure.

6.1 Two-Point Activation control

Back to the result inspection in Section 5.3.1, the temperature profiles (Copied below in Figure 6.1) show regular activation patterns of the control input (cooling energy flow) even under scenario uncertainty. In fact, there are only two activation points from the MPC that intervene with the original temperature setpoints. The first activation point occurs before 9:00, at which the HVAC system pre-cool the building to meet the control band. The second activation point occurs after the first one, at which the building is pre-cooled

to enable load shifting. After the first activation point, the room air temperature is controlled to the desired room air temperature (T_D); and after the second activation point, it is controlled to the lower bound of the comfort band (T_{lb}). Since the temperature profile in the cases without uncertainty (AAL, AALP) shows a flat line elsewhere from 9:00 to 14:00, it is reasonable to believe that the temperature fluctuation (marked in Figure 6.1) occurring in other cases are resulted from the prediction error introduced by scenario uncertainty. Therefore, the question arises whether these two activation points can be the control input to the HVAC system instead of the energy flow rate?

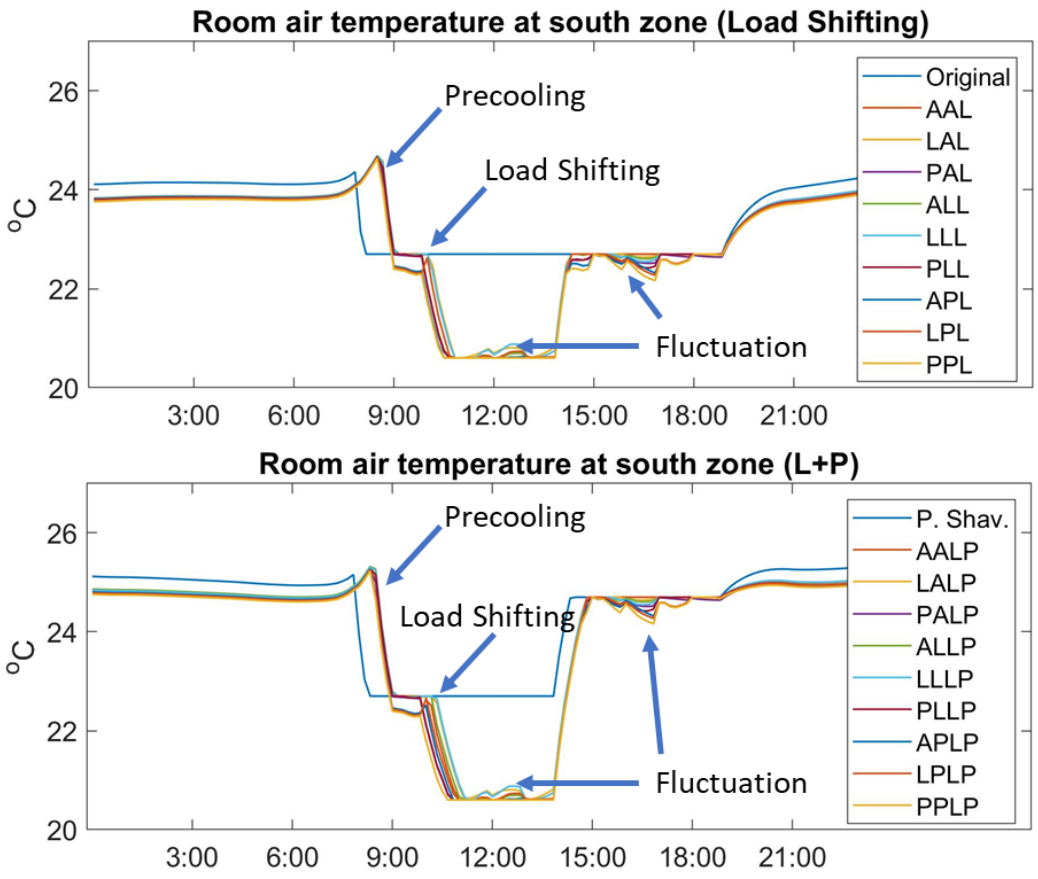

Figure 6.1 Temperature profiles based on MPC in levels of scenario uncertainty

6.1.1 The form of TPA control

The simulation of 18 case setups used in Chapter 5 is repeated with the two-point activation (TPA) control introduced below. Given $\hat{x}$, $\hat{u}$ acquired from the MPC controller, the setpoint temperature profile at each zone ($T_{ub,i,k}$) can be translated as

$$T^{+}_{ub,i+1,k} = \begin{cases} T_D, & if\ \hat{x}_{i+1,k} < T_{NS}\ and\ \hat{u}_{i,k} < 0\ and\ T_{ub,i,k} = T_{NS} \\ T_{lb}, & if\ \hat{x}_{i+1,k} < T_D - T_{err}\ and\ \hat{u}_{i,k} < 0\ and\ T_{ub,i,k} = T_D \\ T^{+}_{ub,i+1,ori}, & after\ 14{:}00\ today\ until\ 6{:}00\ next\ day \end{cases} \quad (93)$$

Where i is the time step in the building model, k denotes a specific zone. $T^{+}_{ub,i}$ represents temperature setpoint at step i and beyond, T_{NS} is the setback temperature during the night, T_{err} is the tolerance of the prediction error of the MPC controller in the previous prediction interval; it is set to be 0.2 ^{o}C in this case. $T_{ub,i,ori}$ is the setpoint temperature in the original or peak shaving scenario at step i. The first and second conditions in Equation 93 describe the starting point of pre-cooling the building and the activation of load shifting; the third condition resets the HVAC system to its original operation by ignoring the MPC. Therefore, the cooling energy flow rate at each zone ($u^{*}_{i,k}$) is calculated in Equation 94

$$u^{*}_{i,k} = \begin{cases} 0, & if\ x_{i+1,k} \le T_{ub,i+1,k} \\ B_k^{-1}(T_{ub,i+1,k} - (A_k x_i + D_k w_i)), & if\ \hat{x}_{i+1,k} > T_{ub,i+1,k} \end{cases} \quad (94)$$

As introduced in Section 5.1.2, this control logic is implemented as a one-step predictive control in the simulation, but it should be recognized that this control logic can be realized by the temperature setpoint control currently embedded in thermostats.

The cost-saving performance of the 18 cases with TPA control is shown in Table 6.1, and the temperature profiles of AA, LL, and PP scenarios are shown in Figure 6.2, in which the hash sign (#) denotes the cases with TPA control.

Table 6.1 Comparison of the performance using original / TPA MPC control

Strategy and uncertainty setups	HVAC operation cost (USD)	Cost savings (USD)	Cost-saving percentage (%)	Strategy and uncertainty setups	HVAC operation cost (USD)	Cost savings (USD)	Cost-saving percentage (%)
Original	1354.43	-	-	-	-	-	-
AAL	1245.54	108.89	8.0%	AAL#	1247.52	106.91	7.9%
LAL	1253.64	100.79	7.4%	LAL#	1253.41	101.02	7.5%
PAL	1261.30	93.14	6.9%	PAL#	1255.88	98.56	7.3%
ALL	1253.34	101.09	7.5%	ALL#	1253.84	100.59	7.4%
LLL	1257.37	97.06	7.2%	LLL#	1256.76	97.68	7.2%
PLL	1264.57	89.86	6.6%	PLL#	1259.07	95.37	7.0%
APL	1261.56	92.87	6.9%	APL#	1261.56	92.87	6.9%
LPL	1264.29	90.15	6.7%	LPL#	1262.77	91.66	6.8%
PPL	1271.36	83.07	6.1%	PPL#	1264.72	89.71	6.6%
Peak Shaving	1027.34	327.09	24.1%	-	-	-	-
AALP	949.18	405.26	29.9%	AALP#	952.73	401.70	29.7%
LALP	956.16	398.28	29.4%	LALP#	957.65	396.78	29.3%
PALP	961.49	392.95	29.0%	PALP#	958.99	395.44	29.2%
ALLP	955.31	399.12	29.5%	ALLP#	957.18	397.25	29.3%
LLLP	959.01	395.42	29.2%	LLLP#	960.04	394.39	29.1%
PLLP	964.00	390.43	28.8%	PLLP#	961.80	392.63	29.0%
APLP	961.89	392.54	29.0%	APLP#	966.36	388.07	28.7%
LPLP	964.61	389.82	28.8%	LPLP#	965.57	388.87	28.7%
PPLP	969.76	384.67	28.4%	PPLP#	967.50	386.94	28.6%

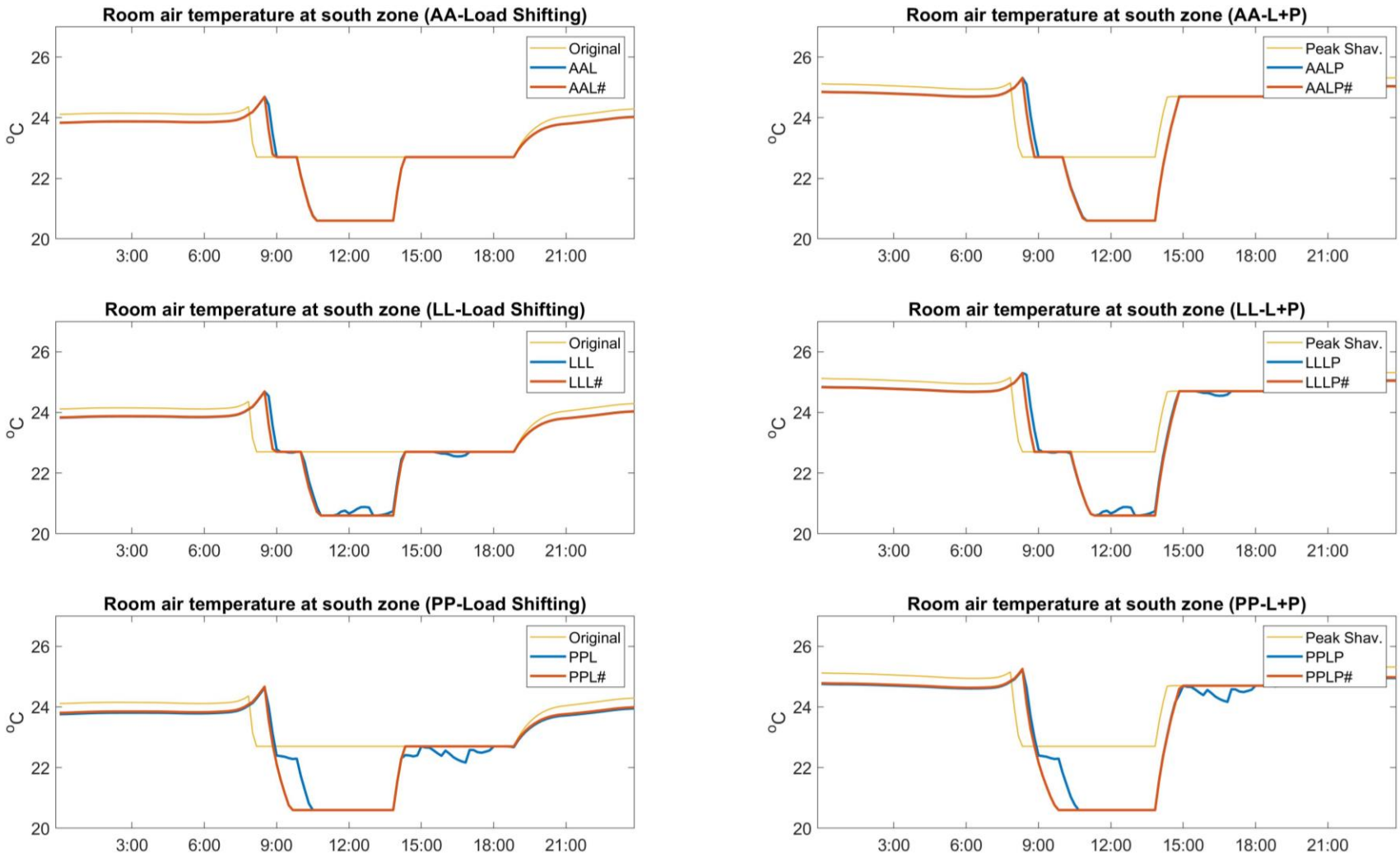

Figure 6.2 Temperature profiles in AA, LL, and PP scenarios

The temperature profiles in Figure 6.2 confirm that the TPA control is able to translate the output from MPC (optimized energy flow rate) to the actuated control input (temperature setpoint) to the HVAC system with a certain degree of accuracy. The discrepancy of TPA control occurs when the predicted energy flow rate of the first step in the pre-cooling period is very low or when the prediction error of MPC is higher than the tolerance T_{err}. Beyond the function of translation, the TPA control is also able to regulate the MPC output by 1) making up for the insufficient cooling in the load shifting period and 2) avoiding overcooling in the peak shaving period. Hence, the "insurance" control introduced in Section 5.1.2 is no longer required.

As shown in Table 6.1, the TPA control is able to realize the cost-saving performance of the MPC that uses the energy flow rate as the control variable. Even more cost-saving by the TPA control is observed in the cases with higher uncertainty levels, mainly due to the regulation function mentioned above. Thus, it is proved that the TPA control is trustable in actuating the optimized energy flow rate from MPC.

6.1.2 The significance of TPA control

In the last section, TPA control is implemented as an actuator of the original MPC, which effectively translates the optimized energy flow rate to temperature setpoints. In fact, the concept of TPA control has its own significance serving as the objective of optimizations.

Again, taking the 5-zone office building as an example, the objective function of the original MPC is shown in Equation 50-51 in Chapter 3, for convenience copied below.

Assuming the prediction horizon is 24 hours, and the step length is 10 mins in MPC, there are 144 control variable values that need to be optimized for every single zone. Due to the interzonal heat transfer, a 720-dimensional optimization is theoretically required at every prediction interval. Even without the consideration of interzonal heat transfer, a 144-dimensional optimization still needs to be performed five times in the MPC. Assuming the prediction interval is 1 hour, the aforementioned optimizations need to be run 24 times in a single day. As explained in Chapter 1, this high-dimensional optimization prevents most forms of the prediction model from being implemented in an actual MPC. In the theoretical investigations throughout this dissertation, the linear nodal-network model with linear programming optimization is employed to ensure the global optimum in analyzing the theoretical potential of MPC in different scenarios.

$$\min_{U_i} R_i \Omega_{i(U_i)} \tag{50}$$

Subj.to $$X_{lb,i} \leq X_i \leq X_{ub,i} \tag{51}$$

However, in the form of TPA control, there are only 2 control variables that need to be optimized for each zone. By ignoring the interzonal heat transfer, the solutions space is at the dimensionality of 2. Moreover, these 2 control variables are in discrete form if a fixed control interval is used in the HVAC system. An additional advantage is that finding the optimal solution in discrete variables does not require the prediction model to have very high accuracy. In other words, the optimization may only need to be performed once on a certain day in order to ensure that the two optimal activation points are accurate. The solution space of the TPA control is calculated in Equation 95-99.

Assuming the earliest starting time of precooling is at t_s, the working period starts at t_w, and the control interval is Δt, then there exists $\mathcal{C}_1$ possibilities for the activation point of precooling t_1 ($t_s \leq t_1 \leq t_w$). Where

$$\mathcal{C}_1 = (t_w - t_s)/\Delta t \tag{95}$$

Assuming that peak shaving starts at t_p, the set of all possible activation points of load shifting $\mathcal{C}_2$ and its minimum and maximum set can be calculated as

$$\mathcal{C}_2 = (t_p - t_1)/\Delta t \tag{96}$$

hence

$$\mathcal{C}_{2,min} = (t_p - t_w)/\Delta t \tag{97}$$

$$\mathcal{C}_{2,max} = (t_p - t_s)/\Delta t \tag{98}$$

Thus, the solution space of TPA control ($\mathcal{S}_{TPA}$) can be calculated as the sum of arithmetic progression that

$$\mathcal{S}_{TPA} = \frac{\mathcal{C}_1}{2}(\mathcal{C}_{2,min} + \mathcal{C}_{2,max}) \tag{99}$$

With the same assumption that 10 min is the control interval, the earliest starting time of precooling at 6:00, working hour starting at 9:00, and peak shaving starting at 14:00, then the solution space can be calculated accordingly, which is a set of 702 elements for every zone or 3510 elements for the entire building. Thus, due to the minimal size of the solution space in TPA formulation, the optimization process is no longer an Achilles' heel of MPC.

6.2 An example of TPA control

To verify the advantages of TPA control, a case study is performed in this section. In which a reduced-order RC model is trained initially from the represented historical building operation conditions. A TPA-MPC is established accordingly based on this RC model in order to generate the optimal setpoint temperature profiles for each zone. The performance of this TPA-MPC is analyzed at the end of this section.

6.2.1 Assumptions about the building

The chosen building is represented by the 5-zone nodal-network building model developed in Chapter 3. The term "building" used in the rest of this section indicates this building model. Several assumptions are made to reflect the knowledge about the chosen building.

1) A thermostat is installed in each zone of the building. Only the room air temperature is monitored and recorded without sensor error.
2) Energy consumptions of the cooling and heating system of the entire building are recorded separately with no sensor error. The seasonal COPs of the cooling and heating system are assumed to be known, but the energy flow rate for each zone is not available.
3) Historical weather and zonal internal gain profiles are known. The future profiles are acquired from local predictors. Thus, the scenario uncertainty level is set the same as the LL setup defined in Section 5.2.2.

4) It is acknowledged that the building has exterior walls that are using the same construction on every façade, and the window to wall ratio on each façade is the same.

6.2.2 RC modeling

Given the assumptions, it is hardly possible to derive a five-zone RC model directly, mainly due to the lack of data about the historical energy flow rate of the HVAC unit in each thermal zone. Therefore, a single-zone RC model, representing the entire building, is calibrated initially to identify the properties of materials. Then the zonal RC models are established based on the information given from the calibrated building-level RC model. A schematic diagram of this modeling process is shown in Figure 6.3.

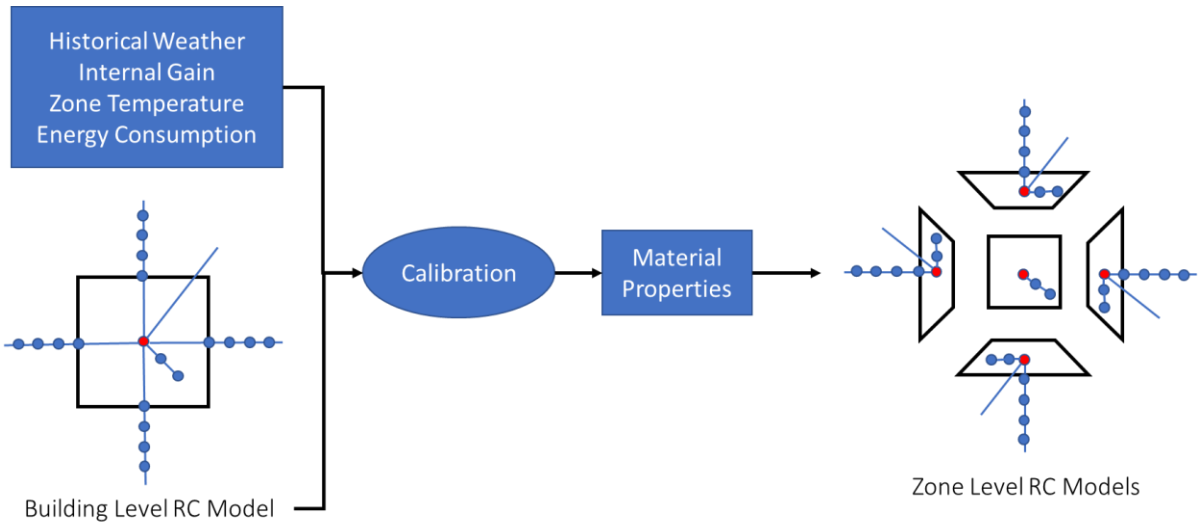

Figure 6.3 Modeling process of the RC model

In the RC models, the layers in the exterior wall are represented by 4 capacitors, and the thermal mass of floor and other internal constructions are represented by 2 connected capacitors. The internal layers of the constructions are connected to the zone capacitor only through convection heat transfer. The heat transfer from attic and soil and

the infrared radiation between interior construction surfaces are ignored in the RC models. Equation 100-102 describes the general form of the governing equations used in the RC models, as evaluated for capacitor m.

$$\dot{Q}_{mn,T} = -A_{mn}\frac{(T_m - T_n)}{r_{mn}} \tag{100}$$

$$\dot{Q}_{m,sol} = A_m\frac{\dot{q}_{m,sol}}{r_m} \tag{101}$$

$$c_m A_m\frac{dT_m}{dt} = \dot{Q}_{mn,T} + \dot{Q}_{m,sol} + \dot{Q}_{m,int} + \dot{Q}_{m,HVAC} \tag{102}$$

Where $\dot{Q}_{mn,T}$ is the energy flow rate of heat transfer due to temperature difference, $\dot{Q}_{m,sol}$ is the solar heat gain, $\dot{Q}_{m,int}$ is the internal heat gain, and $\dot{Q}_{m,HVAC}$ is the energy flow rate of the HVAC system; in the building level RC model, $\dot{Q}_{m,HVAC}$ is calculated by HVAC electricity consumption rate times seasonal COP. $\dot{q}_{m,sol}$ is the solar radiation intensity on the surface m. r_{mn} is the normalized thermal resistance, which has the unit of m^2K/W. r_m is the resistance of solar radiation, which is essentially the inverse of surface emissivity. c_m is the normalized thermal capacity in the unit of $J/(m^2K)$. A_{mn} is the effective area of heat transfer, and A_m is the area of the capacitor m itself. For all the capacitors representing the zone air (the red nodes in Figure 6.3), the A_m and c_m are evaluated based on the floor area.

Based on the governing equations, the building level RC model is established, as shown in Figure 6.4. The RC parameters are calculated given in Table 6.2, in which A_{bf}, A_{sw}, A_{ew}, A_{nw}, and A_{ww} are the area of building floor, south wall, east wall, north wall, and west wall, respectively.

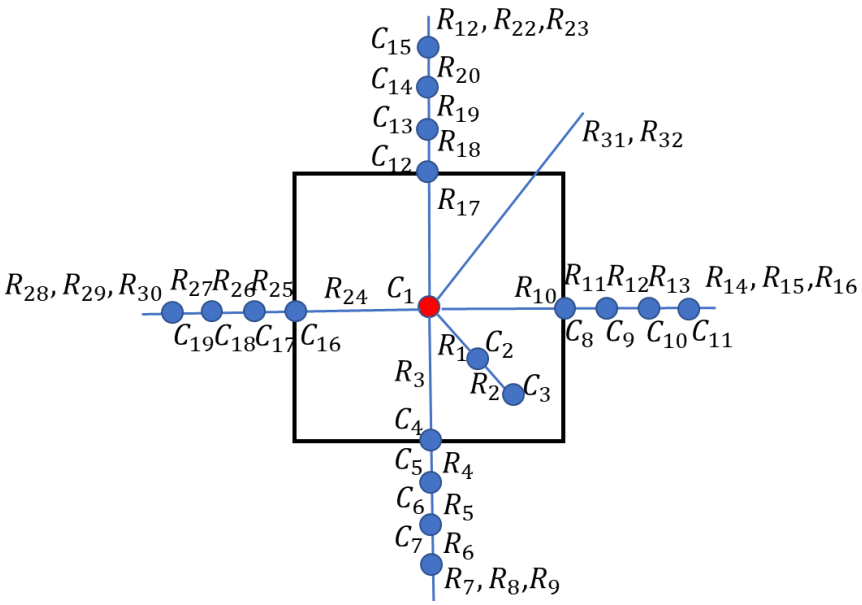

Figure 6.4 Structure of the building level RC model

Table 6.2 RC parameters in the building level RC model

Capacitor	Calculated by	Physical Representation	Resistor	Calculated by	Physical Representation
C_1	$c_1 \times A_{bf}$	Room	R_1	r_1/A_{bf}	Convection C_1-C_2
C_2	$c_2 \times A_{bf}$	Floor, Layer 1	R_2	r_2/A_{bf}	Conduction C_2-C_3
C_3	$c_3 \times A_{bf}$	Floor, Layer 2	R_3	r_3/A_{sw}	Convection C_1-C_4
C_4	$c_4 \times A_{sw}$	S. Wall, Layer 1	R_4	r_4/A_{sw}	Conduction C_4-C_5
C_5	$c_5 \times A_{sw}$	S. Wall, Layer 2	R_5	r_5/A_{sw}	Conduction C_5-C_6
C_6	$c_6 \times A_{sw}$	S. Wall, Layer 3	R_6	r_6/A_{sw}	Conduction C_6-C_7
C_7	$c_7 \times A_{sw}$	S. Wall, Layer 4	R_7	r_7/A_{sw}	Convection C_7-outdoor air
C_8	$c_4 \times A_{ew}$	E. Wall, Layer 1	R_8	r_8/A_{sw}	Solar Rad. at C_7
C_9	$c_5 \times A_{ew}$	E. Wall, Layer 2	R_9	r_9/A_{sw}	Long-wave Rad. C_7-sky
C_{10}	$c_6 \times A_{ew}$	E. Wall, Layer 3	R_{10}	r_3/A_{ew}	Convection C_1-C_8
C_{11}	$c_7 \times A_{ew}$	E. Wall, Layer 4	R_{11}	r_4/A_{ew}	Conduction C_8-C_9
C_{12}	$c_4 \times A_{nw}$	N. Wall, Layer 1	R_{12}	r_5/A_{ew}	Conduction C_9-C_{10}
C_{13}	$c_5 \times A_{nw}$	N. Wall, Layer 2	R_{13}	r_6/A_{ew}	Conduction C_{10}-C_{11}
C_{14}	$c_6 \times A_{nw}$	N. Wall, Layer 3	R_{14}	r_7/A_{ew}	Convection C_{11}-outdoor air
C_{15}	$c_7 \times A_{nw}$	N. Wall, Layer 4	R_{15}	r_8/A_{ew}	Solar Rad. at C_{11}
C_{16}	$c_4 \times A_{ww}$	W. Wall, Layer 1	R_{16}	r_9/A_{ew}	Long-wave Rad. C_{11}-sky
C_{17}	$c_5 \times A_{ww}$	W. Wall, Layer 2	R_{17}	r_3/A_{nw}	Convection C_1-C_{12}
C_{18}	$c_6 \times A_{ww}$	W. Wall, Layer 3	R_{18}	r_4/A_{nw}	Conduction C_{12}-C_{13}
C_{19}	$c_7 \times A_{ww}$	W. Wall, Layer 4	R_{19}	r_5/A_{nw}	Conduction C_{13}-C_{14}
			R_{20}	r_6/A_{nw}	Conduction C_{14}-C_{15}
			R_{21}	r_7/A_{nw}	Convection C_{15}-outdoor air
			R_{22}	r_8/A_{nw}	Solar Rad. at C_{15}
			R_{23}	r_9/A_{nw}	Long-wave Rad. C_{15}-sky
			R_{24}	r_3/A_{ww}	Convection C_1-C_{16}
			R_{25}	r_4/A_{ww}	Conduction C_{16}-C_{17}
			R_{26}	r_5/A_{ww}	Conduction C_{17}-C_{18}
			R_{27}	r_6/A_{ww}	Conduction C_{18}-C_{19}
			R_{28}	r_7/A_{ww}	Convection C_{19}-outdoor air
			R_{29}	r_8/A_{ww}	Solar Rad. at C_{19}
			R_{30}	r_9/A_{ww}	Long-wave Rad. C_{19}-sky
			R_{31}	r_{10}/A_{bf}	Solar Rad. at C_1
			R_{32}	r_{11}/A_{bf}	Infiltration C_1-outdoor air

Using the same transformation shown in Equation 33-39 in Chapter 3, this RC model can be written in the state space form in Equation 103.

$$\hat{x}_{i+1} = \mathcal{A}^o \hat{x}_i + \mathcal{B}^o u_i + \mathcal{D}^o w_i \tag{103}$$

Where $\mathcal{A}^o$, $\mathcal{B}^o$, and $\mathcal{D}^o$ are the state space, control space, and disturbance space matrix in the RC model, in which the parameters will be determined from RC model calibration.

6.2.3 RC model calibration

Assuming the areas (A) in Table 6.2 are known, there are only 18 parameters that need to be calibrated in this 32R-19C model, which are c_1-c_7 and r_1-r_{11}. In fact, only the proportional estimation, rather than the absolute value, of the area terms are needed to perform the variable reduction, since the area terms always occur with c or r terms in the RC model, where the c and r terms are all calibration parameters. Thus, the absolute value of any area term is never needed alone.

The following two aspects are considered in the calibration process to acquire the RC model that fits TPA control. 1) According to the formulation of TPA control, only the two activation points are determined by the optimizer, while the predicted states (x) or energy flow rate (u) are not required. 2) The "prediction accuracy" and the "ability to capture the dynamics of the building system" are usually regarded as the same objective in model calibration. However, depending on the definitions, the objectives of "accuracy" and "ability" may not always be identical.

With these considerations, the calibration performed in this study only focuses on maximizing the RC model's ability to capture the dynamics of the building system, in which the ability is defined as to reduce the difference between the actual and predicted temperature change (ΔT). Thus, the calibration aims to reduce the error in predicting the first-order derivative of the temperature profile. Accordingly, the objective function is given in Equation 104-106. In contrast, the most commonly used objective function in

minimizing the sum of squared error (SSE) in temperature prediction is given in Equation 107.

$$\hat{r}, \hat{c} = \underset{r,c}{argmin} \sum_{i} (\Delta \hat{T}_i - \Delta T_i)^2 \tag{104}$$

Where

$$\Delta \hat{T}_i = \hat{T}_i - \hat{T}_{i-1} \tag{105}$$

$$\Delta T_i = T_i - T_{i-1} \tag{106}$$

$$\hat{r}', \hat{c}' = \underset{r,c}{argmin} \sum_{i} (\hat{T}_i' - T_i)^2 \tag{107}$$

Where T_i is the mean temperature of the 5 zones recorded in thermostats. $\hat{T}_i$=$\hat{x}_{i(1)}$ is the predicted zone temperature from the building level RC model.

In this example, the RC model is calibrated based on the historical building operation condition in May 2019. The particle swarm optimization (PSO) is used as the optimization algorithm with the swarm size of 180. In this study, the RC model is only initialized once (on May 1st at 00:00) within the calibration period. It could also be initialized on a daily basis in order to fit the prediction structure of TPA control, which is running once a day (explained later in this section). Of course, the initial condition for model calibration is another factor that influences the performance of the trained model, especially when the RC model has a large size of capacitors. It is worthwhile for a separate study to discuss the training structure. In this study, the initial condition of this 32R-19C model is acquired by solving the steady-state heat transfer equation of the RC system, in which the room air temperature, outdoor air temperature, sky temperature, and internal heat

gain are used as the boundary conditions, given no solar radiation or HVAC operation at midnight. The temperature profiles of the calibration period are shown in Figure 6.5, and the training error's distribution is shown in Figure 6.6.

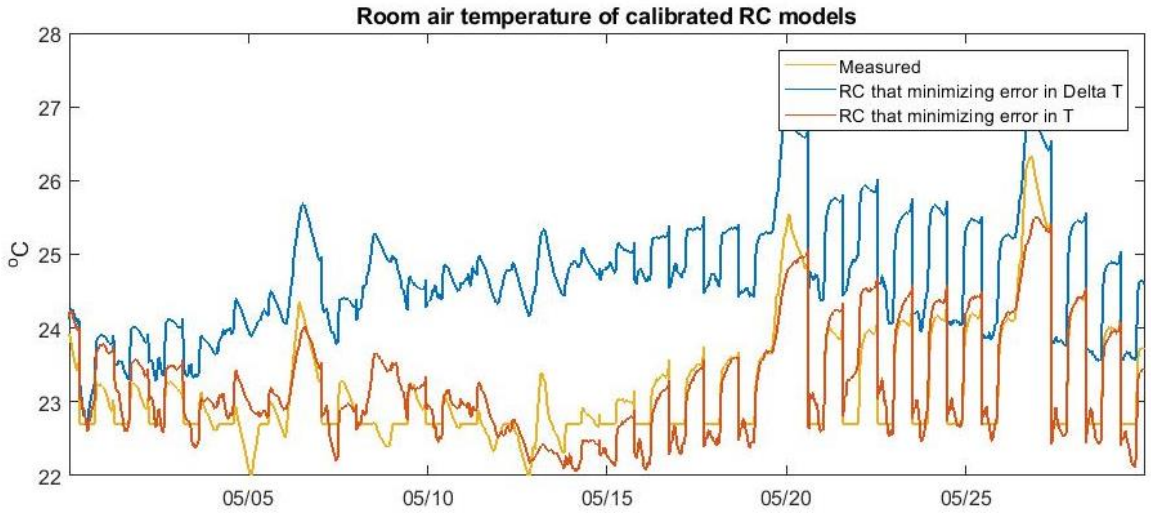

Figure 6.5 Room air temperature profiles of the calibrated RC models

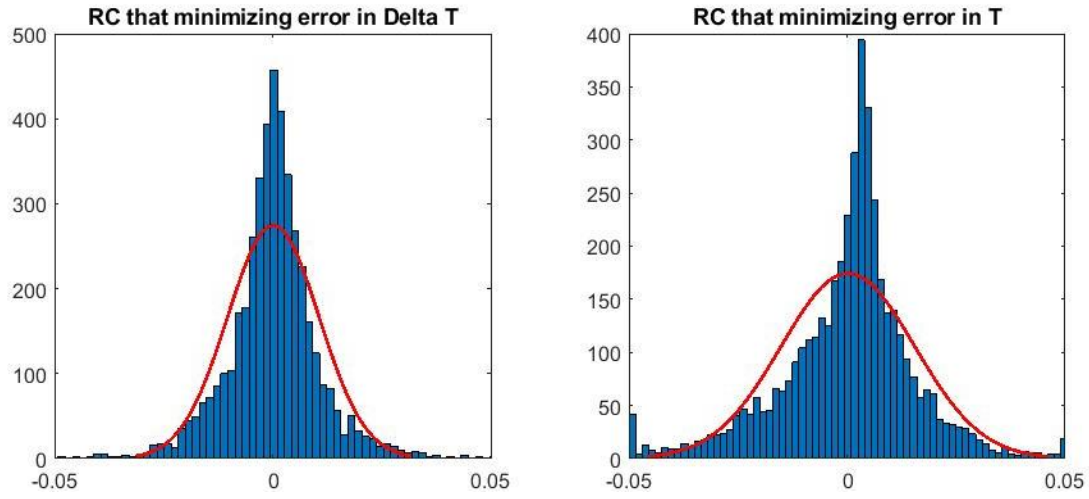

Figure 6.6 Error distributions of the calibrated RC models

It is not surprising that the RC model calibrated by minimizing the error in ΔT (ΔT model) provides the long-period temperature prediction that is way off from the measured data, as the prediction is significantly biased. On the other hand, the prediction error in ΔT

is reduced compared to the RC model calibrated by minimizing the prediction error in temperature (T model). An interpretation of the functionality of these two RC models is that the T model is trained to provide an accurate prediction for an extended period, and the ΔT model only focuses on the prediction accuracy of the next step. In other words, since the prediction error of ΔT in the ΔT model is unbiased and smaller than the T model, the "one-step" or say "next-step" temperature prediction of the ΔT model should be more accurate if it is initialized at every step. Given the fact that the prediction structure of the TPA control is on a daily initialized basis, to the author's belief, the ΔT model will perform better than the T model in providing one-day predictions for TPA control.

Therefore, the parameters $\hat{r}$ and $\hat{c}$ are calibrated according to the objective function in Equation 104, which serves as the material information in establishing the zone level RC models. The RC model of the south zone is shown as an example in Figure 6.7, and its parameters are listed in Table 6.3, in which A_{sf} is the floor area of the south zone. The other RC models of the perimeter zones have the same model form as for the south zone; the center zone model has only 3 capacitors representing the room air, the first and second layer of the floor.

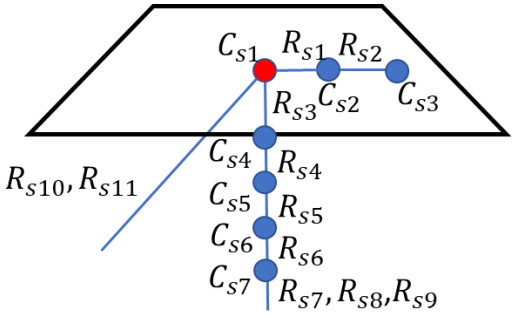

Figure 6.7 Structure of the south zone RC model

Table 6.3 RC parameters in the south zone RC model

Capacitor	Calculated by	Physical Representation	Resistor	Calculated by	Physical Representation
C_{s1}	$c_1 \times A_{sf}$	South Zone	R_{s1}	r_1/A_{sf}	Convection C_{s1}-C_{s2}
C_{s2}	$c_2 \times A_{sf}$	S. Floor, Layer 1	R_{s2}	r_2/A_{sf}	Conduction C_{s2}-C_{s3}
C_{s3}	$c_3 \times A_{sf}$	S. Floor, Layer 2	R_{s3}	r_3/A_{sw}	Convection C_{s1}-C_{s4}
C_{s4}	$c_4 \times A_{sw}$	S. Wall, Layer 1	R_{s4}	r_4/A_{sw}	Conduction C_{s4}-C_{s5}
C_{s5}	$c_5 \times A_{sw}$	S. Wall, Layer 2	R_{s5}	r_5/A_{sw}	Conduction C_{s5}-C_{s6}
C_{s6}	$c_6 \times A_{sw}$	S. Wall, Layer 3	R_{s6}	r_6/A_{sw}	Conduction C_{s6}-C_{s7}
C_{s7}	$c_7 \times A_{sw}$	S. Wall, Layer 4	R_{s7}	r_7/A_{sw}	Convection C_{s7}-outdoor air
			R_{s8}	r_8/A_{sw}	Solar Rad. at C_{s7}
			R_{s9}	r_9/A_{sw}	Long-wave Rad. C_{s7}-sky
			R_{s10}	r_{10}/A_{sf}	Solar Rad. At C_{s1}
			R_{s11}	r_{11}/A_{sf}	Infiltration C_{s1}-outdoor air

6.2.4 Optimization and simulation result

In order to illustrate the advantage of the TPA control structure for optimization, the exhaustive search method is used as the algorithm to find the optimal temperature setpoint profile in this study. The optimization process is performed in steps listed below.

1) The possible starting point of precooling is limited to 6:00 to 9:00, and the possible starting point of load shifting is between precooling and 14:00. The control interval is set at 10 mins, and the prediction horizon is 24 hours.
2) Every day at 0:00, the TPA-MPC is performed to provide the optimal temperature setpoints for the entire day. In which the RC models are initialized based on the steady-state heat transfer equation. Then the full-combination of the activation points is generated to form the candidate schedules for every zone. Through the simulation in RC models, the optimal setpoint temperature profiles are selected as the ones with the lowest zonal HVAC operation cost. The uncertain scenario parameters are used in RC models in prediction.

3) The optimal temperature setpoints of the day are sent to the thermostats in each zone, and the actual HVAC operation cost is recorded for evaluation.

Figure 6.8 shows the objective values in the solution space of all 5 zones, on a typical day in July, in which load shifting is used as the control strategy. If an activation point of precooling cannot make the room air temperature within the thermal comfort band before working hour starts, the HVAC operation cost based on this activation point will be assigned by the highest objective value in the solution space. The optimal solution of each zone is marked in a red block.

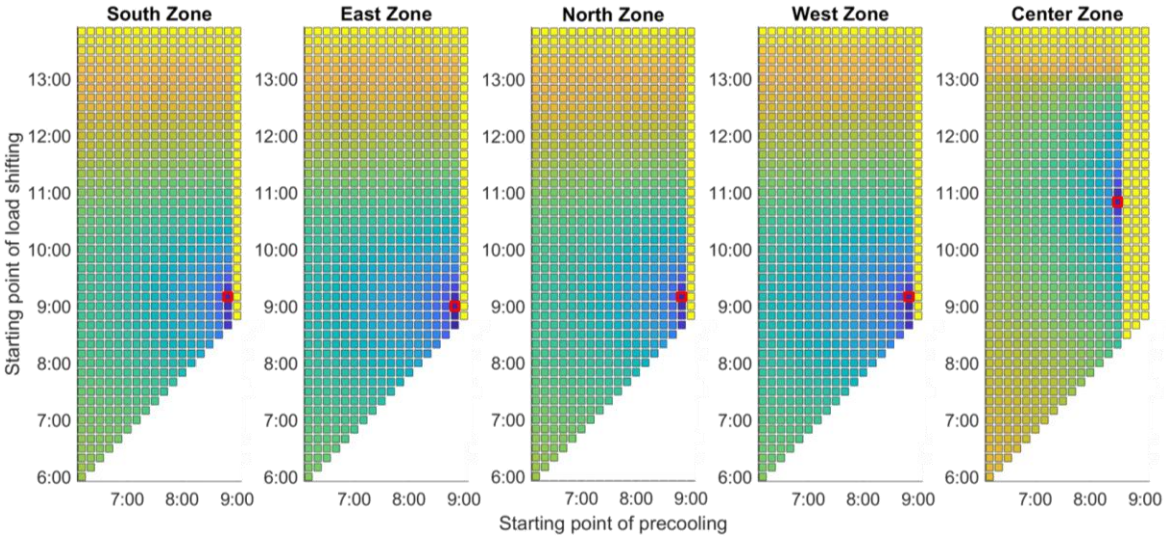

Figure 6.8 Objective value and optimum in the solution space of each RC model

Several points are made from observing Figure 6.8. 1) The solution space is visually very smooth, even though the mathematical smoothness cannot be defined due to the discrete form of the solution space. 2) The objective value is monotonically decreasing across the x-axis, and it is concave across the y-axis. Based on the results, this RC model enabled TPA control can be interpreted as finding the best starting time for load shifting and the latest feasible starting time for precooling.

The south zone temperature profiles based on the RC model enabled TPA control are shown in Figure 6.9, in comparison with the AA, LL, and LL# cases. The detailed case setups are listed in Table 6.4. The same-day temperature profiles of other zones are shown in Appendix B

Table 6.4 Detailed case setups

Case Code	Prediction model	Optimization algorithm	Scenario uncertainty in prediction	Control strategy	Control input to HVAC
Original	-	-	-	Original	Setpoint T.
AAL	Nodal network	Linear programming	No uncertainty	Load shifting	Energy flow rate
LLL	Nodal network	Linear programming	Local prediction	Load shifting	Energy flow rate
LLL#	Nodal network	Translated from LLL	Local prediction	Load shifting	Setpoint T.
RCL#	Zonal RC models	Exhaustive search	Local prediction	Load shifting	Setpoint T.
P. Shav.	-	-	-	Peak shaving	Setpoint T.
AALP	Nodal network	Linear programming	No uncertainty	L+P	Energy flow rate
LLLP	Nodal network	Linear programming	Local prediction	L+P	Energy flow rate
LLLP#	Nodal network	Translated from LLLP	Local prediction	L+P	Setpoint T.
RCLP#	Zonal RC models	Exhaustive search	Local prediction	L+P	Setpoint T.

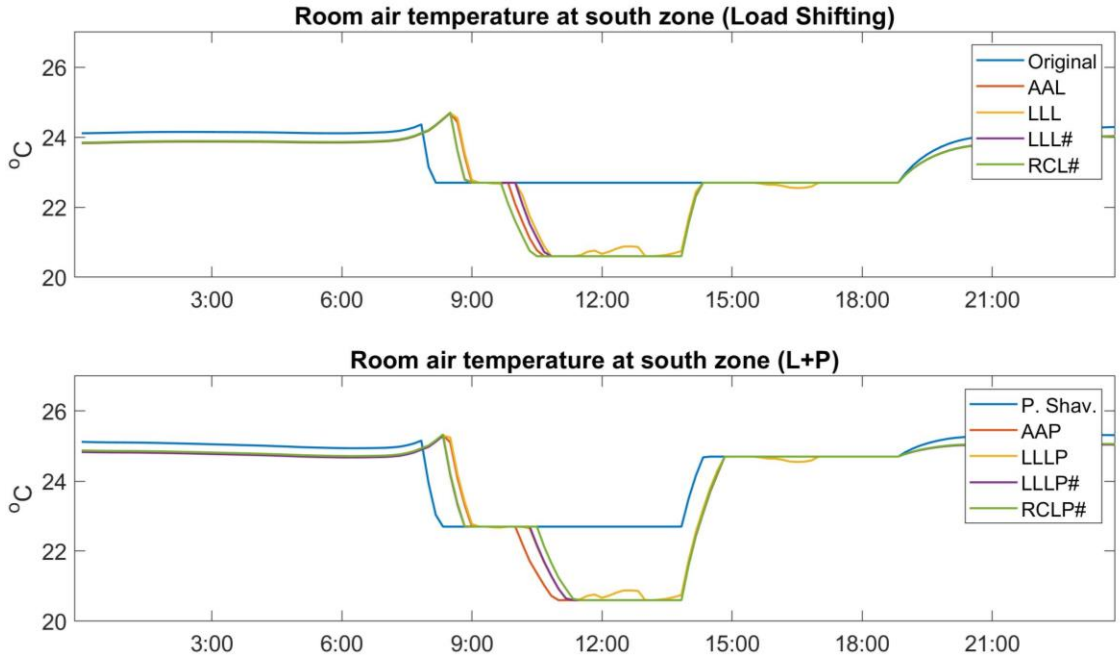

Figure 6.9 Comparison of temperature profiles in different MPC cases

The temperature profiles show that the RC model based TPA control is able to provide similar setpoint temperature schedules to the ones translated from the results of linear programming optimization. To summarize, the cost-saving performance of all cases above is compared in Table 6.5.

Table 6.5 Comparison of cost-saving performance in different MPC cases

Case Code	HVAC operation cost (USD)	Cost savings (USD)	Cost-saving percentage (%)
Original	1354.43	-	-
AAL	1245.54	108.89	8.0%
LLL	1257.37	97.06	7.2%
LLL#	1256.76	97.68	7.2%
RCL#	1255.64	98.79	7.3%
Peak Shav.	1027.34	327.09	24.1%
AALP	949.18	405.26	29.9%
LLLP	959.01	395.42	29.2%
LLLP#	960.04	394.39	29.1%
RCLP#	959.25	395.18	29.2%

The results show that the RC model based TPA control has exceptional cost-saving performance, and more cost saving is realized in the RCL# case than the LLL and LLL# cases. To be noticed, since the LLL and LLL# cases are not the theoretical optimum due to the influence of scenario uncertainty, the RC model based TPA control is, in fact, able to outperform these cases. An intuitive explanation for this outperformance is that since the RC model has less dynamics than the nodal-network model, it is more reluctant to the fluctuations of the scenario parameters hence less sensitive to the influence of scenario uncertainty. However, proving or rejecting this hypothesis is beyond the scope of this study. Anyhow, the effectiveness of the RC model based TPA control is proved through the obtained result.

6.3 Conclusion

Two-Point Activation control is developed in this chapter as a simple but effective MPC implementation basis, which explicitly fits the purpose of building thermal load control. Due to its structure, TPA control dramatically reduces the computational complexity of the optimization. This advantage indirectly relieves the strain on the form of prediction models used in MPC. Therefore, the RC model used in the case study can be replaced by any building model as long as it can be acquired and provide predictions efficiently.

There is a limitation of TPA control. Its control structure stands alone if the HVAC operation cost at a certain control interval only depends on the energy flow rate through the terminal units within that interval, that $C_i = g(u_i)$, where C_i is the operation cost at step i, $g(u_i)$ is the HVAC model that calculates the HVAC operation cost from energy flow rate. In the case study, $g(u_i) = TOU_i \cdot u_i / COP_{season}$. To be noticed, this condition does not mean that the TPA control is not able to work with a complicated HVAC system, but the $g(u_i)$ should be able to receive additive u_i from each zone as input and does not rely on the building or HVAC states. In other words, as the optimal setpoint temperature schedule is generated by TPA control, the optimal energy flow rate profile is also generated simultaneously but implicitly. The HVAC model can only take this profile as a disturbance term rather than adjust it based on its own characteristics.

A counterexample is to use a thermal storage tank as a component added to the HVAC system with building thermal load control to realize the overall minimum of operation cost. In this setup, the operation cost at a specific control interval should be

calculated based on both the energy flow rate and the state of the tank, as $C_i = g(u_i, x_{tank,i})$. The rationale would be that energy in the storage tank represents saved energy for later use. Defining u_i solely based on the building model may only lead to sub-optimum of the entire system. In fact, a holistic optimization can be approached by augmenting the building model with the storage whose future state is predicted by the complete building model. Of course, the feasibility of TPA control on this augmented building model requires more study as the control of the charging and discharging of the storage tank may not easily lend itself to a small set of discrete actions.

CHAPTER 7. CONCLUSION AND FUTURE WORKS

This dissertation puts focus on building thermal load control with the aim to analyze its theoretical potential, its control strategies, the way that performance is influenced by variability and scenario uncertainty, and verification of possible implementation methods. The research outcomes serve to expand the understanding of building thermal load control from these perspectives. Since the substudies in this research are composed in a relatively independent structure, the conclusions have been drawn at the end of each chapter. Several substantial points deserve repeating.

1) The range of zonal control flexibility is significant. The study in Chapter 2 provides a method to sample the zonal control flexibility for research purposes. In reality, it should be carefully defined for each thermal zone separately.
2) An MPC workflow for analyzing the theoretical potential of building thermal load control is illustrated in Chapter 3. The result proves the potential for cost-saving by using multiple control strategies but questions the MPC's utility in increasing organizational benefits. The result also shows that the contribution by pure load shifting through the use of passive thermal mass is limited.
3) The influence of climates and construction types on the cost-saving performance is analyzed in Chapter 4. It is shown that climate conditions have a substantial influence on the performance, while the influence from construction type is minimal. An emulator is developed to provide a quick estimation of the saving percentages in any given location.

4) From the study in Chapter 5, it is apparent that the influence of scenario uncertainty on the performance of MPC is marginal. A properly defined MPC proves to have adequate robustness for cost saving under scenario uncertainties.
5) The study in Chapter 6 illustrates that the theoretical control sequence of energy flow rate can be characterized by a simple control regime, consisting of two activation points that modifying the original setpoint temperature schedule. A case study further demonstrates the effectiveness of this TPA control.

On the other hand, there are some limitations and imperfections of this study. Firstly, as elaborated at the end of Chapter 3, this control method heavily relies on the knowledge of the thermal comfort requirements. An arbitrarily defined control band may result in the violation of thermal comfort or the unrealization of saving potential or even both. Secondly, TPA control may not be readily executable for any HVAC system. If an HVAC system does not satisfy the required formulation of TPA control, a re-evaluation of the entire system is needed. Last but not least, it should be understood that the thermal comfort requirement is not time-invariant, hence control flexibility will vary over time. Ideally, an explanatory model should be added ahead to predict the thermal comfort requirements over time. Unfortunately, our understanding on this research topic is still immature.

Based on the research outcomes and the identified limitations of this dissertation, the following research topics are expected to be addressed in the future.

1) Since the objective building defined in this dissertation only includes the office work as zone function, other building types may lead to distinctly different

performances of building thermal load control. The methodology developed in this research may serve as a reference for future parallel studies

2) Due to the conclusive format (satisfied/unsatisfied) of thermal dissatisfaction recorded in the database, the study performed in Chapter 2 failed to provide control flexibilities of the zones with very few occupants (below 5). This problem can be solved by taking the quantitatively defined dissatisfaction of individuals and tracking in which zones they reside at a given moment, but the data gathering requires a huge amount of effort. An example is seen in [130].
3) The control flexibility is defined only based on the room air temperature in this research. A more comprehensive definition could be given if more evidence supports it. Ideally, control flexibility should be defined dynamically.
4) The adaptability of TPA control to HVAC systems could be further analyzed, especially when the building model requires to be augmented by the HVAC model, especially in the presence of components with latency. If there exists a TPA control (or similar control type) that effectively optimizes the control sequences utilizing the active and passive thermal mass simultaneously, the cost-saving will be substantial, while the implementation of the MPC would still be straightforward.
5) As building thermal load control is fundamentally a strategy under the topic of Energy Flexibility Buildings, further analyzes are required to understand its influence and coeffects at grid scale. The study presented in this dissertation can serve as a starting point in extending the analysis.

APPENDIX A. PARAMETERS IN THE EMULATOR FOR COST-SAVING POTENTIAL ESTIMATION

Given the seasonal cost-saving percentage is calculated by the emulator as

$$S_{season} = c \sum_{d} w_d S_d \tag{59}$$

$$w_d = \frac{C_d}{\sum_d C_d} \tag{60}$$

There are 4 sets of parameters in estimating 1) daily saving percentage of load shifting ($S_{d,L}$), 2) daily saving percentage of peak shaving ($S_{d,L}$), 3) daily saving percentage of load shifting + peak shaving ($S_{d,L+P}$), and 4) daily HVAC operation cost (C_d). The regression model is in the form of

$$Y = X\beta \tag{108}$$

The parameter c in Equation 59 is about 0.968, and the 4 sets of regression parameters are given in the table below:

Parameters	$S_{d,L}$	$S_{d,L}$	$S_{d,L+P}$	C_d
$\bar{T}_a^2$	0.00034686	0.00077242	0.00056912	-0.01309964
$\tilde{T}_a^2$	-0.00006534	0.00025148	0.00000057	-0.01258717
$\bar{T}_s^2$	-0.00007220	-0.00043475	-0.00034112	0.03271755
$\tilde{T}_s^2$	0.00006260	0.00033140	0.00073443	-0.00286125
$\bar{Q}_s^2$	0.00000076	0.00000141	0.00000222	-0.00006411
$\tilde{Q}_s^2$	-0.00000010	-0.00000025	-0.00000039	0.00000289
$\bar{T}_a$	-0.02386799	-0.06891049	-0.05309684	1.24386216
$\tilde{T}_a$	0.00531426	0.00271596	0.01047758	-0.23146703
$\bar{T}_s$	0.04179336	0.25646407	0.20086244	-18.23682372
$\tilde{T}_s$	-0.00166757	-0.00117060	-0.00928246	0.25677054
$\bar{Q}_s$	-0.00032837	-0.00009210	-0.00060128	0.02332065
$\tilde{Q}_s$	0.00008469	0.00028664	0.00043943	-0.00172435
1	-5.55455401	-36.38441081	-28.31891744	2526.33445437

APPENDIX B. COMPARISON OF TEMPERATURE PROFILES IN DIFFERENT MPC CASES

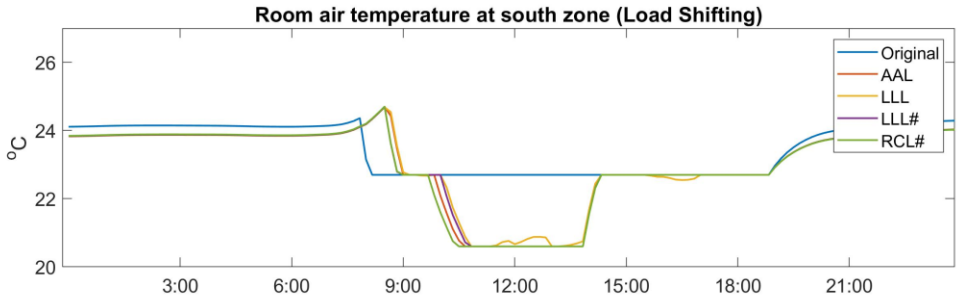

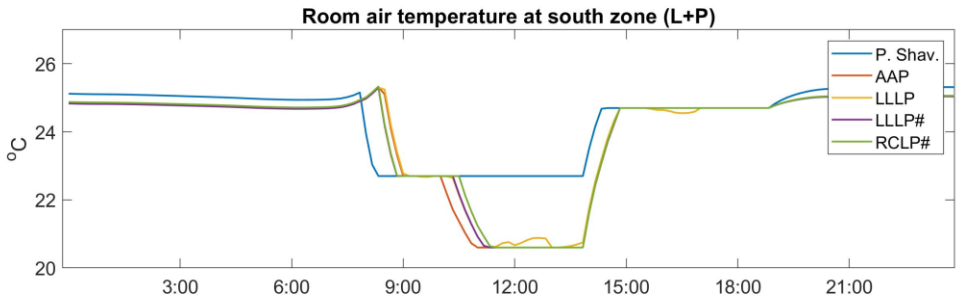

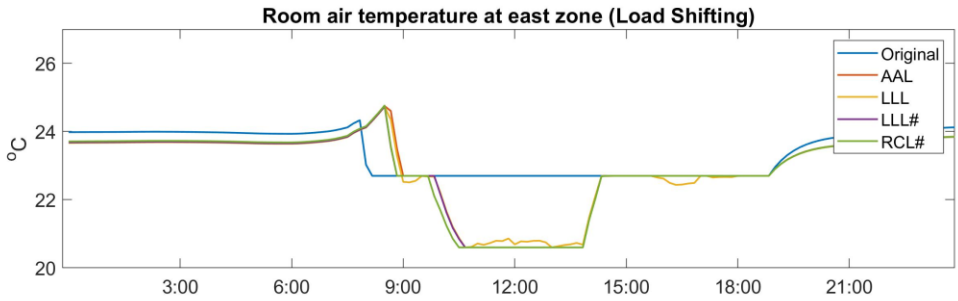

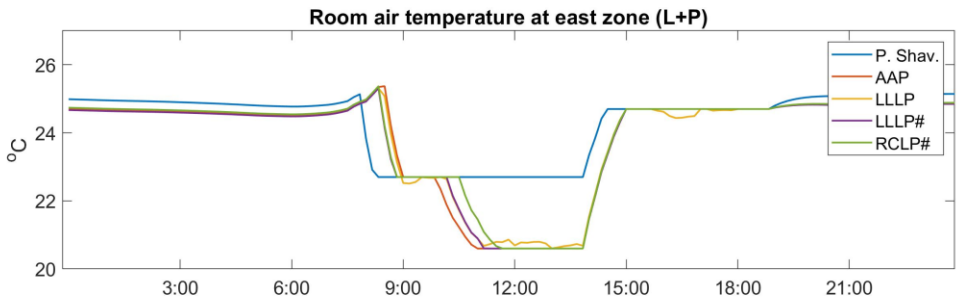

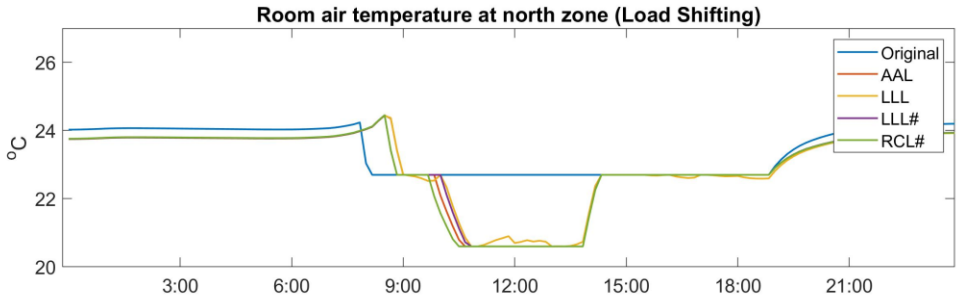
Room air temperature at north zone (Load Shifting)
°C
26
24
22
20
3:00
6:00
9:00
12:00
15:00
18:00
21:00
Original
AAL
LLL
LLL#
RCL#

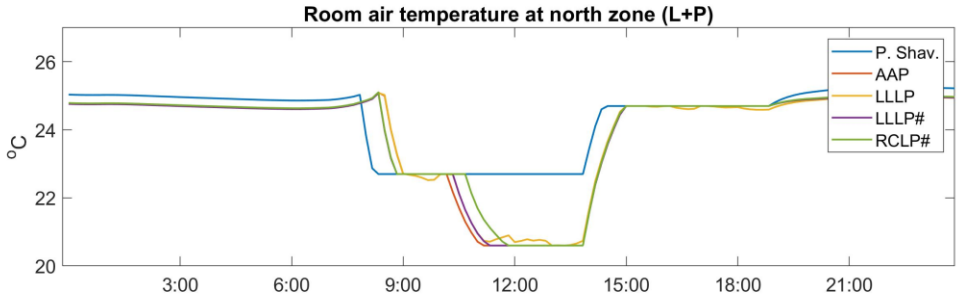
Room air temperature at north zone (L+P)
°C
26
24
22
20
3:00
6:00
9:00
12:00
15:00
18:00
21:00
P. Shav.
AAP
LLLP
LLLP#
RCLP#

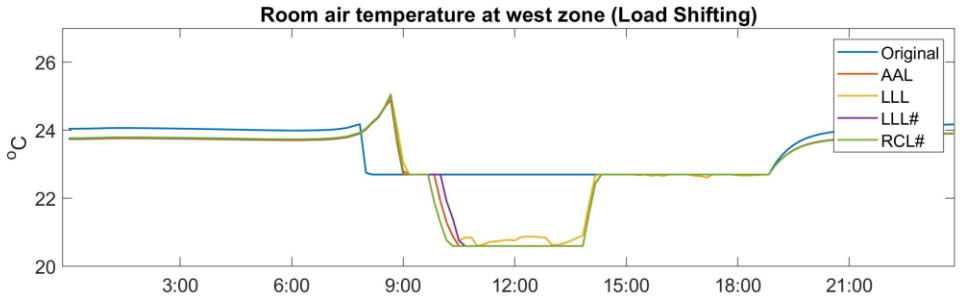
Room air temperature at west zone (Load Shifting)
°C
26
24
22
20
3:00
6:00
9:00
12:00
15:00
18:00
21:00
Original
AAL
LLL
LLL#
RCL#

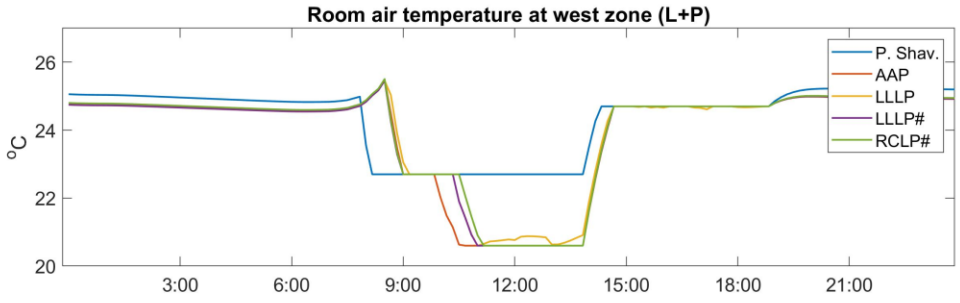
Room air temperature at west zone (L+P)
°C
26
24
22
20
3:00
6:00
9:00
12:00
15:00
18:00
21:00
P. Shav.
AAP
LLLP
LLLP#
RCLP#

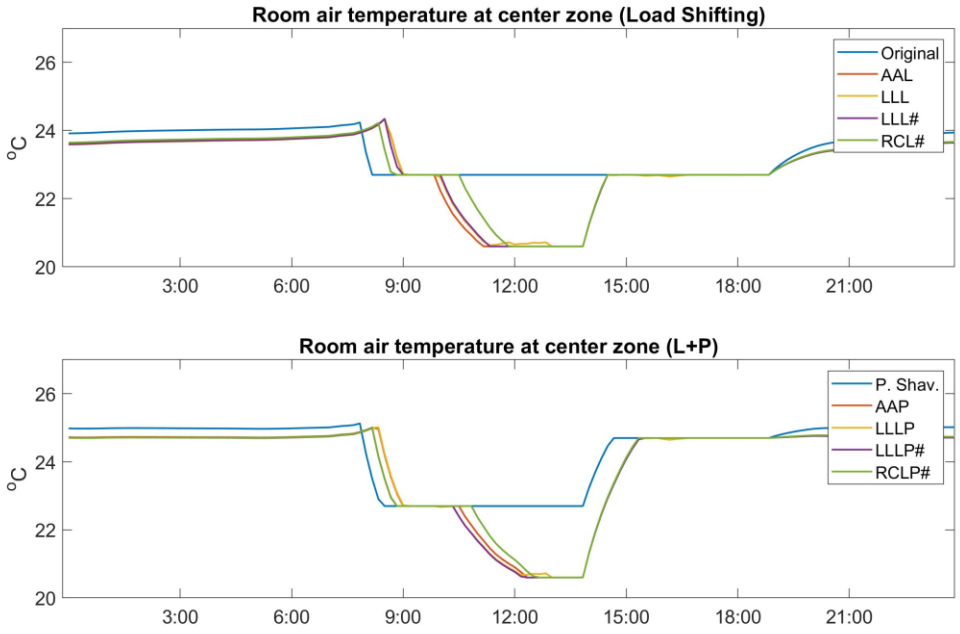
Room air temperature at center zone (Load Shifting)
°C
26
24
22
20
3:00
6:00
9:00
12:00
15:00
18:00
21:00
Original
AAL
LLL
LLL#
RCL#
Room air temperature at center zone (L+P)
°C
26
24
22
20
3:00
6:00
9:00
12:00
15:00
18:00
21:00
P. Shav.
AAP
LLLP
LLLP#
RCLP#

REFERENCES

[1] U.S. Energy Information Administration, "Annual Energy Outlook 2018 with projections to 2050"

[2] Jensen, S. Ø., et al. (2017). "IEA EBC Annex 67 Energy Flexible Buildings." Energy and Buildings **155**: 25-34.

[3] Fanger, Poul O. "Thermal comfort. Analysis and applications in environmental engineering." Thermal comfort. Analysis and applications in environmental engineering. (1970).

[4] ASHRAE, " ASHRAE/ANSI Standard 55-2017 Thermal environmental conditions for human occupancy. " 2017, American Society of Heating, Refrigerating, and Air-Conditioning Engineers: Atlanta, GA.

[5] REHVA Guidebook No. 6 - Indoor Climate and Productivity in Offices - How to Integrate Productivity in Life-Cycle Cost Analysis of Building Services. (2006). REHVA.

[6] Lan, L., P. Wargocki, D. P. Wyon, and Z. Lian. "Effects of Thermal Discomfort in an Office on Perceived Air Quality, SBS Symptoms, Physiological Responses, and Human Performance." Indoor Air 21.5 (2011): 376-90. Web.

[7] WGBC (2014 September). Health, wellbeing and productivity. (2014 September). Retrieved February 28, 2017, from http://www.ukgbc.org/campaigns-policy/campaigns/health-wellbeing-and-productivity

[8] Wang, Z., et al. (2018). "Individual difference in thermal comfort: A literature review." Building and Environment 138: 181-193

[9] Killian, M., and M. Kozek. "Ten questions concerning model predictive control for energy efficient buildings." Building and Environment 105 (2016): 403-412.

[10] Gregor P. Henze (2013) "Model predictive control for buildings: a quantum leap? ", Journal of Building Performance Simulation, 6:3, 157-158, DOI: 10.1080/19401493.2013.778519

[11] Henze, Gregor P., Clemens Felsmann, and Gottfried Knabe. "Evaluation of optimal control for active and passive building thermal storage." International Journal of Thermal Sciences43.2 (2004): 173-183.

[12] Kim, Sean Hay. "Building demand-side control using thermal energy storage under uncertainty: An adaptive multiple model-based predictive control (mmpc) approach." Building and Environment 67 (2013): 111-128.

[13] Ma, Yudong, Jadranko Matuško, and Francesco Borrelli. "Stochastic model predictive control for building HVAC systems: Complexity and conservatism." IEEE Transactions on Control Systems Technology 23.1 (2014): 101-116.

[14] Henze, Gregor P., et al. "Experimental analysis of model-based predictive optimal control for active and passive building thermal storage inventory." HVAC&R Research 11.2 (2005): 189-213.

[15] Corbin, Charles D., Gregor P. Henze, and Peter May-Ostendorp. "A model predictive control optimization environment for real-time commercial building application." Journal of Building Performance Simulation 6.3 (2013): 159-174.

[16] May-Ostendorp, Peter, et al. "Model-predictive control of mixed-mode buildings with rule extraction." Building and Environment 46.2 (2011): 428-437.

[17] Sloup, Charles J., Daniel Karnes, and Gregor P. Henze. "Real-time global optimization of building setpoints and sequence of operation." U.S. Patent No. 7,894,943. 22 Feb. 2011.

[18] Nikovski, D., J. Xu, and M. Nonaka. "A method for computing optimal set-point schedules for HVAC systems." Proceedings of the 11th REHVA World Congress CLIMA. 2013.

[19] Afram, Abdul, et al. "Artificial neural network (ANN) based model predictive control (MPC) and optimization of HVAC systems: A state of the art review and case study of a residential HVAC system." Energy and Buildings 141 (2017): 96-113.

[20] Tanaskovic, Marko, et al. "Robust adaptive model predictive building climate control." Ifac-Papersonline 50.1 (2017): 1871-1876.

[21] Afram, Abdul, et al. "Development and performance comparison of low-order black-box models for a residential HVAC system." Journal of Building Engineering 15 (2018): 137-155.

[22] Afram, Abdul, et al. "Development of an accurate gray-box model of ubiquitous residential HVAC system for precise performance prediction during summer and winter seasons." Energy and Buildings 171 (2018): 168-182.

[23] Huang, Hao, Lei Chen, and Eric Hu. "A neural network-based multi-zone modelling approach for predictive control system design in commercial buildings." Energy and buildings 97 (2015): 86-97.

[24] Ferreira, P. M., et al. "Neural networks based predictive control for thermal comfort and energy savings in public buildings." Energy and buildings 55 (2012): 238-251.

[25] Hazyuk, Ion, Christian Ghiaus, and David Penhouet. "Optimal temperature control of intermittently heated buildings using Model Predictive Control: Part I–Building modeling." Building and Environment 51 (2012): 379-387.

[26] Hazyuk, Ion, Christian Ghiaus, and David Penhouet. "Optimal temperature control of intermittently heated buildings using Model Predictive Control: Part II–Control algorithm." Building and Environment 51 (2012): 388-394.

[27] Sharma, Isha, et al. "A modeling framework for optimal energy management of a residential building." Energy and Buildings130 (2016): 55-63.

[28] Cole, Wesley J., et al. "Reduced-order residential home modeling for model predictive control." Energy and Buildings74 (2014): 69-77.

[29] Lefort, Antoine, et al. "Hierarchical control method applied to energy management of a residential house." Energy and Buildings 64 (2013): 53-61. [30] Huang, Hao, et al. "A new zone temperature predictive modeling for energy saving in buildings." Procedia Engineering 49 (2012): 142-151.

[31] Li, Xiwang, and Ali Malkawi. " Multi-objective optimization for thermal mass model predictive control in small and medium size commercial buildings under summer weather conditions." Energy 112 (2016): 1194-1206.

[32] Široký, Jan, et al. "Experimental analysis of model predictive control for an energy efficient building heating system." Applied energy 88.9 (2011): 3079-3087.

[33] Afram, Abdul, and Farrokh Janabi-Sharifi. "Supervisory model predictive controller (MPC) for residential HVAC systems: Implementation and experimentation on archetype sustainable house in Toronto." Energy and Buildings 154 (2017): 268-282.

[34] Reynolds, Jonathan, et al. "A zone-level, building energy optimisation combining an artificial neural network, a genetic algorithm, and model predictive control." Energy 151 (2018): 729-739.

[35] Maasoumy, Mehdi, et al. "Handling model uncertainty in model predictive control for energy efficient buildings." Energy and Buildings 77 (2014): 377-392.

[36] Avci, Mesut, et al. "Model predictive HVAC load control in buildings using real-time electricity pricing." Energy and Buildings 60 (2013): 199-209.

[37] Oldewurtel, Frauke, et al. "Use of model predictive control and weather forecasts for energy efficient building climate control." Energy and Buildings 45 (2012): 15-27.

[38] Liu, Xiaoqi, et al. "Model predictive control under forecast uncertainty for optimal operation of buildings with integrated solar systems." Solar Energy 171 (2018): 953-970.

[39] Chen, Yuxiang, Khaled E. Galal, and Andreas K. Athienitis. "Design and operation methodology for active building-integrated thermal energy storage systems." Energy and Buildings 84 (2014): 575-585.

[40] Chen, Yuxiang, Andreas K. Athienitis, and Khaled E. Galal. "A charging control strategy for active building-integrated thermal energy storage systems using frequency domain modeling." Energy and Buildings 84 (2014): 651-661.

[41] Khakimova, Albina, et al. "Optimal energy management of a small-size building via hybrid model predictive control." Energy and Buildings 140 (2017): 1-8.

[42] Bălan, Radu, et al. "Parameter identification and model based predictive control of temperature inside a house." Energy and Buildings 43.2-3 (2011): 748-758.

[43] Yu, Zhun Jerry, et al. "Control strategies for integration of thermal energy storage into buildings: State-of-the-art review." Energy and Buildings 106 (2015): 203-215.

[44] Li, Xiwang, and Jin Wen. "Review of building energy modeling for control and operation." Renewable and Sustainable Energy Reviews 37 (2014): 517-537.

[45] Afram, Abdul, and Farrokh Janabi-Sharifi. "Theory and applications of HVAC control systems–A review of model predictive control (MPC)." Building and Environment 72 (2014): 343-355.

[46] Privara, Samuel, et al. "Building modeling: Selection of the most appropriate model for predictive control." Energy and Buildings 55 (2012): 341-350.

[47] Patteeuw, Dieter, Gregor P. Henze, and Lieve Helsen. "Comparison of load shifting incentives for low-energy buildings with heat pumps to attain grid flexibility benefits." Applied energy 167 (2016): 80-92.

[48] PC Reviews, "The Best Smart Thermostats for 2019", https://www.pcmag.com/article/356755/the-best-smart-thermostats (Accessed September 2019).

[49] DeLand, Seth, MathWorks MathWorks, "Solving Large-Scale Optimization Problems with MATLAB: A Hydroelectric Flow Example", https://www.mathworks.com/company/newsletters/articles/solving-large-scale-optimization-problems-with-matlab-a-hydroelectric-flow-example.html (Accessed September 2019)

[50] BSI. "BS EN ISO 7730: 2005: Ergonomics of the Thermal Environment. Analytical Determination and Interpretation of Thermal Comfort Using Calculation of the PMV and PPD Indices and Local Thermal Comfort Criteria." (2005).

[51] ASHRAE, "ASHRAE Thermal Comfort Tool CD", v2. Atlanta: ASHRAE (2011).

[52] Brager, G., et al. "A comparison of methods for assessing thermal sensation and acceptability in the field." (1993).

[53] Wall Street Mojo, "Revenue Per Employee Ratio Formula", https://www.wallstreetmojo.com/revenue-per-employee/ (Accessed September 2019).

[54] Fountain, Marc, Gail Brager, and Richard De Dear. "Expectations of indoor climate control." Energy and Buildings 24.3 (1996): 179-182.

[55] Mahdavi, Ardeshir, and Satish Kumar. "Implications of indoor climate control for comfort, energy and environment." Energy and Buildings 24.3 (1996): 167-177.

[56] Humphreys, Michael A., and J. Fergus Nicol. "The validity of ISO-PMV for predicting comfort votes in every-day thermal environments." Energy and buildings 34.6 (2002): 667-684.

[57] Van Hoof, Joost, Mitja Mazej, and Jan LM Hensen. "Thermal comfort: research and practice." Frontiers in Bioscience 15.2 (2010): 765-788.

[58] Hensen, Jan LM, and Roberto Lamberts, eds. Building performance simulation for design and operation. Routledge, Expanded Second Edition 2019.

[60] Pepler R, Warner R, “Temperature and Learning: An experimental study”. Paper No 2089. Transactions of ASHRAE annual meeting, (Lace Placid 1967), 211-219.

[61] Seppanen, Olli, William J. Fisk, and David Faulkner. "Control of temperature for health and productivity inoffices." ASHRAE transactions 111.LBNL-55448 (2004).

[62] Al Horr, Yousef, et al. "Occupant productivity and office indoor environment quality: A review of the literature." Building and environment 105 (2016): 369-389.

[63] Kekäläinen, Pirjo, et al. "Effect of reduced summer indoor temperature on symptoms, perceived work environment and productivity in office work: An intervention study." Intelligent Buildings International 2.4 (2010): 251-266.

[64] Zhang, Fan, et al. "The effects of higher temperature setpoints during summer on office workers' cognitive load and thermal comfort." Building and Environment 123 (2017): 176-188.

[65] Niemelä, Raimo, et al. "The effect of air temperature on labour productivity in call centres—a case study." Energy and buildings 34.8 (2002): 759-764.

[66] Federspiel, Clifford C., et al. Worker performance and ventilation: Analyses of individual data for call-center workers. No. LBNL-50124. Lawrence Berkeley National Lab.(LBNL), Berkeley, CA (United States), 2002.

[67] Seppanen, O., William J. Fisk, and Q. H. Lei. "Room temperature and productivity in office work." (2006).

[68] Ghahramani, Ali, Farrokh Jazizadeh, and Burcin Becerik-Gerber. "A knowledge based approach for selecting energy-aware and comfort-driven HVAC temperature set points." Energy and Buildings 85 (2014): 536-548.

[69] Zhang, Yuna. Optimal strategies for demand charge reduction by commercial building owners. Diss. Georgia Institute of Technology, 2017.

[70] Wang, Zhe, et al. "Individual difference in thermal comfort: A literature review." Building and Environment 138 (2018): 181-193.

[71] De Dear, Richard J. "A global database of thermal comfort field experiments." ASHRAE transactions 104 (1998): 1141.

[72] Ličina, Veronika Földváry, et al. "Development of the ASHRAE global thermal comfort database II." Building and Environment 142 (2018): 502-512.

[73] ASHRAE, ASHRAE Global Thermal Comfort Database II, http://www.comfortdatabase.com/, (Accessed September 2019).

[74] Tian, Wei, et al. "A review of uncertainty analysis in building energy assessment." Renewable and Sustainable Energy Reviews 93 (2018): 285-301.

[75] Li, Qi, et al. "Calibration of dynamic building energy models with multiple responses using Bayesian Inference and Linear Regression models." Energy Procedia 78 (2015): 979-984.

[76] De Dear, Richard, and Gail Schiller Brager. "Developing an adaptive model of thermal comfort and preference." (1998).

[77] Georgia Power, “Time of use – energy only schedule:TOU-EO-10”, https://www.georgiapower.com/content/dam/georgia-power/pdfs/business-pdfs/rates-schedules/small-business/3.30_TOU-EO.pdf (Accessed September 2019).

[78] Underwood, Chris P., and Francis Yik. Modelling methods for energy in buildings. Oxford: Blackwell Science, 2004.

[79] Augenbroe, Godfried, et al. "Lessons from an advanced building simulation course." Proceedings of SimBuild 3.1 (2008): 261-268.

[80] Borrelli, Francesco, Alberto Bemporad, and Manfred Morari. Predictive control for linear and hybrid systems. Cambridge University Press, 2017.

[81] Nicol, J. Fergus, and Michael A. Humphreys. "Adaptive thermal comfort and sustainable thermal standards for buildings." Energy and buildings 34.6 (2002): 563-572.

[82] Nicol, Fergus, Michael Humphreys, and Susan Roaf. Adaptive thermal comfort: principles and practice. Routledge, 2012.

[83] U.S. Department of Energy, EnergyPlus, https://energyplus.net/, (Accessed November 2019)

[84] The University of Wisconsin Madison, TRNSYS, https://sel.me.wisc.edu/trnsys/features/ , (Accessed November 2019)

[85] Drgoňa, Ján, et al. "All you need to know about model predictive control for buildings." Annual Reviews in Control (2020).

[86] ASHRAE. 2013. ASHRAE Standard 169-2013, Weather Data for Building Design Standards. American Society of Heating, Refrigerating and Air-Conditioning Engineers, Atlanta, Georgia.

[87] ICC. 2014. 2015 International Energy Conservation Code and ANSI/ASHRAE/IES Standard 90.1- 2013: Energy Standard for Buildings Except LowRise Residential Buildings. International Code Council, Washington, DC.

[88] Baechler, M. C., Williamson, J. L., Gilbride, T. L., Cole, P. C., Hefty, M. G., & Love, P. M. (2010). Building America best practices series: volume 7.1: guide to determining climate regions by county (No. PNNL-17211 Rev. 1). Pacific Northwest National Lab.(PNNL), Richland, WA (United States).

[89] Florida Power & Light, Summary of your rates, https://www.fpl.com/rates/pdf/new-customer-overview.pdf, (Accessed May 2020)

[90] Xcel Energy, Texas Time of Use Rate, https://www.xcelenergy.com/staticfiles/xe-responsive/Programs%20and%20Rebates/Business/TX-Time-of-use-rate-FAQ.pdf, (Accessed May 2020)

[91] Salt River Project, Business Time-of-Use Price Plan (E-32), https://www.srpnet.com/prices/business/tou.aspx, (Accessed May 2020)

[92] NV Energy, Commercial Electric RATES, https://www.nvenergy.com/publish/content/dam/nvenergy/brochures_arch/about-nvenergy/rates-regulatory/np_com_rate.pdf, (Accessed May 2020)

[93] Pacific Gas and Electric Company, Time-of-Use rate plans, https://www.pge.com/en_US/small-medium-business/your-account/rates-and-rate-options/time-of-use-rates.page, (Accessed May 2020)

[94] Baltimore Gas and Electric Company, Electric Retail, https://www.bge.com/MyAccount/MyBillUsage/Documents/Electric/Rdr_1.pdf, (Accessed May 2020)

[95] Xcel Energy, New Mexico Time of Use Rate, https://www.xcelenergy.com/staticfiles/xe-responsive/Marketing/NM-Time-of-use-rate-FAQ.pdf, (Accessed May 2020)

[96] Commonwealth Edison Co, https://hourlypricing.comed.com/live-prices/, (Accessed May 2020)

[97] Xcel Energy, Time of Use Pricing – How it works, https://www.xcelenergy.com/billing_and_payment/understanding_your_bill/residential_rate_plans/time_of_use_pricing/time_of_use_pricing_how_it_works, (Accessed May 2020)

[98] Xcel Energy, Xcel Energy Minnesota Commercial and Industrial Electric Prices, https://www.xcelenergy.com/staticfiles/xe/Regulatory/Regulatory%20PDFs/rates/MN/MNBusRateCard.pdf, (Accessed May 2020)

[99] International Code Council, 2018 IECC - International Energy Conservation Code, Chapter 4 [CE], Commercial Energy Efficiency.

[100] DoE, U. S. (2010). Energyplus engineering reference. The reference to energyplus calculations.

[101] DoE, U. S. (2010). EnergyPlus Input output reference. US Department of Energy.

[102] International Organization for Standardization (2017). ISO 13786. Thermal performance of building components–Dynamic thermal characteristics–Calculation methods.

[103] Gregor P. Henze , Doreen E. Kalz , Clemens Felsmann & Gottfried Knabe (2004) Impact of Forecasting Accuracy on Predictive Optimal Control of Active and Passive Building Thermal Storage Inventory, HVAC&R Research, 10:2, 153-178

[104] Petersen, Steffen, and Katrine Wieck Bundgaard. "The effect of weather forecast uncertainty on a predictive control concept for building systems operation." Applied Energy 116 (2014): 311-321.

[105] Oldewurtel, Frauke, David Sturzenegger, and Manfred Morari. "Importance of occupancy information for building climate control." Applied energy 101 (2013): 521-532.

[106] Goyal, Siddharth, Herbert A. Ingley, and Prabir Barooah. "Occupancy-based zone-climate control for energy-efficient buildings: Complexity vs. performance." Applied Energy 106 (2013): 209-221.

[107] Sun, Yuming. "Closing the building energy performance gap by improving our predictions." PhD diss., Georgia Institute of Technology, 2014.

[108] Wang, Qinpeng. "Accuracy, validity and relevance of probabilistic building energy models." PhD diss., Georgia Institute of Technology, 2016.

[109] ForecastWatch.com , "Analysis of Combined One- to Five-Day-Out Global Temperature Forecasts, January-June 2016", https://www.forecastwatch.com/wp-content/uploads/Global_Temperatures_One_to_Five_Day_Out_Jan-June_2016.pdf (Accessed June 2020)

[110] ForecastWatch.com , "Analysis of High Temperature Forecast Accuracy of Consumer Weather Forecasts from 2005-2016", https://www.forecastwatch.com/wp-content/uploads/High_Temperature_Accuracy_Study_12_Years.pdf (Accessed June 2020)

[111] Browning, Keith Anthony. "Review lecture: Local weather forecasting." Proceedings of the royal society of London. A. Mathematical and Physical Sciences 371, no. 1745 (1980): 179-211.

[112] Wong, L. T., and W. K. Chow. "Solar radiation model." Applied energy 69, no. 3 (2001): 191-224.

[113] Florita, Anthony R., and Gregor P. Henze. "Comparison of short-term weather forecasting models for model predictive control." HVAC&R Research 15, no. 5 (2009): 835-853.

[114] Lazos, Dimitris, Alistair B. Sproul, and Merlinde Kay. "Optimisation of energy management in commercial buildings with weather forecasting inputs: A review." Renewable and Sustainable Energy Reviews 39 (2014): 587-603.

[115] Yadav, Amit Kumar, and S. S. Chandel. "Solar radiation prediction using Artificial Neural Network techniques: A review." Renewable and sustainable energy reviews 33 (2014): 772-781.

[116] Dong, Jin, Mohammed M. Olama, Teja Kuruganti, Alexander M. Melin, Seddik M. Djouadi, Yichen Zhang, and Yaosuo Xue. "Novel stochastic methods to predict short-term solar radiation and photovoltaic power." Renewable Energy 145 (2020): 333-346.

[117] Wang, Zhe, Tianzhen Hong, and Mary Ann Piette. "Data fusion in predicting internal heat gains for office buildings through a deep learning approach." Applied Energy 240 (2019): 386-398.

[118] Wang, Zhaoxia, and Yan Ding. "An occupant-based energy consumption prediction model for office equipment." Energy and Buildings 109 (2015): 12-22.

[119] Mahdavi, Ardeshir, Farhang Tahmasebi, and Mine Kayalar. "Prediction of plug loads in office buildings: Simplified and probabilistic methods." Energy and Buildings 129 (2016): 322-329.

[120] Saha, Homagni, Anthony R. Florita, Gregor P. Henze, and Soumik Sarkar. "Occupancy sensing in buildings: A review of data analytics approaches." Energy and Buildings 188 (2019): 278-285.

[121] Hong, Tianzhen, Yixing Chen, Zsofia Belafi, and Simona D'Oca. "Occupant behavior models: A critical review of implementation and representation approaches in building performance simulation programs." In Building Simulation, vol. 11, no. 1, pp. 1-14. Tsinghua University Press, 2018.

[122] WeatherSTEM, http://gatech.weatherstem.com/data?refer=/stadium (Accessed May 2020)

[123] World Weather Online, Hstorical Forecast Weather, https://www.worldweatheronline.com/hwd/hfw.aspx (Accessed Octcober 2020)

[124] Chen, Yixing, Xuan Luo, and Tianzhen Hong. "An agent-based occupancy simulator for building performance simulation." (2016).

[125] ASHRAE, ANSI. "ASHRAE/IES Standard 90.1-2016: Energy Standard for Buildings Except Low-Rise Residential Buildings." Atlanta, USA: American Society of Heating, Refrigerating, and Air Conditioning Engineers (2016).

[126] Malkawi, Ali, and Godfried Augenbroe, eds. Advanced building simulation. Routledge, 2004.

[127] Kim, Il Yong, and Oliver L. De Weck. "Adaptive weighted-sum method for bi-objective optimization: Pareto front generation." Structural and multidisciplinary optimization 29, no. 2 (2005): 149-158.

[128] Hazelrigg, George A. Fundamentals of decision making for engineering design and systems engineering. 2012.

[129] Augenbroe, Godfried, and Sten de Wit. "Web-hosted opportunities for cost-effective expert judgement studies." In Proceedings of the Institution of Civil Engineers-Civil Engineering, vol. 150, no. 6, pp. 57-62. Thomas Telford Ltd, 2002.

[130] Chen, Jianli. "INVESTIGATION OF HYBRID VENTILATION POTENTIAL OF COMMERCIAL BUILDINGS IN US." PhD diss., Georgia Institute of Technology, 2018.